Università degli Studi dell'Aquila

Dipartimento di Scienze cliniche applicate e biotecnologiche

Dottorato di Ricerca in "Medicina Sperimentale"

Curriculum "Biotecnologie Mediche"

XXXIV ciclo

The Extracellular Vesicles (EVs) and their role in primary and metastatic bone tumors

SSD: BIO/17 – ISTOLOGIA

Dottorando:
Argia Ucci

Coordinatore del corso:
Prof.ssa Mariagrazia Perilli

Tutor:
Prof.ssa Nadia Rucci

A.A. 2020-2021

TABLE OF CONTENTS

SUMMARY **5**

CHAPTER 1: "INTRODUCTION"

1. INTRODUCTION **7**

1.1 THE BONE TISSUE 7
1.1.1 BONE CELLS 7
1.1.2 BONE REMODELING 12
1.2 PRIMARY MALIGNANT BONE TUMORS 14
1.3 BONE METASTASES 16
1.4 EXTRACELLULAR VESICLES (EVs) 20
1.5 EVs AND BONE CANCER 26

2. AIM AND OUTLINE OF THE WORK **28**

3. REFERENCES **29**

CHAPTER 2: "EXTRACELLULAR VESICLES FROM OSTEOTROPIC BREAST CANCER CELLS AFFECT BONE RESIDENT CELLS"

1. ABSTRACT **39**

2. INTRODUCTION **40**

3. MATERIALS AND METHODS **41**

3.1 MATERIALS 41
3.2 ANIMALS 42
3.3 CELL LINES 42
3.4 OSTEOBLAST PRIMARY CULTURES 43
3.5 ALP ACTIVITY ASSAY 43
3.6 OSTEOCLAST PRIMARY CULTURES 43
3.7 EVs ISOLATION 44
3.8 TRANSMISSION ELECTRON MICROSCOPY 44
3.9 RT^2 PROFILER REAL-TIME PCR ARRAY 44
3.10 COMPARATIVE REAL-TIME RT-PCR 45
3.11 ENDPOINT RT-PCR 46
3.12 CYTOKINE PROFILER ARRAYS 46
3.13 WESTERN BLOT ANALYSIS 47
3.14 FLUORESCENCE-ACTIVATED CELL SORTING OF EVS 47
3.15 CELL VIABILITY ASSAY 48
3.16 IN VITRO TUBE FORMATION ASSAY 48
3.17 MATRIGEL PLUG ASSAY 48
3.18 MOUSE CALVARIAE ORGAN CULTURE 49
3.19 μCT ANALYSIS 49
3.20 IN VIVO TUMOR EV TARGETING TO BONE 50

4. RESULTS **51**

4.1 BREAST CANCER–DERIVED CM AFFECTS OSTEOBLAST DIFFERENTIATION 51
4.2. CHARACTERIZATION OF MDA-DERIVED EVS 55
4.3 EFFECT OF BREAST CANCER–DERIVED EVS ON OSTEOBLAST BEHAVIOR 58

4.4 BREAST CANCER CELL–EVS AND OB-EVS EDUCATED BY TUMOR CELL CM STIMULATE OSTEOCLASTOGENESIS ... 65
4.5 BREAST CANCER CELL–EVS AND OB-EVS EDUCATED BY TUMOR CELLS CM STIMULATE ANGIOGENESIS ... 68
4.6 IN VIVO BREAST CANCER CELL–EV INTEGRATION INTO THE BONE TISSUE ... 70

5. DISCUSSION ... **72**

6. REFERENCES ... **76**

CHAPTER 3: "ANTI-OSTEOBLASTOGENIC, PRO-INFLAMMATORY AND PRO-ANGIOGENIC EFFECT OF EXTRACELLULAR VESICLES ISOLATED FROM THE HUMAN OSTEOSARCOMA CELL LINE MNNG/HOS"

1. ABSTRACT ... **81**

2. INTRODUCTION ... **82**

3. MATERIALS AND METHODS ... **83**

3.1 MATERIALS ... 83
3.2 ANIMALS ... 84
3.3 CELL LINES ... 84
3.4 EXTRACELLULAR VESICLES (EVS) ISOLATION ... 85
3.5 TRANSMISSION ELECTRON MICROSCOPY (TEM) ... 85
3.6 EV INTERNALIZATION ASSAY ... 85
3.7 OSTEOBLAST PRIMARY CULTURES ... 85
3.8 ALKALINE PHOSPHATASE (ALP) ACTIVITY ASSAY ... 86
3.9 MINERALIZATION ASSAY ... 86
3.10 OSTEOCLAST PRIMARY CULTURES ... 86
3.11 BONE RESORPTION ASSAY ... 87
3.12 EVALUATION OF BONE TURNOVER MARKERS ON CONDITIONED MEDIA ... 87
3.13 CELL METABOLIC ACTIVITY ... 87
3.14 CRYSTAL VIOLET ASSAY ... 87
3.15 *IN VITRO* TUBE FORMATION ASSAY ... 87
3.16 MATRIGEL PLUG ASSAY ... 88
3.17 RT^2 PROFILER REAL TIME PCR ARRAY ... 88
3.18 COMPARATIVE REAL TIME RT-PCR ... 88
3.19 ENDPOINT RT-PCR ... 89
3.20 CYTOKINE ARRAY ... 90
3.21 WESTERN BLOT ANALYSIS ... 91
3.22 STATISTICS ... 91

4. RESULTS ... **91**

4.1 MNNG/HOS-EV CHARACTERIZATION AND BONE TRANSCRIPTIONAL PROFILING ... 91
4.2 MNNG/HOS-EVS INTEGRATION INTO RECIPIENT BONE CELLS IN VITRO ... 92
4.3 EFFECT OF MNNG/HOS-EVS ON OSTEOBLAST DIFFERENTIATION AND ACTIVITY ... 94
4.4 EFFECT OF MNNG/HOS-EVS ON OSTEOCLAST DIFFERENTIATION AND ACTIVITY ... 97
4.5 EFFECT OF MNNG/HOS-EVS ON OSTEOBLAST INFLAMMATORY AND OSTEOCLASTOGENIC CYTOKINES ... 99
4.6 EFFECT OF MNNG/HOS-EV ON ANGIOGENESIS ... 103

5. DISCUSSION ... **105**

6. REFERENCES ... **108**

CHAPTER 4: “CONCLUSIONS”

CONCLUSIONS **114**

REFERENCES **114**

CHAPTER 5: “ACHIEVEMENTS”

CURRICULUM VITAE **119**

SUMMARY

Extracellular vesicles (EVs) are defined as spherical structures surrounded by a lipid bilayer released by cells into various biological fluids. EVs represent an important means of communication and transport of signal molecules between cells, playing a crucial role as mediators of many physiological and pathological processes, including cancer. In recent years, several studies have been emerging on their involvement in the onset and progression of primary bone tumors and metastases, both addressed in Chapter 1 of this PhD thesis.

In a previous work conducted in our lab, it was shown that there is extensive EV-mediated communication among the cells of the bone tissue. Since the latter is one of the most common sites for breast cancer metastases, we set out to evaluate the EVs-mediated interaction between MDA-MB-231 cells, a human osteotropic breast cancer cell line, and bone resident cells. In particular, we showed that EVs from MDA-MB-231 have a direct role on bone cell physiology, stimulating osteoclastogenesis, angiogenesis, and inhibiting osteoblast differentiation. We also observed that soluble factors, released by MDA-MB-231 cells, educate osteoblasts, increasing the osteoclastogenic potential of the EVs isolated from the latter and thus creating a microenvironment conducive to bone destruction and to tumor growth. These results are reported in more detail in Chapter 2.

Subsequently, we focused on the mechanisms underlying the progression of primary bone tumors, studying the EVs-mediated interaction between the human osteosarcoma cell line MNNG/HOS and the bone cells. We treated osteoblasts with EVs from MNNG/HOS, observing a significant reduction in their number, as well as their metabolic and alkaline phosphatase (Alp) activity. We found a reduction in the expression of genes associated with the cell cycle and osteoblast differentiation. Furthermore, we observed that osteoblasts were induced by tumor EVs to produce and release pro-inflammatory and pro-tumoral factors in the bone microenvironment. In addition to these results, described in Chapter 3, we found that EVs from MNNG/HOS increase the expression of Serpin b2 in osteoblasts, a protein often overexpressed in tumor tissues and still under our investigation. Furthermore, we found that EVs from MNNG/HOS promote angiogenesis, both *in vitro* and *in vivo*.

In conclusion, the results obtained during my PhD underline the importance of tumor-derived EVs in the crosstalk between cancer cells and resident cells in the bone microenvironment, and show their role in influencing bone cells behavior, in particular of osteoblasts, and their release of determining factors, hopefully useful in advancing the current research on therapeutic and prognostic potential of EVs in cancer treatment.

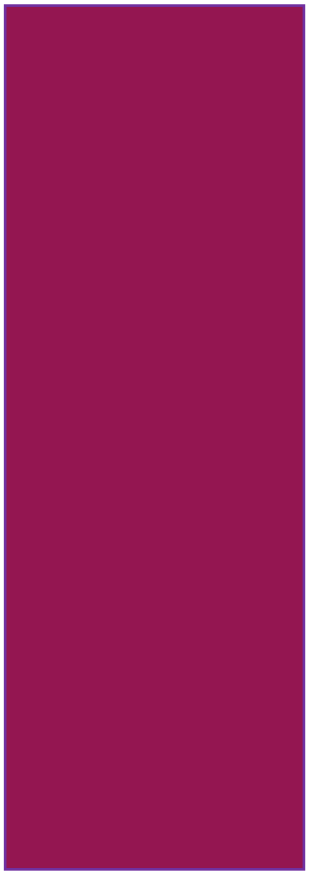

Chapter 1

"Introduction"

1. INTRODUCTION

1.1 The bone tissue

Bone is a specialized connective tissue and the main constituent of the skeletal system, which exerts many important functions in the body other than mechanical support and protection of soft organs, such as being a metabolic reserve of calcium and phosphate[1].

Its internal organization is very peculiar and consists of cells and an abundant extracellular matrix (ECM), in which an organic and an inorganic component can be distinguished. The first is composed of collagen type I fibers (90% of the total proteins), immersed in an amorphous matrix of non-collagenous proteins, glycoproteins and proteoglycans; while the latter (65% of the dry weight of the tissue), consists mainly of mineral salts, among which the most abundant is present in the form of small crystals of hydroxyapatite [$Ca_{10}(PO_4)_6(OH)_2$]. The inorganic or mineralized matrix provides to the bone tissue the typical mechanical properties of rigidity, hardness and tensile strength, whereas the organic component ensures an extraordinary elasticity and flexibility[2,3].

The bone has been recognized as a very complex and dynamic tissue, which is constantly renewed through a process named bone remodeling. This ensures the replacement of old or damaged bone with a new and mechanically competent one, maintaining the integrity and stability of the tissue.

Three main cell types, actively involved in this process, can be distinguished: osteoblasts, cells with osteogenic function; osteoclasts, responsible for bone resorption; and osteocytes, mechanosensitive bone-resident cells deriving from mature osteoblasts and embedded in the bone matrix. They interact each other's to guarantee a correct tissue homeostasis[4].

1.1.1 Bone cells

Osteoblasts

Osteoblasts are responsible for bone formation[5,6]. They arise from mesenchymal stem cells (MSCs), pluripotent stem cells able to commit to the osteoprogenitors cells under stimulation of specific local growth factors, such as Bone Morphogenetic Proteins (BMPs), Wingless-related integration site (Wnt) family proteins[7] and Fibroblast Growth Factor (FGF)[8]. In

particular, Wnt proteins (Wint 1a, 3a, 10b) play an important role in this process through the canonical Wnt/β-catenin signaling pathway, binding to Frizzled (Fzd) receptor and Low-density lipoprotein Receptor–related Proteins 5 or 6 (LRP-5/6) coreceptors expressed on the plasma membrane of osteoprogenitor cells[9]. This promotes an intracellular signaling cascade involving a multi-protein complex [made of Glycogen Synthase Kinase 3b (GSK3b), Axin, Adenomatous Polyposis Coli (APC), Dishevelled (Dsh) proteins], which in turn inhibit the GSK3b-mediated β-catenin phosphorylation and its ubiquitin-mediated degradation, leading to β-catenin stabilization and accumulation in the cytoplasm and its subsequent translocation into the nucleus. Nuclear β-catenin in turn interacts with transcription factors TCF/LEF (T cell-specific transcription factor/Lymphoid Enhancer-binding Factor) and promotes osteoblastic differentiation by promoting the transcription of specific genes, such as Runt-related transcription factor 2 (Runx2) and Osterix[10,11]. Moreover, during the last stage of differentiation, some osteoblasts can become bone-lining cells, which are quiescent flat-shaped cells located on the bone surface, others remain embedded in the newly formed matrix becoming osteocytes, while others die by apoptosis[12,13].

Mature osteoblasts are characterized by a cuboidal shape (Figure 1) and a plasma membrane rich in Alkaline Phosphatase (ALP), used as a serum marker of bone formation. In addition, they express receptors for parathyroid hormone (PTH), oestrogens, vitamin D3, and they produce bone matrix proteins, such as osteocalcin (OCN), bone sialoproteins and collagen type I[5].

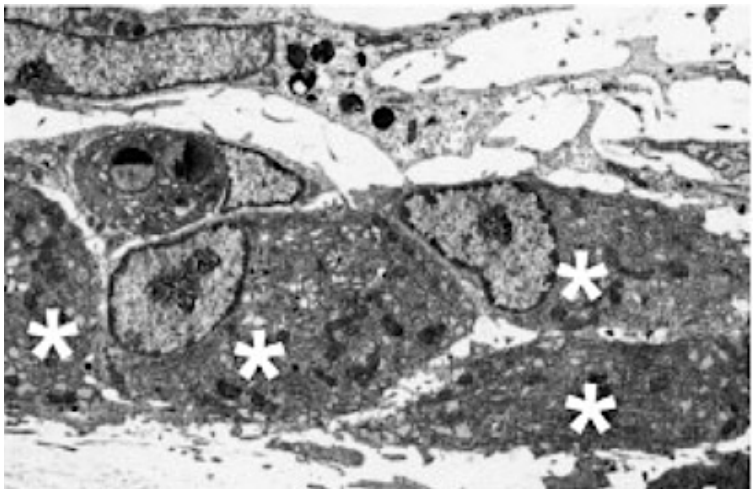

Figure 1: Mature osteoblasts. Transmission electron micrograph of active osteoblasts (marked by asterisks, *), having a cuboidal shape and well-developed organelles, necessary to produce and secrete the bone matrix. *(Source: adapted from Johannesdottir and Bouxsein, 2018[14])*

Above all, osteoblasts are responsible for the secretion of organic components of the ECM and deposition of mineral salts, producing new bone matrix in form of the so called "osteoid" and managing its subsequent mineralization[12]. Another important function attributable to osteoblasts is the regulation of osteoclasts formation and function, by means of three main cytokines: the Macrophages-Colony Stimulating Factor (M-CSF), involved in pre-osteoclasts growth and survival, the Receptor Activator of Nuclear Factor-κB Ligand (RANKL), which regulates their fusion and differentiation, and the osteoprotegerin (OPG), a decoy receptor for RANKL able to antagonize its binding to RANK and to inhibit osteoclastogenesis and subsequent bone resorption[15,16] (Figure 2).

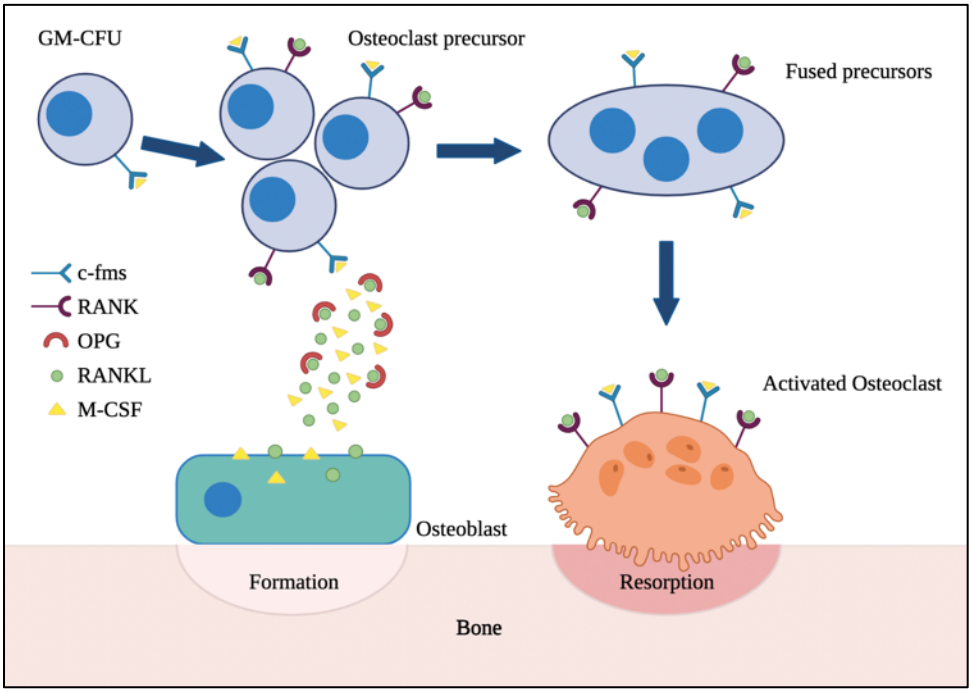

Figure 2: Osteoblasts produce cytokines involved in osteoclast formation and differentiation. Cartoon illustrating the mechanism by which osteoblasts regulate osteoclastogenesis through the production of cytokines such as M-CSF, RANKL and OPG. *(Source: adapted from Owen and Reilly, 2018[17], created in BioRender.com)*

Osteocytes

Osteocytes are the most abundant cells in bone, representing 90-95% of the total bone cells[5]. They originate from osteoblasts, which became embedded in the bone mineralized matrix that they produced, in small cavities (lacunae). They are non-proliferative and terminally differentiated cells.

Despite the morphology of the osteocytes varies according to the age and functional activity, they generally appear as spider-shaped cells with a small, flattened cell body and numerous long cytoplasmic protrusions called dendritic processes, that extend through a complex network of tubular canaliculi (Figure 3) and by which they interconnect with each other, with osteoblasts or lining cells at the bone surface and with the vasculature, forming gap junctions[18,19].

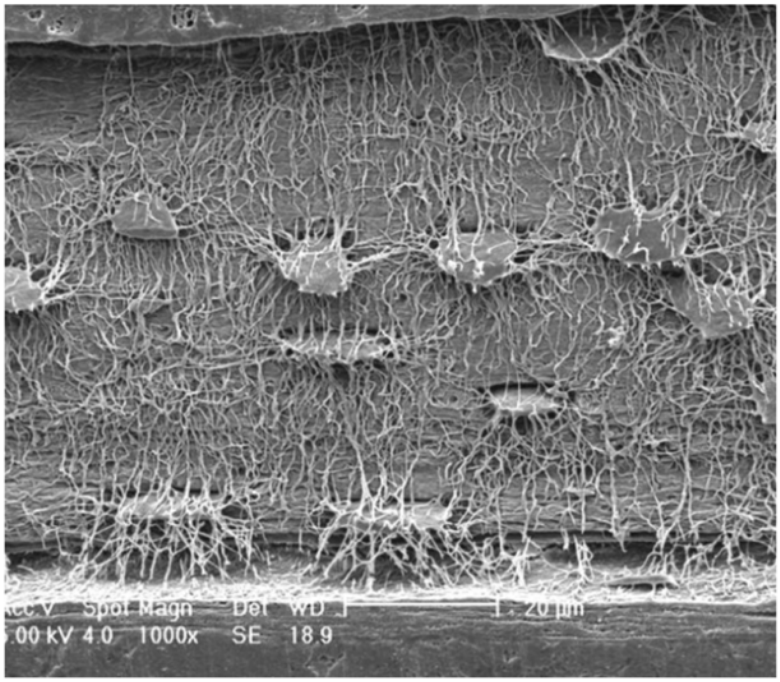

Figure 3: The osteocytes and their canalicular network. Scanning electron microscopy (SEM) image of murine osteocytes within the bone matrix, connected through dendritic processes. Magnification 1000 X. *(Source: Manolagas and Parfitt, 2010[20])*

A mature osteocyte persists in the matrix per years, playing a role as mechanosensor and regulating load-driven bone remodeling, via intercellular interactions with osteoblasts and osteoclasts and the release of soluble mediators[21,22]. In the last stages of differentiation, they highly express characteristic markers by which they actively contribute to the regulation of bone turnover, such as Dentin matrix protein 1 (DMP1), FGF23, BMPs and Sclerostin (Sost), the latter being an inhibitor of osteoblasts differentiation and function by blocking the canonical Wnt/β-catenin pathway[12,18]. In this regard, it has been widely demonstrated that they release also RANKL and OPG, regulating osteoclastogenesis[23].

Osteoclasts

Osteoclasts are giant multinucleated cells, containing 4-30 nuclei, derived from fusion of mononuclear precursors of the monocyte-macrophage lineage[16]. These cells are mainly responsible for the degradation of the bone matrix, to which they adhere in small resorption area called Howship lacunae, produced by their erosive action. Precisely, they play an important role in bone remodeling and regulation of mineral homeostasis[24].

Osteoclasts contain a vacuolized cytoplasm, sign of an intense secretory activity, are rich in mitochondria, lysosomes with acid hydrolases and multiple Golgi apparati, disposed around each nucleus. They are polarized cells showing different plasma membrane domains: the apical membrane, characterized by the "sealing zone", bone-facing area with specialized adhesion structures called podosomes[25]; the "ruffled border" membrane, a system of membrane expansions that allow the fusion and the release of the lysosomal enzymes and H^+ ions into the resorption lacuna, with its subsequent acidification and dissolution of hydroxyapatite crystals[16,26,27]; and the basolateral membrane, rich of several ion channels and presenting a secretory domain essential for releasing the digested matrix components (Figure 4). This last domain also expresses receptors for RANKL (RANK) and for M-CSF (c-Fms), responsible for osteoclastogenesis[28].

Osteoclast differentiation process is achieved by several factors, mainly derived from T cells or osteoblasts, among which M-CSF and RANKL stand out in importance. The first cytokine binds and activates the c-Fms receptor by dimerization, causing trans-phosphorylation of tyrosine residues in its cytoplasmatic tail and starting different signaling pathways binding proteins such as c-Src (phosphatidylinositol 3-kinase PI3K/AKT pathway) and Grb2 (ERK pathway), promoting the proliferation and survival of osteoclast precursors. The RANKL, instead, interacts with the RANK receptor on the osteoclast precursor surface, thus recruiting TNF receptor-associated factor family proteins (TRAFs), which in turn allows the nuclear translocation of Nuclear Factor k-light-chain-enhancer of activated B cells (NFkB) and Nuclear factor of activated T cells 1 (NFATc1), osteoclastogenesis regulators[28]. At this point, several mature osteoclast-specific genes are expressed: Tartrate Resistant Acid Phosphatase (TRAcP), (used as a cellular marker for functional osteoclasts), cathepsin K, Osteoclast Associated Receptor (OSCAR), Dendritic Cell-Specific Transmembrane Protein (DC-STAMP) and Matrix Metalloproteinase (MMP)-9 and -14[29,30]. Moreover, osteoclastogenesis can be promoted also by different inflammatory molecules,

such as Tumor Necrosis Factor-α (TNF-α) and Interleukins (IL-) 1β and 6, through the activation of the NFkB pathway[31,32].

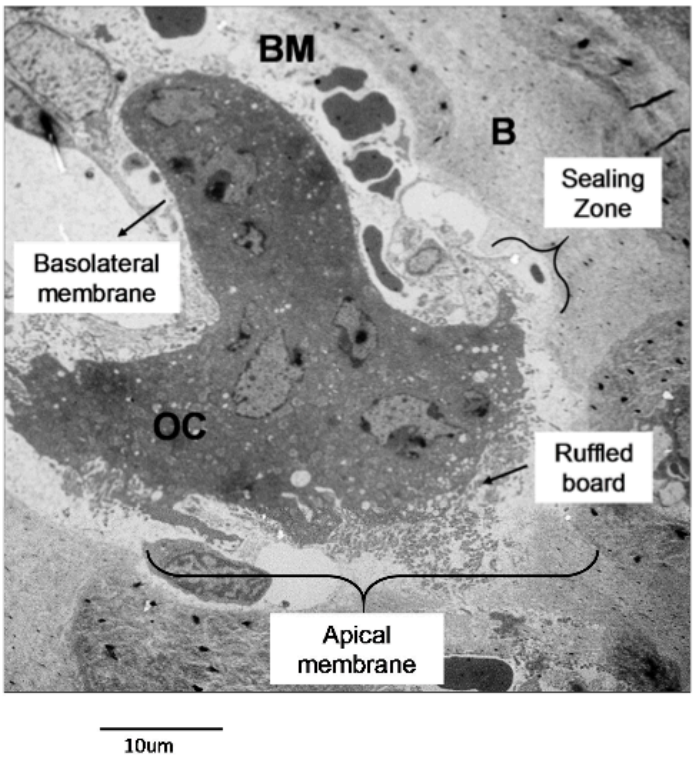

Figure 4: Osteoclast morphology. Transmission electron microscopy (TEM) image of a murine osteoclast and its different plasma membrane domains. Scale bar: 10 µm. B=bone, OC=osteoclast and BM=bone marrow. *(Source: Maurizi and Rucci, 2018[33])*

1.1.2 Bone remodeling

The bone remodeling is a well-organized process, consisting in the cyclic removal and deposition of the bone matrix, performed by osteoclasts and osteoblasts, respectively. As already mentioned, it confers the maintenance of the bone microarchitecture and the mechanical properties of the tissue and is essential for the metabolic regulation of calcium and phosphate levels[34].

The process occurs in four different sequential steps[35,36] (Figure 5):

1. *Activation phase*: triggered by several stimuli, such as bone micro damages, mechanical stress or soluble factors released in the bone microenvironment, including Insulin-like Growth Factor-1 (IGF-1), PTH, or inflammatory cytokines, such as TNF-α, IL-1β and IL-6. It results in the activation of bone lining cells, exposure of the bone surface and secretion of chemokines involved in the recruitment of osteoclasts precursors from the bloodstream. Once arrived in the remodeling site,

pre-osteoclasts differentiation is stimulated by osteogenic cells expression of m-CSF and RANKL, which bind to their specific receptors.

2. *Resorption phase*: characterized by polarization of mature osteoclasts, which start the acidification of the bone matrix, to dissolve the inorganic component, followed by the release of lysosomal enzymes (Cathepsin K) and metalloproteinases (MMP-9) which degrade the organic part. Bone degradation allows the release of breakdown products of type I collagen, including terminal peptide fragments [N-terminal (NTx)] and C-terminal [(CTx) telopeptides], calcium and of several factors, such as BMPs, FGFs, IGF-2 and Transforming Growth Factor-β (TGF-β), which are involved in the subsequent osteoblast precursors recruitment and commitment.
3. *Reversal phase*: involves the arrest of osteoclasts activity by apoptosis and the appearance on the bone surface of the reverse cells, macrophage-like cells involved in the removal of residual debris produced during matrix degradation and in the stimulation of osteoblasts' anabolic activity.
4. *Formation phase*: the longest phase, characterized by the differentiation of osteoblasts precursors and their secretion and deposition of new bone matrix, initially not calcified (osteoid) and then mineralized, through the precipitation of hydroxyapatite crystals. The entire process ends when the resorbed bone is entirely replaced and osteoblasts undergo apoptosis or become osteocytes embedded in the ECM.

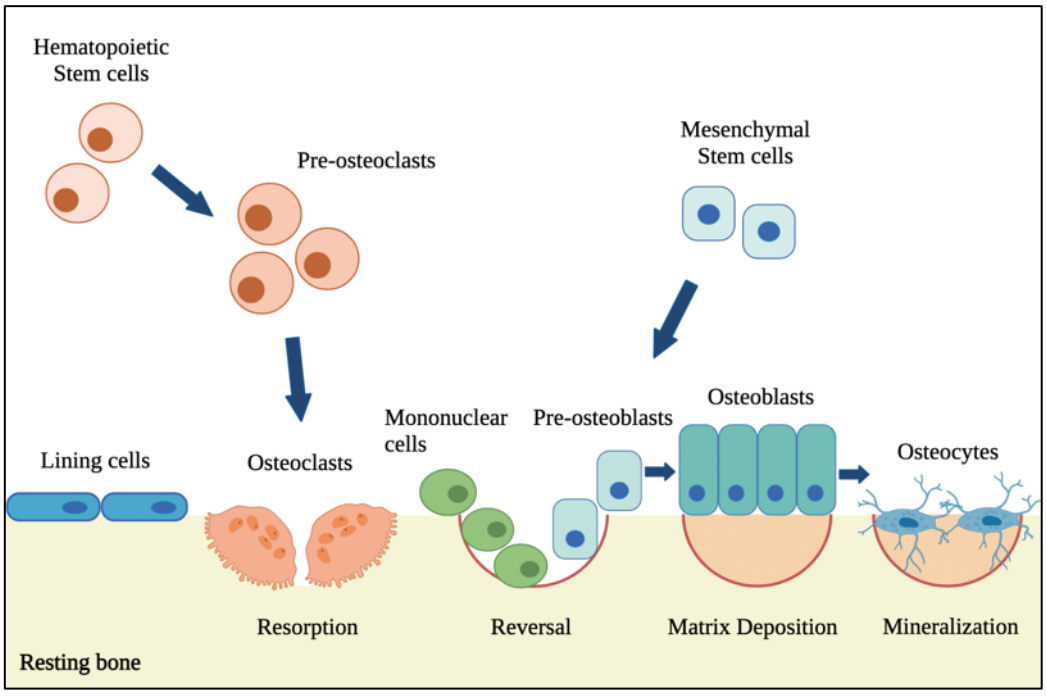

Figure 5: The bone remodeling process. The bone remodeling process begins with the exposure of bone surface by bone lining cells and migration of pre-osteoclasts in the resorption area. They differentiate into mature osteoclasts and resorb the bone matrix, releasing breakdown products. Then, reverse cells absorb the debris in the resorbed surface and help recruiting osteoblasts, which depose newly synthetized organic matrix, the osteoid. The remodeling cycle is completed with matrix mineralization and differentiation of some osteoblasts in osteocytes. *(Source: adapted from Kapinas and Delany, 2011[37], created in BioRender.com)*

The combined activity of osteoblasts and osteoclasts is finely regulated, thus preventing excessive bone deposition respect to its degradation and *viceversa*. In contrast, any alteration of this *equilibrium* affects the bone mass, eventually leading to several bone pathologies, including cancer[17].

1.2 Primary malignant bone tumors

Primary malignant bone tumors are quite rare (1:100,000 individuals)[38]. There are three main types of cancers affecting the bone, according to the cells that give rise to them: osteosarcoma, Ewing's sarcoma and chondrosarcoma.

Chondrosarcomas are the rarest, characterized by the production of cartilaginous tissue and are often registered in adults (40 to 70 years of age), with an increasing risk in old age. They occur mostly in pelvis, vertebrae, around hip and proximal long bones. Different subtypes can be distinguished, of which conventional chondrosarcomas are the most common (80-90%). To date, these tumors can be treated only by surgery, being resistant to chemotherapy and radiotherapy[39].

Ewing's sarcoma (ES) occurs in children and adolescents, between the ages of 5 and 20. Identified for the first time in 1921 by James Ewing and described as a "diffused endothelioma of the bone"[40], this tumor belongs to the Ewing's sarcoma Family Tumors (EFT), together with extraosseous ES (EES), Askin's tumor and peripheral primitive neuroectodermal bone tumor (pPNET)[41]. ES develops especially in diaphysis of long bones, pelvis and ribs; is very aggressive and is prone to metastasize in lungs, lymph nodes and brain. The cellular origin is still under investigations.

Osteosarcoma (OS), instead, represent the most common tumor among primary bone malignancies (annual incidence 3:1,000,000 in the general population), mostly affecting children and young adults and, in a small percentage (10%) people over 60s, thus showing a bimodal distribution. Of note, OS are more common in males than in females (3:2)[42]. These tumors are fairly aggressive and divided in several histological subtypes, among which the

high-grade subtype (intramedullary osteosarcoma) is the most common. Typically, OS develops in the metaphysis of long bones, especially the distal femur and proximal tibia and humerus, and can spread systemically, mostly developing lung metastases. There are still doubts about the origin of OS: recent studies suggested that it may arise from malignant MSCs as osteogenic precursor cells[43], while others hypothesized that it originates directly from osteoblasts or pre-osteoblasts. In this regard, OS cells have an osteoblastic phenotype, they deposit bone in form of osteoid and express Alp, Osterix, Osteocalcin and bone sialoproteins[44]. Moreover, OS cells alter the balance between bone resident cells through the expression of pro-osteoclastogenic factors such as RANKL and IL-6, inducing osteoclasts activity and subsequent bone resorption, and also stimulating the stromal cells (fibroblasts, endothelial cells and macrophage) to modify the ECM and create a pro-metastatic microenvironment.

Generally, pain is the most common symptom of bone cancer, followed by swelling, periods of fever and onset of spontaneous fractures. Radiography is the most used imaging modality for diagnosis (Table 1).

Table 1. Descriptive table with radiological features of different types of primary malignant bone cancers (*adapted from Ferguson et al,* 2018[45]).

Cancer type	**Radiographic characteristics**
Osteosarcoma	Dense sclerosis of metaphysis (nearly all) Soft tissue extension Radiating calcification; "sunburst" (60%) Osteosclerotic lesion (45%) Lytic lesion (30%)
Ewing sarcoma	Bone destruction (75%) Soft tissue extension (64%) Reactive bone formation (25%) Lamellated periosteal reaction; "onion skin" (23%) Radiating calcification, "sunburst" (20%) Radiography may be normal
Chondrosarcoma	Calcified eccentric osteolytic lesion

To date, the only therapeutic options for bone sarcomas, except for chondrosarcoma, consist in a combination of neoadjuvant chemotherapy (methotrexate, cisplatin,

doxorubicin) and subsequent local treatment of the primary tumor with surgery and/or radiation, followed by further cycles of chemotherapy[46]. The clinical outcomes depend on the presence of metastatic foci, which lower the 5-years survival rate to 20-30% cases.

1.3 Bone metastases

During tumor progression, cancer cells can acquire the ability to migrate from primary lesions and selectively colonize distant sites to form secondary tumors, because of the presence of a favorable environment ("seed and soil" theory, Stephen Paget)[47,48].

In this contest, the bone tissue is one of the most common sites of metastasis, after liver and lung[49]. In particular, bone metastases are very frequent in advanced breast and prostate cancers, with an incidence exceeding 70%[50]. Less commonly, carcinoma of lung, kidney, colon, thyroid and melanoma can spread to bone[51].

Bone metastases are usually multifocal, predilecting the bone marrow sites in the proximal long bones, as well as vertebrae, pelvis, ribs and skull. Based on histological and clinical features of caused lesions, they can be classified as osteolytic, osteosclerotic and mixed types[52].

Without any type excluded, cancer cells spread to the bone microenvironment and interact pathologically with osteoblasts and osteoclasts, breaking the physiological balance between bone resorption and formation given by the synergistic action of these cells, called "virtuous cycle", and establishing a "vicious cycle" (Figure 6), from which they benefit to grow[53,54]. Furthermore, this bidirectional interaction has proven to be supported by the acquisition by cancer cells in the host tissue of a property called "osteomimicry", that is the propensity to resemble genetically the osteoblasts and to produce their own proteins, such as OPN, OCN, bone sialoproteins, RUNX2 and ALP, influencing the bone physiology and acquiring the ability to escape from immune responses[55].

Lytic lesions are more frequent in breast cancers and are characterized by an exacerbated bone erosion. In particular, tumor cells in bone microenvironment produce several proteins, including RANKL, and inflammatory cytokines, such as IL-1β, IL-6 and TNF-α, that stimulate osteoclasts-mediated bone resorption, leading to the release of growth factors previously stored in the bone matrix (TGF-β, IGFs, FGFs, PDGF and BMPs), which promote cancer cells growth, proliferation and survival[56]. Additionally, tumor cells produce also the parathyroid hormone-related peptide (PTHrP), by which they increase the osteoblast expression of RANKL and indirectly regulate osteoclastogenesis.

Osteosclerotic or osteoblastic lesions, instead, are typical of prostate cancer. They are distinguished by the presence of an aberrant deposition of woven bone, qualitatively not competent[57]. In this case, cancer cells affect osteoblasts differentiation and activity through the release of several factors, such as Wnt-1, Wnt-3a, IGF-1, FGF, PTHrP, BMPs and endothelin-1, causing uncontrolled deposition of new bone matrix. This lead to an osteoblast's RANKL-mediated osteoclastogenesis, followed by abnormal bone resorption and release of factors that stimulate the formation of a pro-metastatic microenvironment[33].

Eventually, in case of mixed-type bone metastases, osteolytic and osteosclerotic lesions can coexist in the same body district or in different sites.

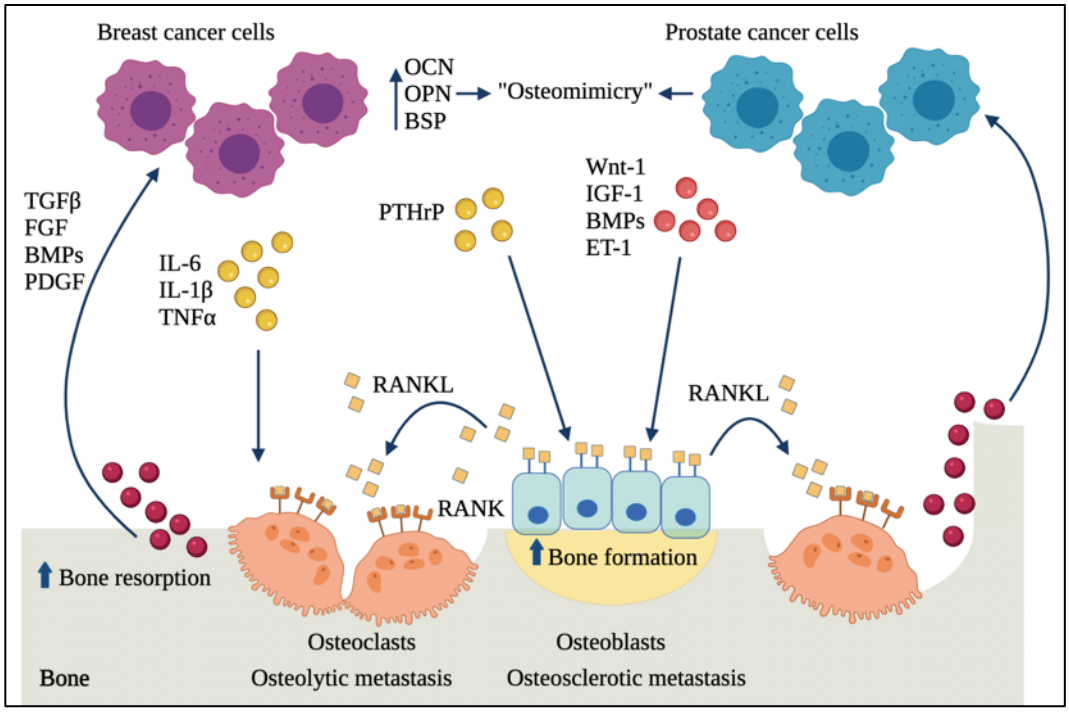

Figure 6: The "vicious cycle". Illustration of the mechanisms by which osteolytic and osteosclerotic lesions develop. In the first case, breast cancer cells release factors that stimulate osteoclasts formation and increase bone resorption; in the second, prostate cancer cells promote bone formation and indirectly stimulate osteoclastogenesis through RANKL-osteoblasts expression. In both cases, factors released from the bone matrix degradation feed tumor cells and create a fertile soil for their growth and survival *(Source: adapted from Maurizi and Rucci, 2018[33], created in BioRender.com).*

Generally, three fundamental steps contribute to the bone metastatic process: (i) escape of cancer cells from the local microenvironment and dissemination through intravasation into the bloodstream, (ii) extravasation, adhesion and invasion to bone, and (iii) colonization and growth in bone[58]. An important additional step to cite is the formation of pre-metastatic niche, a supportive environment established to facilitate metastatic tumor

cells colonization[59]. Various factors and associated pathways regulate this multistep process, providing multiple targets for study and management of bone metastases (Table 2)[58].

Table 2. Descriptive table with regulating factors associated with the bone metastasis process (*adapted from Wang et al, 2020*[58]).

Regulating factors	**Action mechanism**
Tumor cell dissemination	
MMP-2	Acts synergistically with E-cadherin and facilitates tumor angiogenesis
MMP-7	Promotes osteolytic bone metastases by increasing the soluble form of RANKL
MMP-9	Induces tumor angiogenesis
MMP-13	Mediates tumor-induced osteolysis and indicates the invasion and metastasis capacity of tumors
Tumor cell adhesion and invasion	
CXCL12/CXCR4	Facilitates the mobilization of hematopoietic stem cells, tumor proliferation, and angiogenesis
Galectin-3/TF	Promotes adhesion of cancer cells to bone marrow endothelial monolayers
CD44/hyaluronan	Promotes adhesion of cancer cells to bone marrow endothelial monolayers
CCL5/CCR5	Induces tumor cancer cell migration
XCL1/XCR1	Promotes the proliferation and migration of tumor cells
ADAM	Facilitates the degradation of the bone matrix
uPA82	Facilitates the degradation of the bone matrix
COX-2	Facilitates tumor cell adhesion and proliferation in bones
Metastasis formation in bone	
TGF-β	Dual role: suppresses tumor growth at early stage and promotes invasion and metastasis to bones at later stages
IGF-1	Promotes bone colonization of metastasizing tumor cells and facilitates their expansion inside bones
miR-141-3p	Promotes EMT leading to cancer cell invasion and migration
miR-145	Promotes EMT leading to cancer cell invasion and migration
miR-335	Suppresses the development of bone metastases
miR-126	Suppresses the development of bone metastases
miR-206	Suppresses the development of bone metastases
miR-135	Reduces metastasis formations in bone via the downregulation of Runx2
miR-203	Reduces metastasis formations in bone via the downregulation of Runx2
miR-10b	Promotes the bone marrow invasion of tumor cells
miR-21	Promotes the bone marrow invasion of tumor cells
ATX	Regulates the early stage of tumor cell colonization in bones
Osteoclastic metastases	
RANK/RANKL	Activates transcription factor and prevents the apoptosis of mature osteoclasts
PTHrP	Activates the bone resorption activity of osteoclasts
OPG	Competes with RANK for RANKL and thus blocks the RANKL/RANK interaction and osteoclastogenesis
CaSR	Mediates the adhesion, migration and proliferation potential of tumor cells in a calcium-dependent manner
TNF-α	Upregulates the expression of RANKL and induces osteoclast differentiation from TRAF6$^{-/-}$ osteoclast precursors
IL-1	Directly or indirectly promotes osteoclastogenesis by inducing RANKL expression
IL-6	Promotes osteoclastogenesis by inducing RANKL expression in osteoblasts and stromal cells
IL-7	Induces RANKL expression and disturbs the RANKL/OPG balance
GM-CSF	Dual role: stimulates osteoclastogenesis, or suppresses hematopoietic osteoclast precursors
IL-11	Induces the formation of osteoclast-like multinucleated cells
IL-8	Stimulates osteoclastogenesis and bone destruction in metastatic bone diseases

Osteoblastic metastases	
ET-1	Suppresses osteoblast apoptosis and promotes tumor cell adhesion via E-cadherin augmentation
DKK-1	Converts osteolytic metastasis to osteoblastic metastasis
PTHrP	Participates in the bone remodeling process and facilitates tumor cell proliferation, adhesion and survival
MMPs matrix metallopeptidases, *CXCR4* C-X-C chemokine receptor type 4, *TF* Thomsen–Friedenreich, *COX-2* cyclooxygenase-2, *TGF-β* transforming growth factor beta, *IGF* insulin-like growth factor, *miRNA* microRNA, *ATX* autotaxin, *RANL* receptor activator of nuclear factor kappa-B ligand, *PTHrP* parathyroid hormone-related protein, *OPG* osteoprotegerin, *CaSR* calcium-sensing receptor, *TNF* tumor necrosis factor, *GM-CSF* granulocyte-macrophage colony-stimulating factor, *ET-1* endothelin-1, *Dkk-1* Dickkopf-1	

However, the metastatic disease is still incurable, with a high mortality rate, and it causes severe morbidities in patients, reducing their quality of life. Bone pain is the most common symptom, to which pathological fractures, hypercalcemia, spinal cord compression and physical weakness can be added, collectively identified as Skeletal-Related Events (SRE)[50,60,61,62].

Current treatments aim to limit the tumor growth and to alleviate pain[63] and other symptoms, in order to improve the life of patients. Local treatments (radiotherapy and orthopedic surgery) are used in combination with systemic treatments, as combined chemotherapy and hormone therapy. In addition, against the common collateral effect of bone loss, new drugs have been recently introduced as anti-resorptive treatments (Table 3), including c-Src inhibitors (Dasatinib), bisphosphonates (zoledronic acid) and anti-RANKL antibody (Denosumab), which act through inhibition of the osteoclast's formation and activity[53,64]. However, due to the fact that some of those drugs can give some side effects over time such as hypocalcemia and osteonecrosis of the jaw, the research for new targets and new effective treatments is still ongoing.

Table 3. Descriptive table with inhibitors of bone resorption used for the treatment of bone metastases (adapted from D'Oronzo et al, 2019[53]).

Drug class	**Mechanism of action**	**Indication for BM treatment**
BPs	N-BPs: ↓ mevalonate pathway, essential for osteoclast activity and survival Non-N-BPs: ↑ osteoclast apoptosis	Treatment of BM and SRE prevention in MM, BC, CRPC and other solid tumors (if clinically indicated)
Denosumab	Anti-RANKL mAb: ↓ osteoclast differentiation and activity	Treatment of BM and SRE prevention in BC, CRPC and other solid tumors (if clinically indicated). Recently approved by FDA in MM setting

c-Src inhibitors	↓ RANKL-induced osteoclast differentiation	No indications
mTOR inhibitors	↓ osteoclast differentiation and activity ↑ osteoclast apoptosis	Everolimus approved in association with exemestane in advanced HR + HER2-BC with bone-prevalent disease; BPs or Denosumab to be associated
Proteasome inhibitors	↓ osteoclastogenesis ↑ osteoblast differentiation ↑ synthesis of collagen and BMP	Bortezomib and Carfilzomib + BPs (in association, or not, with cht, IMiDs and steroids) approved in MM
Abiraterone acetate	↓ osteoclastogenesis and osteoclast activity ↑ osteoblast differentiation ↑ bone matrix deposition anti-tumor effect	Treatment of BM and SRE prevention in CRPC
Acronyms: BM: bone metastases; BPs: bisphosphonates; N-BPs: nitrogen-containing BPs; non-N-BPs: non-nitrogen-containing BPs; MM: multiple myeloma; BC: breast cancer; CRPC: castration-resistant prostate cancer; receptor activator of nuclear factor-κB ligand; mAb: monoclonal antibody; SRE: skeletal related events; FDA: food and drug administration; mTOR: mammalian target of rapamycin; cht: chemotherapy; IMiDs: immunomodulatory drugs.		

1.4 Extracellular vesicles (EVs)

Intercellular communication is an important biological process, characteristic of multicellular organisms. It can be mediated through direct interaction between cells (juxtracrine) or the secretion of soluble molecules, such as growth factors, hormones and cytokines, in response to physiological or pathological changes.

In recent decades, an additional intercellular communication system has emerged, which involves the transfer of Extracellular Vesicles (EVs)[65,66].

Classification and molecular composition

EVs are complex membranous structures surrounded by a phospholipid bilayer, released by a variety of cells into the extracellular space and divided into different subgroups (Figure 7), based on their size and biogenesis: exosomes (30-100 nm of diameter) released by exocytosis; microvesicles, or shedding vesicles (100-1000 nm of diameter), formed by budding of the plasma membrane; and apoptotic bodies (1000-5000 nm), generally considered as a separate class[67].

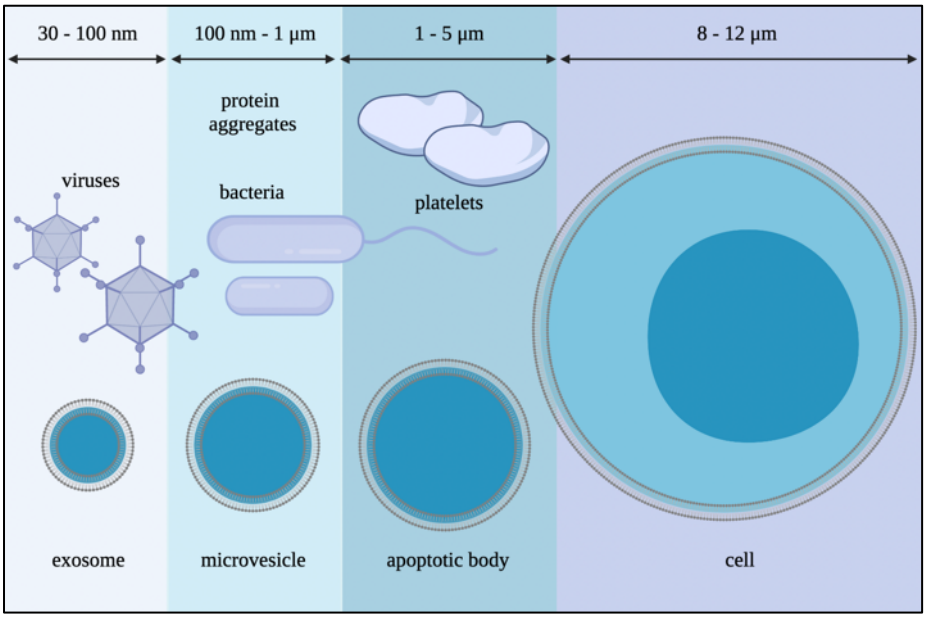

Figure 7. **Different classes of extracellular vesicles.** Exosomes are the smallest, similar in size to viruses, while microvesicles overlap in size with bacteria and protein aggregates. Both apoptotic bodies and platelets, on the other hand, fall in the size range of 1000-5000 nm. (*Source: adapted from György et al., 2011*[67]*, created in BioRender.com*).

Biochemically, their cargo consists of lipids (ceramides and sphingomyelin), nucleic acids (DNA, mRNA, microRNAs and siRNA) and different types of proteins involved in transport and fusion with the membrane [GTPase, Rab, Soluble N-ethylmaleimide-sensitive-factor Attachment protein Receptor (SNAREs) and Annexin], belonging to the family of integrins, tetraspanins (CD9, CD63, CD81, CD82) and heat shock proteins (Hsp90, Hsp70), involved in the biogenesis of multivesicular bodies [Alix and Tumor susceptibility gene 101 (TSG101)] and associated with lipid rafts (phospholipase C, D and aldolase)[68,69]. They are surrounded by a membrane relatively enriched in phosphatidylserine, cholesterol, ceramide and sphingomyelin, glycolipids and free fatty acids, at the expense of phosphatidylcholine and phosphatidylethanolamine[70].

Exosomes

Exosomes are small vesicles with a diameter between 30 and 100 nm, generated within the endosomal compartment and released by exocytosis mainly by B lymphocytes, dendritic cells and other cell types, such as cytotoxic T cells, platelets, mast cells, neurons, Schwann cells, oligodendrocytes, intestinal epithelium and tumor cells[71,72].

The mechanism of exosome formation is one of the most studied, indeed. Exosomes are constitutively formed as intraluminal vesicles (ILVs), generated within the lumen of

multivesicular bodies (MVBs) through invagination of the endosomal membrane, which can follow two distinct ways: fuse with lysosomes for the degradation of their contents or fuse with the plasma membrane, releasing vesicles in the form of exosomes in the extracellular space (Figure 8)[65,73,74]. The biogenesis of MVBs and the accumulation and sorting of molecules into ILVs are driven by the endosomal-sorting complex required for transport (ESCRT), a complex molecular machinery consisting of four main protein complexes (ESCRT-0, -I, -II and -III) and associated to RAS proteins. Interestingly, recent studies showed that the depletion of specific ESCRT-family proteins can alter the rate of exosomes released by cells and their cargo[75]. However, an alternative pathway mediating exosome formation and loading in an ESCRT-independent manner was recently discovered. It seems to involve lipids (neutral sphingomyelinases) and tetraspanins within the endosomal membrane[76,77].

Exosomes morphology changes according to the detection methodologies used: by transmission electron microscopy (TEM) and scanning electron microscope (SEM) they appear biconcave or cup-like shaped, that is thought to reflect a collapse of the dehydrate vesicles during samples preparation and fixation; while, for example, through cryo-electron microscopy (cryo-EM) and atomic-force microscopy (AFM) they show a perfectly round morphology[78].

Microvescicles

Microvescicles (MVs) or microparticles were first described by Chargaff and colleagues in 1946 in plasma, as pro-coagulant factors derived from platelets[79]. For a long time, they were considered to be merely cellular debris, unneeded fragments generated following the turnover of the plasma membrane or resulting from cell damage mediated by apoptosis.

Nowadays, MVs are recognized as regulatory structures originating by direct outward budding from the cellular plasma membrane (Figure 8), with a diameter between 100 and 1000 nm. They are mainly produced by platelets, immune cells, endothelial cells and tumor cells (as tumor-derived microvesicles, TMVs, or oncosomes)[66]. Their formation seems to involve changes in the lipid composition across the membrane bilayer, in Ca^{2+} levels and in the cytoskeleton (actin filaments and microtubules) of the donor cells, as well as associated proteins (kinesin and myosin), and proteins involved in vesicular trafficking (GTPase Rab) and fusion mechanisms (SNAREs proteins).

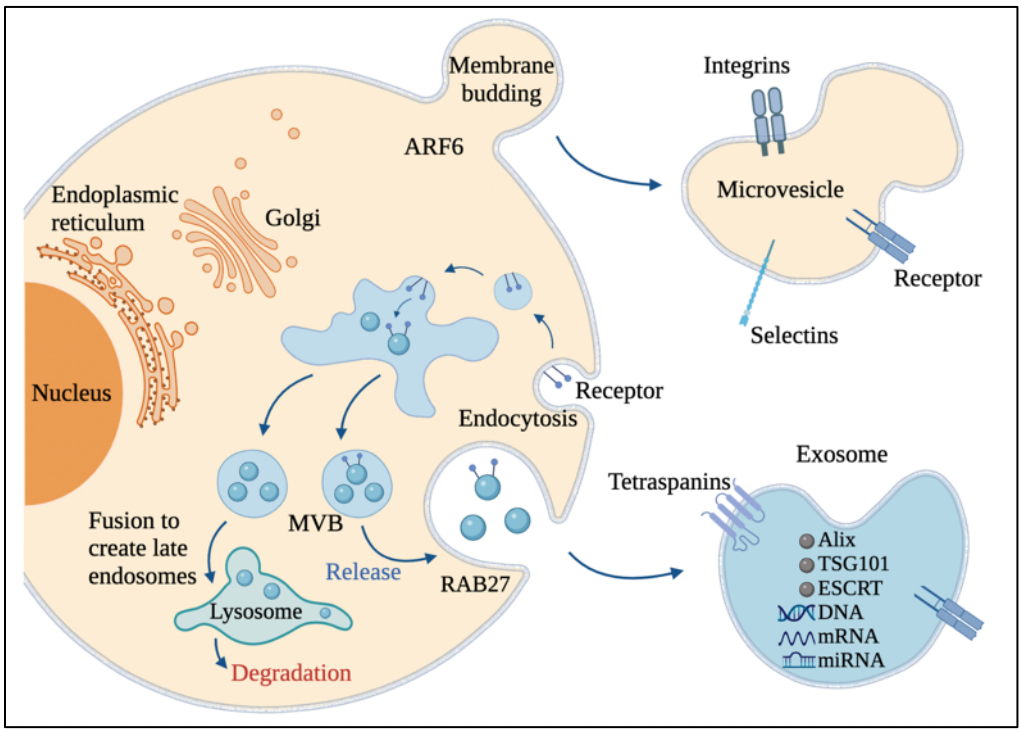

Figure 8. Extracellular vesicles (EVs) biogenesis and secretion. Schematic representation of production and cellular release of EVs into the extracellular space. Microvesicles are generated by outward budding of the plasma membrane. Exosomes are formed as ILVs generated by the inward budding of endosomal membrane and are released by the fusion of MVBs with the plasma membrane. Apoptotic bodies are formed during programmed cell death. EVs shuttle a heterogenous cargo, principally consisting of proteins, lipids and nucleis acids (*Source: adapted from Shao et al., 2018*[78]*, created in BioRender.com*).

Release and biological functions of EVs

Generally, it has been found that the release of EVs increases under cellular stimulation, especially by second messengers such as Ca^{2+} and protein kinase C (PKC)[80]. Upon release, EVs can interact with target cells in several ways: through activation of specific receptors and stimulation of signaling pathways; fusing directly with the plasma membrane, transferring membrane receptors and delivering their cargo, or being internalized by endocytosis[81,82]. A further step forward in the biology of EVs has been the evidence that EVs shuttle both mRNA and miRNA which in turn can be incorporated into recipient cells, regulating post-transcriptional gene expression and causing transient or persistent phenotypic changes[83]. Recently, EVs RNA sequencing has shown that they also contain long non-coding RNA, transfer RNA, ribosomal RNA, and a wide variety of small non-coding RNA species, including repeated sequences, piwi-interacting RNA and siRNA. Therefore, several biological functions have been attributed to all EVs subtypes, recognized as an

important means of communication, aimed at the shuttle of various signal molecules between nearby and distant cells, as well as playing a crucial role as mediators of many physiological and pathological processes, such as coagulation, inflammation and tumorigenesis[84].

Isolation and characterization of EVs

Although purification methods that allow to discriminate completely between the two main types of vesicles are still not completely available, EVs with heterogeneous characteristics have so far been isolated from cell culture serum-free medium, as well as from various biological fluids (blood, sperm, urine, saliva, ascites, amniotic and cerebrospinal fluids).

To date, several groups of EVs isolation techniques have been developed, among which the differential ultracentrifugation-based, size-based, immunoaffinity capture-based, exosome precipitation by polyethylene glycol (PEG), and microfluidics-based techniques can be distinguished.

In this regard, differential ultracentrifugation protocols are commonly used, such as a low-speed centrifugation (to remove dead cells or cellular debris) followed by high-speed ultracentrifugation (to isolate vesicles). Another ultracentrifugation method is the density gradient centrifugation, of which there are two different types employed in research settings: the isopycnic and the rate-zonal centrifugation. Between the size-based isolation methods, instead, one of the most popular and fast is ultrafiltration, followed by sequential filtration, size exclusion chromatography (SEC), and the recently developed flow field-flow fractionation (FFFF) and hydrostatic filtration dialysis (HFD)[73], based on nanoparticles' density and hydrodynamic properties,. The study of the protein composition of EVs and their characterization allowed the development of immunoaffinity capture-based techniques, such as microplate-based enzyme-linked immunosorbent assay (ELISA) and the more sensitive magneto-immunoprecipitation. Lastly, microfluidic technologies, such as the acoustic nanofilter, and easy commercial kits for exosome isolation, such as ExoChip, have also been developed in recent years, allowing to integrate immunoaffinity capture system with a microfluidic chip for the isolation of specific EVs subtypes[85,86].

However, high-speed ultracentrifugation is the most widely employed technique in research settings, which currently remains the gold standard for EVs isolation, especially from conditioned cell culture media. Despite some drawbacks of the technique, when

combined with sucrose-gradient ultracentrifugation it seems to purify better the EVs and clear them from protein complexes and other contaminants, which could be co-isolated with EVs[81]. Furthermore, researchers dealing with complex biological fluid tend to use a combination of different isolation and purification approaches[87].

A useful technique for single EVs detection and characterization in an heterogeneous preparation, determining the size distribution, phenotype and cellular origin, is flow cytometry, despite some limitations in analyzing particles below 500 nm and a tendency to underestimate their actual number[78].

Once isolated, EVs can also be characterized by other methods, such as Western Blot, mass spectrometry and imaging techniques. They can be analyzed in dimension and structure also by microscopy-based methods (TEM, SEM, cryo-EM), despite the fact that these techniques require essential procedures, such as fixation and dehydration, which could be responsible for artifacts, thus influencing their morphology. Recently, new methods have been proposed to determine both size and concentration of vesicles directly in suspension, including Atomic Force Microscopy (AFM), Dynamic Light Scattering (DLS) and Nanoparticles Tracking Analysis (NTA)[74]. Furthermore, the advancement of new techniques and the improvement of the most common ones seem to try to solve a problem that should not be underestimated, such as the possibility that the isolation methodology may influence the molecular composition and functionality of the EVs[67,88]. Therefore, the processes of isolation, characterization, and purification of EVs need to be better standardized to make sure their application.

Clinical applications and therapeutic potential of EVs

Recent scientific advances in the field, focused especially on EVs molecular cargo, are pushing towards their identification as biomarker resources for the diagnosis and prognosis of some pathologies, including cancer. Since they are found in circulating body fluids, EVs are good candidates to be exploited in the field of minimally- or non-invasive liquid biopsy, not only for obtaining a simpler and early diagnosis, but also to monitor and potentially predict disease progression, any patients' relapse or response to therapy[89,90].

Moreover, as biological carriers of bioactive materials, EVs have been recently used, directly after purification or after being modified in order to have targeting ligands on their surface or to deliver drugs, as therapeutic agents with multiple uses, such as in cancer therapy[91], vaccination[92] and immune modulation[93]. In this regard, the therapeutic potential

of EVs is mainly due to their biological characteristics, such as high biocompatibility, stability, specific cell targeting, transport of genetical and molecular information related to the cell of origin, and low immunogenicity.

Some of the mentioned therapeutic applications are still under investigation or involved in ongoing clinical trials, as there are still some limitations and technical issues to be addressed when considering the use of EVs in clinical practice, such as high costs and time involved, half-life, samples heterogeneity, and lack of standardization method for their isolation for large scale production[94].

1.5 EVs and bone cancer

In recent years, many investigations have been conducted to understand the role of EVs in the pathogenesis and progression of cancer, becoming a "hot topic" in the field[95].

Generally, in the tumor microenvironment it has been observed that both malignant, resident and stromal cells, including fibroblasts, endothelial cells, bone-marrow mesenchymal stem cells and immune cells, can communicate each other via EVs, which are able to mediate several cancer-related processes, contributing to tumor growth, invasion and metastatic spread[96,97,98]. Accordingly, tumor-secreted EVs can transfer a huge variety of bioactive and tumor-supportive molecules to target cells, such as oncoproteins, oncogenic mRNAs, miRNAs and pro-EMT factors (TGF-β, HIF1α, Notch1). This allows them to modulate gene expression, intracellular signaling cascades and phenotypic changes within recipient cells (i.e. fibroblasts reprogramming into Cancer Associated Fibroblasts, CAFs), triggering multiple pathological processes in the surrounding microenvironment, such as ECM remodeling and pre-metastatic niche formation, enhanced angiogenesis, immunosuppression, transfer of chemoresistance and tumor cells dormancy, a quiescent state in which cancer cells do not proliferate[99,100,90].

In particular, over the past few years there was a growing interest in studying the role of EVs in bone biology and associated cancer disease, in both primary bone tumors and metastases. In this regard, different interactions have been identified between tumor-derived EVs and bone cells, taking part to the vicious cycle and favoring cancer development and progression[98,101,102].

So far, it has been seen that primary bone tumor-derived EVs, in particular from osteosarcoma, can target and alter the surrounding bone microenvironment and its cellular components, including osteoclasts, macrophages, endothelial cells and MSCs. This is made

possible by EV-mediated transport of mi-RNA (miR-148a, miR-25-3-p, miR-21-5p), mRNAs and proteins (TGF-β, MMPs, VEGF and RANKL)[103] able to promote inflammatory responses, angiogenesis, osteoclast-mediated bone resorption, as well as to increase tumor cells proliferation and invasiveness (Table 4), leading non-aggressive tumor cells towards a pro-metastatic reprogramming for lung colonization[104,105,106].

Table 4: List of molecular educators, cell targets and effects of EVs isolated from primary bone tumors (*adapted from Cappariello and Rucci, 2019*[106]).

Tumor	Educator	Target cell	Effect
Osteosarcoma	TGF beta	MSCs	Increase of IL-6 production
Ewing sarcoma	CD99	Autologous	Increase of miR-34a Inhibition of NFκB
Fibrosarcoma	Rab27a	Autologous	Induction of chemotaxis
Osteosarcoma	uPA	Lung	Pro-metastatic
Fibrosarcoma	MT1-MMP	Extracellular matrix	Activation of MMP2 Degradation of type 1 collagen and gelatine
Osteosarcoma	MMP1/MMP13	Lung	Increase of aggressiveness
Osteosarcoma	RANKL	Osteoclasts	Increase of osteoclastogenesis
Osteosarcoma	miR-148a	Unspecified	Increase of aggressiveness
Osteosarcoma	miR-25-3-p	Unspecified	Increase of aggressiveness

However, research is still ongoing regarding the role of EVs in bone metastases. It is known that the favorable bone microenvironment retrieves metastasized tumor cells escaped from primary sites, which release EVs and educate resident and stromal cells to facilitate their invasion, growth, survival and proliferation towards the formation and remodeling of pre-metastatic niches and promoting angiogenesis and inflammation, important allies of bone metastatic progression[96]. In addition, tumor EVs are also able to affect the release of vesicles by stromal cells, which in turn can promote cancer-related events, such as dormancy of tumor cells and transfer of drug resistance. These events were demonstrated especially in the development of breast cancer induced-bone metastases, where a dormant phenotype was found to be acquired by cancer cells, due to the release of exosomes containing miR-222/233 and miR-23b by bone marrow-derived mesenchymal stem cells [107,97]. Furthermore, among

other pro-metastatic functions exerted by breast cancer-derived EVs, the inhibition of T-cells proliferation and of the cytotoxic activity of Natural Killer (NK) cells has been identified, giving the aggressive tumor cells the ability to escape the immune response[95,108]. Moreover, recent papers have reported that EVs from prostate cancer cells, after invading the bone, impair osteoclast differentiation[109] and stimulate osteoblast differentiation[110,111] and activity[112] by shuttling different miRNAs (miR-940 and miR-141-3p, respectively), thus promoting the development of osteosclerotic metastasis[106,113].

Due to the actual available data on their role in the tumorigenic process and to the fact that their cargo reflects the state and type of the cancer cell of origin, EVs have recently been studied as diagnostic or prognostic serum biomarkers (liquid biopsy) and potential therapeutic tools against malignancies, including bone metastases[74,114].

Currently, scientists are working on general multiple therapeutic approaches, such as targeting the pathways and molecules involved in the biogenesis and release of tumor EVs (ceramides, integrins, ESCRT complex, Rab proteins) or in their uptake by recipient cells (Heparan Sulfate Proteoglycans, HSPGs), trying to reduce their effects on tumor growth and metastasis. Moreover, additional anti-cancer strategies recently rely on (i) the genetic engineering of donor cells in order to promote the production of EVs enriched in proteins, miRNAs or mRNAs of therapeutic interest, and on (ii) the use of exosomes isolated from cancer or bone cells as vehicles to deliver efficiently active drugs (i.e. chemotherapy drugs as doxorubicin) or nucleic acids (i.e. siRNAs and miRNAs for gene therapy), thanks to their characteristic properties of stability, biodistribution and selectivity for target cells[106]. In this regard, exosomes loading is usually performed via electroporation techniques or via their direct incubation with drugs or chemotherapy compounds[69].

However, further research is needed to fully understand the contribution of EVs in the onset and progression of bone malignancies, together with their potential use as therapeutic agents, in order to limit cancer development and improve bone health and life quality in cancer patients.

2. AIM AND OUTLINE OF THE WORK

Bone is a fertile soil for cancer dissemination. In physiologic conditions, the crosstalk between bone resident cells, in particular osteoblasts and osteoclasts, involves the release of EVs. Moreover, these cells can interact also with cancer cells through EVs, the latter of

which seem to play an important role as integral signaling vehicles in tumor development and progression.

To date, the molecular mechanisms of EV-mediated cell-to-cell communication in the bone tumor microenvironment and the specific role of EVs in the mechanism of tumor growth, both for primary and secondary bone malignancies, still need to be more elucidated. Moreover, EVs seem to represent an essential tool for studying the mechanisms underlying the "vicious" cycle among bone resident cells, vascular cells and tumor cells.

Therefore, my PhD project was aimed at understanding whether and how tumor-derived EVs may be directly involved in the pathophysiological regulation of the bone microenvironment, as well as in the onset and progression of bone tumors and metastasis, trying to expand what is currently known in this matter.

In particular, in **Chapter 2**, we conducted a study aimed at evaluating the effect of EVs deriving from a human breast cancer cell line (MDA-MB-231) on bone cells, in order to find out more on the role of EVs in bone metastasis. In **Chapter 3,** instead, we analyzed the effect of EVs derived from a human osteosarcoma cell line (MNNG/HOS), a primary bone tumor, on cells of the bone microenvironment, identifying key pro-tumoral factors and deregulation of physiological pathways. Lastly, in **Chapter 4** we have reported some conclusions drawn from the present PhD thesis, with the aim of discussing the possible impact of our work in the ongoing battle against cancer progression, taking into consideration future research directions.

3. REFERENCES

1. Nather, A. Ong, H. J. C. & Aziz, Z. Structure of Bone. *Bone Grafts and Bone Substitutes: Basic Science and Clinical Applications,* 3-17 (2005).
2. Adamo, S., De Felici, M., Dolfi, A., *et al.* Istologia di Monesi (2018).
3. Feng, X. Chemical and biochemical basis of cell-bone matrix interaction in health and disease. *Curr Chem Biol* **3**, 189-196 (2009).
4. Florencio-Silva, R., Sasso, G. R. da S., Sasso-Cerri, E., Simões, M. J. & Cerri., P. S. Biology of bone tissue: structure, function, and factors that influence bone cells. *Biomed Res Int* **2015**, 421746 (2015).
5. Capulli, M., Paone, R. & Rucci, N. Osteoblast and osteocyte: games without frontiers. *Arch Biochem Biophys* **561**, 3–12 (2014).
6. Harada, S. I. & Rodan, G. A. Control of osteoblast function and regulation of bone

mass. *Nature* **423**, 349–355 (2003).

7. Fakhry, M., Hamade, E., Badran, B., Buchet, R. & Magne, D. Molecular mechanisms of mesenchymal stem cell differentiation towards osteoblasts. *World J Stem Cells* **5**, 136-148 (2013).
8. Marie, P. J. Fibroblast growth factor signaling controlling bone formation: an update. *Gene* **498**, 1-4 (2012).
9. Yavropoulou, M. P. & Yovos, J. G. The role of the Wnt signaling pathway in osteoblast commitment and differentiation. *Hormones* **6**, 279-94 (2007).
10. Ducy, P., Zhang, R., Geoffroy, V., Ridall, A. L. & Karsenty, G. Osf2/Cbfa1: a transcriptional activator of osteoblast differentiation. *Cell* **89**, 747–754 (1997).
11. Nakashima, K. Zhou, X., Kunkel, G., *et al.* The novel zinc finger-containing transcription factor osterix is required for osteoblast differentiation and bone formation. *Cell* **108**, 17-29 (2002).
12. Cappariello, A., Ponzetti, M. & Rucci, N. The 'soft' side of the bone: unveiling its endocrine functions. *Horm Mol Biol Clin Investig* **28**, 5-20 (2016).
13. Jilka, R. L., Weinstein, R. S., Bellido, T., Parfitt, A. M. & Manolagas, S. C. Osteoblast programmed cell death (apoptosis): modulation by growth factors and cytokines. *J Bone Miner Res* **13**, 793–802 (1998).
14. Johannesdottir, F. & Bouxsein, M. L. Bone structure and biomechanics. *Encycl Endocr Dis* **4**, 19–30 (2018).
15. Suda, T., Takahashi, N., Udagawa, N., Jimi, E., Gillespie, M. T. & Martin, T. J. Modulation of osteoclast differentiation and function by the new members of the tumor necrosis factor receptor and ligand families. *Endocr Rev* **20**, 345-57 (1999).
16. Cappariello, A., Maurizi, A., Veeriah, V. & Teti, A. The great beauty of the osteoclast. *Arch Biochem Biophys* **558**, 70-8 (2014).
17. Owen, R. & Reilly, G. C. In vitro models of bone remodelling and associated disorders. *Front Bioeng Biotechnol* **6**, 1–22 (2018).
18. Compton, J. T. & Lee, F. Y. A review of osteocyte function and the emerging importance of sclerostin. *J Bone Joint Surg Am* **96**, 1659–68 (2014).
19. Bonewald, L. F. & Johnson, M. L. Osteocytes, mechanosensing and Wnt signaling. *Bone* **42**, 606-15 (2008).
20. Manolagas, S. C. & Parfitt, A. M. What old means to bone. *Trends Endocrinol Metab* **21**, 369–374 (2010).
21. Goldring, S. R. The osteocyte: key player in regulating bone turnover. *RMD Open* **1**,

1–4 (2015).

22. Teti, A. & Zallone, A. Do osteocytes contribute to bone mineral homeostasis? Osteocytic osteolysis revisited. *Bone* **44**, 11–16 (2008).
23. Bonewald, L. F. The amazing osteocyte. *J Bone Miner Res* **26**, 229–238 (2011).
24. Kalervo Väänänen, H. & Laitala-Leinonen, T. Osteoclast lineage and function. *Arch Biochem Biophys* **473**, 132-8 (2008).
25. Schachtner, H., Calaminus, S. D. J., Thomas, S. G. & Machesky, L. M. Podosomes in adhesion, migration, mechanosensing and matrix remodeling. *Cytoskeleton* **70**, 572–589 (2013).
26. Schlesinger, P. H., Blair, H. C., Teitelbaum, S. L. & Edwards, J. C. Characterization of the osteoclast ruffled border chloride channel and its role in bone resorption. *J Biol Chem* **272**, 18636-43 (1997).
27. Rousselle, A.-V. & Heymann, D. Osteoclastic acidification pathways during bone resorption. *Bone* **30**, 533-40 (2002).
28. Xu, F. & Teitelbaum, S. L. Osteoclasts: new insights. *Bone Res* **1**, 11–26 (2013).
29. Takayanagi, H., Kim, S., Koga, T., *et al.* Induction and activation of the transcription factor NFATc1 (NFAT2) integrate RANKL signaling in terminal differentiation of osteoclasts. *Dev Cell* **3**, 889–901 (2002).
30. Takayanagi, H. Osteoimmunology: shared mechanisms and crosstalk between the immune and bone systems. *Nat Rev Immunol* **7**, 292–304 (2007).
31. Pacifici, R. Estrogen, cytokines, and pathogenesis of postmenopausal osteoporosis. *J Bone Miner Res* **11**, 1043–1051 (2009).
32. Teitelbaum, S. L. Osteoclasts: what do they do and how do they do it? *Am J Pathol* **170**, 427–435 (2007).
33. Maurizi, A. & Rucci, N. The osteoclast in bone metastasis: player and target. *Cancers (Basel).* **10**, 218 (2018).
34. Robling, A. G., Castillo, A. B. & Turner, C. H. Biomechanical and molecular regulation of bone remodeling. *Annu Rev Biomed Eng* **8**, 455–498 (2006).
35. Hill, P. A. Bone remodelling. *Br J Orthod* **25**, 101-7 (1998).
36. Hadjidakis, D. J. & Androulakis, I. I. Bone Remodeling. *Ann N Y Acad Sci* **1092**, 385-96 (2006).
37. Kapinas, K. & Delany, A. M. MicroRNA biogenesis and regulation of bone remodeling. *Arthritis Res Ther* **13**, 1–11 (2011).
38. Ibrahim, T., Mercatali, L. & Amadori, D. Bone and cancer: the osteoncology. *Clin*

Cases Miner Bone Metab **10**, 121–123 (2013).

39. Gelderblom, H., Hogendoorn, P. C. W., Dijkstra, S. D., *et al.* The clinical approach towards chondrosarcoma. *Onchologist* **13**, 320-9 (2008).
40. Ewing, J. Diffuse endothelioma of bone. *Clin Orthop Relat Res* **185**, 2–5 (1984).
41. Tajima, S., Ohkubo, A., Yoshida, M., Koda, K. & Nameki, I. Ewing's sarcoma family of tumors of the maxillary sinus: a case report of multidisciplinary examination enabling prompt diagnosis. *Int J Clin Exp Pathol* **8**, 960–966 (2015).
42. Ottaviani, G. & Jaffe, N. The Epidemiology of osteosarcoma. *Cancer Treat Res* **152**, 3–13 (2009).
43. De Azevedo, J. W. V., De Medeiros Fernandes, T. A. A., Fernandes Jr, J. V., *et al.* Biology and pathogenesis of human osteosarcoma. *Oncol Lett* **19**, 1099–1116 (2020).
44. Rozeman, L. B., Cleton-Jansen, A. M. & Hogendoorn, P. C. W. Pathology of primary malignant bone and cartilage tumours. *Int Orthop* **30**, 437–444 (2006).
45. Ferguson, J. L. & Turner, S. P. Bone cancer: diagnosis and treatment principles. *Am Fam Physician* **98**, 205–213 (2018).
46. Zhang, Y. & Rosenberg, A. E. Bone-forming tumors. *Surg Pathol Clin* **10**, 513-535 (2017).
47. Paget S. The distribution of secondary growths in cancer of the breast. *Cancer Metastasis Rev* **133**, 571–573 (1889).
48. Steeg, P. S. Tumor metastasis: Mechanistic insights and clinical challenges. *Nat Med* **12**, 895–904 (2006).
49. Schmid-Alliana, A., Schmid-Antomarchi, H., Al-Sahlanee, R., Lagadec, P., Scimeca, J.-C. & Verron, E. Understanding the progression of bone metastases to identify novel therapeutic targets. *Int J Mol Sci* **19**, 148 (2018).
50. Coleman, R. E. Clinical features of metastatic bone disease and risk of skeletal morbidity. *Clin Cancer Res* **12**, 6243–6250 (2006).
51. Guise, T. A., Mundy, G. R. & Calcium, B. Cancer and Bone. *Endocr Rev* **19**, 18–54 (1998).
52. Coleman, R. E., Croucher, P. I., Padhani, A. R., *et al.* Bone metastases. *Nat Rev Dis Prim* **6**, 1–28 (2020).
53. D'Oronzo, S., Coleman, R., Brown, J. & Silvestris, F. Metastatic bone disease: pathogenesis and therapeutic options: up-date on bone metastasis management. *J Bone Oncol* **15**, 004-4 (2018).
54. Ren, G., Esposito, M. & Kang, Y. Bone metastasis and the metastatic niche. *J Mol*

Med **93**, 1203–1212 (2015).

55. Rucci, N. & Teti, A. Osteomimicry: how the seed grows in the soil. *Calcif Tissue Int* **102**, 131–140 (2018).
56. Virk, M. S. & Lieberman, J. R. Tumor metastasis to bone. *Arthritis Res Ther* **9**, 1–10 (2007).
57. Ibrahim, T., Flamini, E., Mercatali, L., Sacanna, E., Serra, P. & Amadori, D. Pathogenesis of osteoblastic bone metastases from prostate cancer. *Cancer* **116**, 1406–1418 (2010).
58. Wang, M., Xia, F., Wei, Y. & Wei, X. Molecular mechanisms and clinical management of cancer bone metastasis. *Bone Res* **8**, 30 (2020).
59. Ponzetti, M. & Rucci, N. Switching homes: how cancer moves to bone. *Int J Mol Sci* **21**, 1–25 (2020).
60. Cui, Y. X., Evans, B. A. J. & Jiang, W. G. New roles of osteocytes in proliferation, migration and invasion of breast and prostate cancer cells. *Anticancer Res* **36**, 1193–1202 (2016).
61. Macedo, F., Ladeira, K., Pinho, F., *et al.* Bone metastases: an overview. *Oncol Rev* **11**, 312 (2017).
62. Coleman, R. E. Bone cancer in 2011: prevention and treatment of bone metastases. *Nat Rev Clin Oncol* **9**, 76–78 (2012).
63. Aielli, F., Ponzetti, M. & Rucci, N. Bone metastasis pain, from the bench to the bedside. *Int J Mol Sci* **20**, (2019).
64. Ibrahim, T., Farolfi, A., Mercatali, L., Ricci, M. & Amadori, D. Metastatic bone disease in the era of bone-targeted therapy: clinical impact. *Tumori* **99**, 1–9 (2013).
65. Raposo, G. & Stoorvogel, W. Extracellular vesicles: exosomes, microvesicles, and friends. *J Cell Bio* **200**, 373-83 (2013).
66. Van Niel, G., D'Angelo, G. & Raposo, G. Shedding light on the cell biology of extracellular vesicles. *Nat Rev Mol Cell Biol* **19**, 213–228 (2018).
67. György, B., Szabò, T. G., Pàsztòi, M., *et al.* Membrane vesicles, current state-of-the-art: emerging role of extracellular vesicles. *Cell Mol Life Sci* **68**, 2667–2688 (2011).
68. Mir, B. & Goettsch, C. Extracellular vesicles as delivery vehicles of specific cellular cargo. *Cells* **9**, 1601 (2020).
69. Xu, R., Rai, A., Chen, M., Suwakulsiri, W., Greening, D. W. & Simpson, R. J. Extracellular vesicles in cancer-implications for future improvements in cancer care. *Nat Rev Clin Oncol* **15**, 617–638 (2018).

70. Haraszti, R. A., Didiot, M.-C., Sapp, E., *et al.* High-resolution proteomic and lipidomic analysis of exosomes and microvesicles from different cell sources. *J Extracell Vesicles* **5**, 32570 (2016).
71. Simons, M. & Raposo, G. Exosomes-vesicular carriers for intercellular communication. *Curr Opin Cell Biol* **21**, 575–581 (2009).
72. Raposo, G., Nijman, H. W., Stoorvogel, W., *et al.* B Lymphocytes Secrete Antigen-presentingVesicles. *J Exp Med* **183**, 1161-72 (1996).
73. Yánez-Mo, M., Siljander, P. R.-M., Andreu, Z., *et al.* Biological properties of extracellular vesicles and their physiological functions. *J Extracell Vesicles* **4**, 27066 (2015).
74. Minciacchi, V. R., Freeman, M. R. & Di Vizio, D. Extracellular vesicles in cancer: exosomes, microvesicles and the emerging role of large oncosomes. *Semin Cell Dev Biol* **40**, 41–51 (2015).
75. Colombo, M., Moita, C., Van Niel, G., *et al.* Analysis of ESCRT functions in exosome biogenesis, composition and secretion highlights the heterogeneity of extracellular vesicles. *J Cell Sci* **126**, 5553–65 (2013).
76. Zhang, Y., Liu, Y., Liu, H. & Ho Tang, W. Exosomes: biogenesis, biologic function and clinical potential. *Cell Biosci* **9**, 19 (2019).
77. Catalano, M. & O'Driscoll, L. Inhibiting extracellular vesicles formation and release: a review of EV inhibitors. *J Extracell Vesicles* **9**, 1703244 (2019).
78. Shao, H., Im, H., Castro, C. M., Breakefield, X., Weissleder, R. & Lee, H. New technologies for analysis of extracellular vesicles. *Chem Rev* **118**, 1917–1950 (2018).
79. Chargaff, E. & West, R. The biological significance of the thromboplastic protein of blood. *J Biol Chem* **166**, 189-97 (1946).
80. Ratajczak, J., Wysoczynski, M., Hayek, F., Janowska-Wieczorek, A. & Ratajczak, M. Z. Membrane-derived microvesicles: important and underappreciated mediators of cell-to-cell communication. *Leukemia* **20**, 1487–1495 (2006).
81. Vlassov, A. V., Magdaleno, S., Setterquist, R. & Conrad, R. Exosomes: current knowledge of their composition, biological functions, and diagnostic and therapeutic potentials. *Biochim Biophys Acta* **1820**, 940–948 (2012).
82. Mathieu, M., Martin-Jaular, L., Lavieu, G. & Théry, C. Specificities of secretion and uptake of exosomes and other extracellular vesicles for cell-to-cell communication. *Nat Cell Biol* **21**, 9–17 (2019).
83. Valadi, H., Ekström, K., Bossios, A., Sjöstrand, M., Lee, J. J. & Lötvall, J. O.

Exosome-mediated transfer of mRNAs and microRNAs is a novel mechanism of genetic exchange between cells. *Nat Cell Biol* **9**, 654–659 (2007).

84. Cocucci, E., Racchetti, G. & Meldolesi, J. Shedding microvesicles: artefacts no more. *Trends Cell Biol* **19**, 43–51 (2009).
85. Doyle, L. & Wang, M. Overview of extracellular vesicles, their origin, composition, purpose, and methods for exosome isolation and analysis. *Cells* **8**, 727 (2019).
86. Li, P., Kaslan, M., Lee, S. H., Yao, J. & Gao, Z. Progress in exosome isolation techniques. *Theranostics* **7**, 789 (2017).
87. Ludwig, N., Whiteside, T. L. & Reichert, T. E. Challenges in exosome isolation and analysis in health and disease. *Int J Mol Sci* **20**, 4684 (2019).
88. Hartjes, T. A., Mytnyk, S., Jenster, G. W., Van Steijn, V. & Van Royen, M. E. Extracellular vesicle quantification and characterization: common methods and emerging approaches. *Bioeng* **6**, 7 (2019).
89. Cappariello, A. & Rucci, N. Extracellular vesicles in bone tumors: how to seed in the surroundings molecular information for malignant transformation and progression. *Front Oncol* **11**, 3654 (2021).
90. Xavier, C. P. R., Caires, H. R., Barbosa, M. A. G., Bergantim, R., Guimarães, J. E. & Vasconcelos, M. H. The role of extracellular vesicles in the hallmarks of cancer and drug resistance. *Cells* **9**, 1–34 (2020).
91. Kamerkar, S., LeBleu, V. S., Sugimoto, H., *et al.* Exosomes facilitate therapeutic targeting of oncogenic KRAS in pancreatic cancer. *Nature* **546**, 498–503 (2017).
92. György, B., Hung, M. E., Breakefield, X. O. & Leonard, J. N. Therapeutic applications of extracellular vesicles: clinical promise and open questions. *Annu Rev Pharmacol Toxicol* **55**, 439–464 (2015).
93. Whiteside, T. L. Exosomes and tumor-mediated immune suppression. *J Clin Invest* **126**, 1216–1223 (2016).
94. Herrmann, I. K., Wood, M. J. A. & Fuhrmann, G. Extracellular vesicles as a next-generation drug delivery platform. *Nat Nanotechnol* **16**, 748–759 (2021).
95. Lucchetti, D., Tenore, C. R., Colella, F. & Sgambato, A. Extracellular vesicles and cancer: a focus on metabolism, cytokines, and immunity. *Cancers* **12**, 171 (2020).
96. Morhayim, J., Baroncelli, M. & Van Leeuwen, J. P. Extracellular vesicles: specialized bone messengers. *Arch Biochem Biophys* **561**, 38–45 (2014).
97. Becker, A., Thakur, B. K., Weiss, J. M., Kim, H. S., Peinado, H. & Lyden, D. Extracellular vesicles in cancer: cell-to-cell mediators of metastasis. *Cancer Cell* **30**,

836–848 (2016).

98. Zhao, H., Achreja, A., Iessi, E., *et al.* The key role of extracellular vesicles in the metastatic process. *Biochim Biophys Acta Rev Cancer* **1869**, 64–77 (2018).
99. Jurj, A., Zanoaga, O., Braicu, C., *et al.* A comprehensive picture of extracellular vesicles and their contents. Molecular transfer to cancer cells. *Cancers (Basel)* **12**, 298 (2020).
100. Kalluri, R. The biology and function of exosomes in cancer. *J Clin Invest* **126**, 1208–1215 (2016).
101. Kahlert, C. & Kalluri, R. Exosomes in tumor microenvironment influence cancer progression and metastasis. *J Mol Med* **91**, 431–437 (2013).
102. Atay, S. & Godwin, A. K. Tumor-derived exosomes: a message delivery system for tumor progression. *Commun Integr Biol* **7**, 1–6 (2014).
103. Garimella, R., Washington, L., Isaacson, J., *et al.* Extracellular membrane vesicles derived from 143b osteosarcoma cells contain pro-osteoclastogenic cargo: a novel communication mechanism in osteosarcoma bone microenvironment. *Transl Oncol* **7**, 331–340 (2014).
104. Chicón-Bosch, M. & Tirado, O. M. Exosomes in bone sarcomas: key players in metastasis. *Cells* **9**, 241 (2020).
105. Li, Q., Huang, Q. P., Wang, Y. L. & Huang, Q. S. Extracellular vesicle-mediated bone metabolism in the bone microenvironment. *J Bone Miner Metab* **36**, 1-11 (2018).
106. Cappariello, A. & Rucci, N. Tumour-derived extracellular vesicles (EVs): a dangerous 'message in a bottle' for bone. *Int J Mol Sci* **20**, 4805 (2019).
107. Bliss, S. A., Sinha, G., Sandiford, O. A., *et al.* Mesenchymal stem cell-derived exosomes stimulate cycling quiescence and early breast cancer dormancy in bone marrow. *Cancer Res* **76**, 5832–5844 (2016).
108. Green, T. M., Alpaugh, M. L., Barsky, S. H., Rappa, G. & Lorico, A. Breast cancer-derived extracellular vesicles: characterization and contribution to the metastatic phenotype. *Biomed Res Int* **2015**, 634865 (2015).
109. Karlsson, T., Lundholm, M., Widmark, A. & Persson, E. Tumor cell-derived exosomes from the prostate cancer cell line TRAMP-C1 impair osteoclast formation and differentiation. *PLoS One* **11**, e0166284 (2016).
110. Hashimoto, K., Ochi, H., Sunamura, S., *et al.* Cancer-secreted hsa-miR-940 induces an osteoblastic phenotype in the bone metastatic microenvironment via targeting ARHGAP1 and FAM134A. *Proc Natl Acad Sci U S A* **115**, 2204–2209 (2018).

111. Itoh, T., Ito, Y., Ohtsuki, Y., *et al.* Microvesicles released from hormone-refractory prostate cancer cells facilitate mouse pre-osteoblast differentiation. *J Mol Histol* **43**, 509–515 (2012).
112. Ye, Y., Li, S.-L., Ma, Y.-Y., *et al.* Exosomal miR-141-3p regulates osteoblast activity to promote the osteoblastic metastasis of prostate cancer. *Oncotarget* **8**, 94834–94849 (2017).
113. Vlaeminck-Guillem, V.-G. Extracellular vesicles in prostate cancer carcinogenesis, diagnosis, and management. *Front Oncol* **8**, 222 (2018).
114. Zhang, X., Yuan, X., Shi, H., Wu , L., Qian, H. & Xu, W. Exosomes in cancer: small particle, big player. *J Hematol Oncol* **8**, 1–13 (2015).

Chapter 2

"Extracellular vesicles from osteotropic breast cancer cells affect bone resident cells"

Published in JBMR, 2020. Vol. 35 (2): Pag. 396-412 (doi: 10.1002/jbmr.3891).
Loftus, A., Cappariello, A., George, C., **Ucci, A.**, Shefferd, K., Green, A., Paone, R., Ponzetti, M., Delle Monache, S., Muraca, M., Teti, A., Rucci, N.

1. ABSTRACT

Extracellular vesicles (EVs) are emerging as mediators of a range of pathological processes, including cancer. However, their role in bone metastases has been poorly explored. We investigated EV-mediated effects of human osteotropic breast cancer cells (MDA-MB-231) on bone resident cells and endothelial cells. Pretreatment of osteoblasts with conditioned medium (CM) of MDA-MB-231 (MDA) cells promoted pro-osteoclastogenic and pro-angiogenic effects by osteoblast EVs (OB-EVs), as well as an increase of RANKL-positive OB-EVs. Moreover, when treating osteoblasts with MDA-EVs, we observed a reduction of their number, metabolic activity, and alkaline phosphatase (Alp) activity. MDA-EVs also reduced transcription of *Cyclin D1* and of the osteoblast-differentiating genes, while enhancing the expression of the pro-osteoclastogenic factors *Rankl*, *Lipocalin 2* (*Lcn2*), *Il1b* and *Il6*. Interestingly, a cytokine array on CM from osteoblasts treated with MDA-EVs showed an increase of the cytokines C-C motif Chemokine Ligand (CCL)-3, CXC motif Chemokine Ligand (CXCL)-2, Regenerating islet-derived protein 3 Gamma (Reg3G), and Vascular Endothelial Growth Factor (VEGF), while OPG and WNT1 Inducible Signaling Pathway Protein 1 (WISP1) were downregulated. MDA-EVs contained mRNAs of genes involved in bone metabolism, as well as cytokines, including Platelet-derived growth factor (PDGF)-BB, CCL3, CCL27, VEGF, and Angiopoietin 2. In line with this profile, MDA-EVs increased osteoclastogenesis and in vivo angiogenesis. Finally, intraperitoneal injection of MDA-EVs in mice revealed their ability to reach the bone microenvironment and be integrated by osteoblasts and osteoclasts. In conclusion, we showed a role for osteoblast-derived EVs and tumor cell-derived EVs in the deregulation of bone and endothelial cell physiology, thus fuelling the vicious cycle induced by bone tumors.

2. INTRODUCTION

Bone metastasis is a frequent complication of advanced breast cancer, with up to 70% incidence[1]. Although patients with bone metastases present with better prognosis than those with visceral metastases[2], they experience severe morbidity, due to bone pain, increased risk of fracture, and hypercalcemia, resulting in a poor quality of life[2]. Bone mass is maintained in the physiological range by the concerted action of two cell types: bone-depositing osteoblasts and bone-resorbing osteoclasts, in a series of tightly coordinated molecular events. Osteoblasts produce macrophage-colony stimulating factor (M-CSF) and receptor activator of NF-κB ligand (RANKL), which interact with the osteoclast-expressed receptors c-fms and RANK, respectively[3,4]. RANK activation results in generation of mature osteoclasts, which form acidified seals on the bone surface to dissolve the mineral matrix components and into which proteases are subsequently secreted to degrade the underlying organic matrix[5]. The resulting release of growth factors and cytokines from the bone matrix and from osteoclasts stimulates osteoblasts to depose new bone matrix, closing the bone remodeling cycle[5].

In metastatic breast cancer, the balance of bone remodeling is tilted toward a state of exacerbated bone destruction, whereby cancer cells secrete factors enhancing bone resorption and employ the subsequently released cytokines as stimuli for bone colonization[6]. Importantly, premetastatic cancer cells can establish bone lesions prior to metastasis, which suggests that a premetastatic niche is educated by breast cancer cells through mechanisms that are only partially known[7].

Extracellular vesicles (EVs) are becoming established mediators of metastasis in a wide range of cancers[8]. They are membrane-derived carriers of biomolecules exchanged by cells *in vivo*, which allow direct transfer of functionally active proteins and nucleic acids to modify the behavior of recipient cells[9]. Despite the growing evidence that EVs are central to the metastatic process, their role in bone metastases is still an open field, which deserves to be more investigated. Results obtained so far demonstrate the ability of tumor-derived EVs to influence behavior of bone cells toward a microenvironment favoring their homing. Indeed, recent evidence indicates that exosomes isolated from metastatic breast cancer cells shuttle different protein cargoes, allowing breast cancer cell dissemination towards specific metastatic sites[10]. These exosomes are enriched in proteins related to migration and invasion, compared to exosomes isolated from non-metastatic breast cancer cells[10]. Consistent with the ability of tumor cell–derived EVs to drive organotropism, Hashimoto and colleagues[11] found that hsa-miR-940 shuttled by prostate cancer EVs enhances human mesenchymal stem

cell differentiation toward an osteoblastic phenotype by targeting *ARHGAP1* and *FAM134A*. Moreover, forced expression of hsa-miR-940 in the osteotropic breast cancer cell line MDA-MB-231 reverts its propensity to induce osteolytic lesions toward an osteosclerotic phenotype[11], thus indicating that the phenotype of bone metastases is also influenced by EV-shuttled miRNAs. Finally, a recent paper showed that exosomal release of L-plastin by MDA-MB-231 cells promotes their ability to induce osteolytic bone metastases in mouse models[12].

Our recent studies have demonstrated extensive EV-mediated crosstalk between cells in the bone microenvironment[13]. Given these findings and the accumulating evidence showing that cancer cells can communicate with distant cells via EVs, we evaluated the impact of breast cancer cell-derived EVs on cells resident in the bone microenvironment, finding a broad spectrum of pro-angiogenic, pro-osteoclastogenic, and anti-osteoblastogenic molecular events. Our data suggest a crucial role for breast cancer cell–derived EVs in the premetastatic dysregulation of bone remodeling.

3. MATERIALS AND METHODS

3.1 Materials

Dulbecco's modified minimum essential medium (DMEM), fetal bovine serum (FBS), penicillin, streptomycin, and trypsin were from GIBCO (Uxbridge, UK). Sterile plasticware was from Falcon Becton-Dickinson (Oxford, UK). The RNeasy Mini™ kit (cat#74104), the RT^2 First Strand Kit (cat# 330401), and the Human Osteoporosis RT^2 Profiler PCR Array (cat# PAHS-170Z) were purchased from Qiagen (Düsseldorf, Germany). SYBR Green reagent was from Bioline (Memphis, TN, USA). DreamTaq Green master mix was from Thermo Scientific (Waltham, MA, USA). The mouse XL Cytokine Array Kit (cat#ARY028) was purchased from R&D Systems (Minneapolis, MN, USA). The human cytokine array kit (cat# ab193656) was from Abcam (Cambridge, UK). The Matrigel Matrix (cat#354262) was purchased by Corning (Corning, NY, USA), the in vitro Angiogenesis Assay (cat#ECM625) was from Millipore (Burlington, MA, USA). Anti-CD31 antibody (cat#ab124432), human recombinant VEGF (hrVEGF; cat#ab9751), and the human cytokine antibody array membrane (cat#ab193656) were from Abcam (Cambridge, UK), anti-Annexin II antibody (cat#71-3400), and anti-RANKL antibody (cat#sc-7628) were from Santa Cruz Biotechnology Inc. (Santa Cruz, CA, USA). The phycoerythrin (PE)-

conjugated anti-RANKL antibody (cat#560295) and the endothelial cell growth supplement (ECGS; cat#354006) were purchased from BD Biosciences (Franklin Lakes, NJ, USA). The allophycocyanin (APC) anti-human Cd254 (RANKL; cat#347508) was from Biolegend (San Diego, CA, USA). The chemiluminescence reagent kit was purchased from Thermo Scientific (Waltham, MA, USA). The 3-(4,5-dimethylthiazol-2-yl)-2,5-diphenyltetrazolium (MTT) bromide reduction assay and all other reagents were from Sigma-Aldrich (St. Louis, MO, USA).

3.2 Animals

All procedures involving animals and their care were conducted in conformity with national and international laws and policies (European Economic Community Council Directive 86/609, OJ L 358, 1, December 12, 1987; Italian Legislative Decree 4.03.2014 n.26, *Gazzetta Ufficiale della Repubblica Italiana* no. 61, March 4, 2014; National Institutes of Health guide for the Care and Use of Laboratory Animals, National Institutes of Health Publication no. 85-23, 1985) and the Animal Research: Reporting of in vivo Experiments (ARRIVE) guidelines. Animal procedures also received institutional approval by the Italian Ministry of Health (Approval N. 173/2016-PR). Mice used for osteoblasts and osteoclast primary cultures were male and female, 7-day-old WT CD1; mice for the Matrigel plug assay experiments were female, 8-week-old WT CD1; mice for the in vivo tissue targeting were 7-day-old male and female WT of the CD1 strain. Mice were purchased by Charles River (Milan, Italy) and were housed in the animal facility of the University of L'Aquila, Italy, at the following conditions: temperature: 20°C to 24°C; humidity: 60% ± 5%; dark/light cycle: 12/12 hours. They had access to food and water ad libitum and were fed a standard diet (Mucedola, Milan, Italy. Code: 4RF21) composed of 60.8% carbohydrates, 21% proteins, 3.45% fat, 6.8% fibers, 7.95% trace elements, and 12% humidity. For these studies, mice were littermates and were randomized via software. Analyses were conducted in double-blind. No adverse events were observed during the course of the experiment.

3.3 Cell lines

The human breast cancer cell lines MDA-MB-231 (MDA) and MCF7, and the mouse breast cancer cell line 4T1 were from the American Tissue Culture Collection (ATCC, Rockville, MD, USA) and were cultured in DMEM supplemented with 10% FBS, 100IU/mL penicillin, 100µg/mL streptomycin, and 2mM L-glutamine.

Human umbilical vein endothelial cells (HUVECs) were purchased from Lonza (Basel, Switzerland) and cultured in endothelial cell growth medium (EGM)-2. All cells were grown in a humidified 95% air/5% CO_2 incubator at 37°C.

3.4 Osteoblast primary cultures

Calvariae from 7-day-old CD1 mice were explanted, cleaned free of soft tissues, and digested three times with 1 mg/mL *Clostridium histolyticum* type IV collagenase and 0.25% trypsin, for 20 min at 37°C, with gentle agitation. Cells from the second and third digestions were plated following centrifugation at 200*g* for 7 min and grown in DMEM plus 10% FBS. At confluence, cells were trypsinized and plated according to the experimental protocol. The purity of the culture was evaluated by the transcriptional expression of the osteoblast markers alkaline phosphatase (Alp), Runt-related transcription factor 2 (Runx2), type I collagen, and osteocalcin and by the cytochemical evaluation of Alp activity[14].

3.5 Alp activity assay

Primary mouse osteoblasts were fixed in 4% buffered paraformaldehyde (PFA) for 15 min and washed twice with PBS. Alp activity was evaluated cytochemically by the Sigma-Aldrich kit n.85 L1, according to the manufacturer's instruction.

3.6 Osteoclast primary cultures

Femurs and tibiae of 7-day-old CD1 mice were cleaned of soft tissues, chopped with a sterile blade, and bone marrow was collected, diluted 1:1 in Hank's balanced salt solution (HBSS), layered over Histopaque 1077 solution, and centrifuged at 400*g* for 30 min. Buffy coat cells were collected, washed twice with HBSS, resuspended in DMEM plus 10% FBS, and plated in culture dishes at a density of 1×10^6 cells/cm^2. After 3 hours, cultures were washed with PBS to remove nonadherent cells and maintained for 7 days in the same medium supplemented with 50 ng/mL human recombinant M-CSF (hrM-CSF) and 120 ng/mL hrRANKL as positive control or with M-CSF alone as negative control[15]. According to the experimental protocol, cells were also treated with EVs derived from osteoblasts and tumor cells for the timeframe of the culture, with or without suboptimal concentrations of hrRANKL (30 ng/mL). Committed precursors and mature osteoclasts were

detected by histochemical staining of tartrate resistant acid phosphatase (TRAcP) activity (Sigma-Aldrich; cat#387A) according to the manufacturer's instructions.

3.7 EVs isolation

EVs were isolated according to Cappariello and colleagues[13] and Kruger and colleagues[16]. Briefly, upon reaching 70% to 80% confluence, cells (osteoblasts, MDA-MB-231, MCF7, and 4T1) were washed in PBS and starved in serum-free DMEM to prevent contamination from FBS EVs. After 24 hours, culture medium was harvested and sequentially centrifuged at 300*g*, 4°C for 5 min to eliminate dead cells and at 5000*g*, 4°C for 25 min to eliminate membrane debris. Then, the supernatant was transferred to a Beckman L7-65 ultracentrifuge in a Beckman SW41-Ti rotor (both from Beckman Coulter, Indianapolis, IN, USA) and centrifuged at 100,000*g*, at 9°C for 70 min. Ultracentrifugation supernatant was discarded while the pellet, containing EVs, was resuspended in PBS, TRIzol, or radioimmunoprecipitation assay (RIPA) buffer according to the experimental protocol.

3.8 Transmission electron microscopy

Five microliters (5 µL) of EVs isolated from MDA-MB-231 CM (12 mL collected from one 175-cm^2 flask, cell density = 6.5×10^4 cells/cm^2) were put onto Formvar-coated grids and allowed to air dry. Grids were washed in PBS and fixed in 1% glutaraldehyde for 5 min. Samples were washed in distilled water and contrasted with 4% uranyl-oxalate solution for 5 min. Finally, grids were air dried for 10 min and observed under a Philips CM 30 transmission electron microscopy (TEM) at 80 kV.

3.9 RT^2 profiler real-time PCR array

RNA was isolated from MDA-MB-231 (MDA) cells and from MDA-derived EV (MDA-EVs) using the RNeasy Mini™ kit (Qiagen), then RNA was reverse-transcribed employing the RT^2 First Strand Kit (Qiagen), according to the manufacturer's instructions. For MDA-EVs, 0.1 µg of RNA were subjected to a preamplification step using the PreAmp cDNA Synthesis Primer mix (Qiagen). cDNAs (from MDA cells or from MDA-EVs) were then mixed with RT^2 SYBR Green qPCR master mix and dispensed in the wells of the human osteoporosis PCR array. Wells were subjected to real-time PCR (Stratagene MX 3000),

following the manufacturer's instructions. Array data were automatically analyzed by the dedicated software, RT^2 Profiler PCR Array data analysis template v3.2 (SuperArray Bioscience, Frederick, MD, USA). Briefly, after the fluorescence signal was collected and the threshold cycles (Cts) calculated by the machine, the average Ct of all genes was used as normalizer (ie, set to 1) to evaluate which genes were more or less expressed compared to the average Ct and plotted as such.

3.10 Comparative real-time RT-PCR

RNA was extracted using TRIzol reagent, then 1 µg of RNA was reverse-transcribed into cDNA using the Moloney Murine Leukemia Virus (M-MLV) reverse transcriptase and subjected to real-time RT-PCR (Roche LightCycler 96; Roche Diagnostics, Mannheim, Germany) using the primer pairs and amplification conditions described in Table 1. All reactions were carried out using a SYBR green–based master mix containing ROX as reference dye. Data analyses were carried out via dedicated software (Roche LightCycler 96 software).

Table 1: Mouse primer sequences (5' to 3'). Primers were designed to anneal at 60°C.

Gene ID	Forward primer	Reverse primer
Alp	CCAGCAGGTTTCTCTCTTGG	CTGGGAGTCTCATCCTGAGC
Bglap	TTCTGCTCACTCTGCTGACC	GGGACTGAGGCTCCAAGGT
Col1a1	GTCCCTCTGGAAATGCTGGAC	GACCGGGAAGACCGACCA
Cyclin D1	TCAAGTGTGACCCGGACTG	ATGTCCACATCTCGCACGTC
Gapdh	TGGCAAAGTGGAGATTGTTGC	AAGATGGTGATGGGCTTCCCG
Il1b	GCCCATCCTCTGTGACTCAT	AGGCCACAGGTATTTTGTCG
Il6	GAGGATACCACTCCCAACAGACC	AAGTGCATCATCGTTGTTCATACA
Lcn2	CCAGTTCGCCATGGTATTTT	CACACTCACCACCCATTCAG
M-csf	GAATCTTCACTGGGCACTAAC	CTTCCCATATGTCTCCTTTCC
Nos2	CACCTTGGAGTTGACCCAGT	ACCACTCGTAGTTGGGATGC
Opg	AAAGCACCCTGTAGAAAACA	CCGTTTTATCCTCTCTACACTC
Osx	GACTGTGACGAGTTGGCTCA	GCCCACAGATTCCTCTTCTG
Rankl	CCAAGATCTCTAACATGACG	CACCATCAGCTGAAGATAGT
Runx2	AACCCACGGCCCTCCCTGAACTCT	ACTGGCGGGGTGTAGGTAAAGGTG

Vegf	CCCTTCCTCATCTTCCCTTC	CACCGATCTGGGAGAGAGAG

3.11 Endpoint RT-PCR

RNA was extracted using TRIzol reagent, then 1 µg was reverse transcribed using the M-MLV reverse transcriptase and subjected to PCR amplification with the DreamTaq Green master mix using the primer pairs and amplification conditions described in Table 2. The PCR products were run in a 2% agarose gel with ethidium bromide.

Table 2: Human primer sequences (5' to 3'). Primers were designed to anneal at 60°C.

Gene ID	Forward primer	Reverse primer
BGLAP	GACTGTGACGAGTTGGCTCA	GCCCACAGATTCCTCTTCTG
CD40	GAGATCAATTTTCCCGACGA	GCTCCAGGGTGAAGTGAGAG
CLCN7	GATTTCAAGATCTTCGAGTACTTCC	TGATTCGAAACATGGTCAGC
GAPDH	CCATCTTCCAGGAGCGAGAT	CAGTGATGGCATGGACTGTG
ITGB3	GACAAGGGCTCTGGAGACAG	ACTGGTGAGCTTTCGCATCT
TGFB1	CCTGCCACAGATCCCCTATT	GTGACCTCCTTGGCGTAGTAG
VEGF	CTACCTCCACCATGCCAAGT	GCAGTAGCTGCGCTGATAGA

3.12 Cytokine profiler arrays

For the mouse cytokine array profiling, 1 mL of conditioned medium (CM) collected from osteoblasts untreated or treated with MDA-EVs (isolated from 12 mL of CM collected from one 175-cm^2 flask, cell density = 6.5 × 10^4/cm^2) were added to the nitrocellulose membranes of the Mouse XL Cytokine Array Kit, which includes 111 capture antibodies printed in duplicate. The membranes were incubated overnight at 4°C, washed three times, and incubated with the detection antibody cocktail for 1 hour at room temperature (RT). After three washes, a 30-min incubation with the streptavidin–horseradish peroxidase (HRP) solution was performed, then membranes were washed and incubated with the Chemi Reagent mix for the detection of the positive spots by chemiluminescence. For data analysis, an Image J software (NIH, Bethesda, MD, USA; https://imagej.nih.gov/ij/) extension (protein array analysis) was used. The intensity of each spot was determined by densitometry, and the average background subtracted. The normalization of the protein was

performed by calculating the ratio between the signal intensity of the protein of interest and of the housekeeping proteins. For cytokine array analysis on EVs, the procedure was similar, but EVs from 10 mL of medium were collected and lysed. Images were subjected to a despeckle algorithm (the ImageJ standard one) and contrast enhancement to improve the quality of the image.

For the human cytokine array, MDA-EVs were isolated from 120 mL of CM collected from ten 175-cm^2 flasks (cell density = 6.5 × $10^4/cm^2$), then the pellet was resuspended in RIPA buffer containing phosphatase and protease inhibitors and lysed by three cycles of freezing and thawing. Fifteen micrograms (15 µg) of proteins extracted from MDA-EVs were added to two separate nitrocellulose membranes after blocking. The membranes contain a total of 120 capture antibodies printed in duplicate, plus positive and negative controls/blanks. Membranes were incubated overnight at 4°C with the protein lysates, washed, and incubated for 2 hours at RT with the biotinylated detection antibody mix. After washing, membranes were incubated overnight at 4°C with streptavidin-HRP, washed, and the bioluminescence signal was detected as described for the human cytokine array. After background subtraction, signal was normalized by the average signal intensity, to evaluate which proteins were expressed above or below average.

3.13 Western blot analysis

For protein extraction, PC3 cells, MDA cells, MDA-EVs, MCF7 cells and MCF7-EVs were lysed in RIPA buffer containing phosphatase and protease inhibitors. Fifty micrograms (50 µg) of protein cell lysates and 5 µg of EV protein lysate were resolved by 12% SDS-PAGE under reducing conditions and transferred to nitrocellulose membranes. Blots were probed with the primary antibody for 1 hour at RT, washed, and incubated with the appropriate HRP-conjugated secondary antibody for 1 hour at RT. Protein bands were visualized with the chemiluminescence reaction kit, according to the manufacturer's instructions and imaged on a Bio-Rad ChemiDoc XR Gel Imaging System (Bio-Rad Laboratories, Hercules, CA, USA).

3.14 Fluorescence-activated cell sorting of EVS

Fluorescence-activated cell sorting (FACS) analysis was performed on both osteoblast-EVs and MDA-EVs. Mouse primary osteoblasts were starved overnight in DMEM and treated with DMEM as control or with MDA- or 4T1-CM for 48 hours.

Osteoblasts and MDA cells were washed three times with PBS, incubated for 24 hours with DMEM without serum before CM collection (12 mL, collected from one 175-cm^2 flask; cell density 3.5 × $10^4/cm^2$ for osteoblasts and 6.5 × $10^4/cm^2$ for MDA cells) and EV isolation. EV pellets were loaded with the membrane-permeant dye 5-chloro-methyl-fluorescein diacetate (CMFDA) for 30 min at 37°C, then incubated with a PE-conjugated anti-RANKL antibody (for OB-EVs) or with APC-conjugated RANKL antibody (for MDA-EVs) for 30 min at 4°C and analyzed on a BD FACSCANTO II (BD Biosciences). Nano-fluorescent standard particles (Spherotech, Lake Forest, IL, USA; cat#NFPPS-52-4 K) were used to set a dimensional gate up to 1 μm.

3.15 Cell viability assay

Viability of HUVECs and osteoblasts was assessed by the 3-(4,5-dimethylthiazol-2-yl)-2,5-diphenyltetrazolium (MTT) bromide reduction assay following the manufacturer's protocol.

3.16 *In vitro* tube formation assay

The tube formation assay was carried out according to Kubota and colleagues[17]. Fifteen-well μ-Slides (Ibidi GmbH, Gräfelfing, Germany) were coated with Matrigel and allowed to solidify at 37°C for 30 min. HUVECs (1.5 × 10^4/well) were then plated and incubated with medium containing the following EVs: osteoblast EVs (OB-EVs), osteoblast EVs pretreated with MDA-CM (MDA_{CM}-OB-EVs), MDA-EVs, OB-EVs pretreated with MCF7-CM ($MCF7_{CM}$-OB-EVs), and MCF7-EVs. Each type of EV was isolated from 6 mL of CM collected from one Petri dish (75 cm^2; cell density: 3.5 × $10^4/cm^2$ for osteoblasts, 6.5 × $10^4/cm^2$ for MDA, and 4.5 × $10^4/cm^2$ for MCF7). As positive control, HUVECs were treated with EGM-2. After 16 hours tube formation was inspected under an inverted light microscope at 40X magnification. Pictures were taken, and the percentage of branching points/area was evaluated (Branching Index) using an Image J extension system for angiogenesis analysis.

3.17 Matrigel plug assay

Eight-week-old male CD1 mice were subcutaneously injected in the ventral area with 0.4 mL Matrigel Matrix with 0.1 mL PBS (Neg.Ctrl), 0.1 mL of EVs isolated from MDA-

CM (MDA-EVs), osteoblasts (OB-EVs), osteoblasts pretreated with MDA-CM (MDA_{CM}-OB-EVs), or with 0.1 mL containing endothelial cell growth supplement (ECGS) plus 150 ng/mL hrVEGF as positive control. Each mouse was injected with the number of EVs isolated from 12 mL of CM collected from one 175-cm^2 flask (cell density: $3.5 \times 10^4/cm^2$ for osteoblasts and $6.5 \times 10^4/cm^2$ for MDA). After 10 days mice were euthanized, and the plugs were removed, fixed in 4% buffered PFA, and processed for histology. No adverse effect or signs of animal distress were noted before euthanasia.

Excised Matrigel plugs were fixed in 4% buffered PFA and embedded in paraffin. Sections were cut using a Leica RM2125RT microtome (Leica, Wetzlar, Germany). Slide-mounted tissue sections (4 µm thick) were deparaffinized in xylene, hydrated serially in 100%, 95%, and 80% ethanol, and stained with hematoxylin/eosin. For immunohistochemistry, sections were deparaffinized, incubated with 0.07M citrate buffer (pH 6), 15 min at 98°C for antigen retrieval and treated with 3% H_2O_2 in PBS for 1 hour to quench endogenous peroxidases. Sections were then incubated with anti-CD31 primary antibody for 1 hour at RT. Finally, after washing, antibody binding was visualized using the Dako En-Vision Detection kit (DAKO, Carpinteria, CA, USA) and 3,3′-Diaminobenzidine (DAB).

3.18 Mouse calvariae organ culture

Ex vivo osteolysis was assessed in mouse calvarial bone using an adaptation of the mouse calvarial organ culture[18]. Seven-day-old mice were euthanized, then calvariae were explanted, cleaned of soft tissues, and cultured in exosome-free DMEM plus FBS 10% with or without MDA-EVs isolated from 12 mL of CM collected from one 175-cm^2 flask (cell density $6.5 \times 10^4/cm^2$, number of mice/group = 3). Organ cultures were maintained for 7 days, the medium was changed twice, then calvariae were fixed in 4% buffered PFA and subjected to microCT (µCT) analysis.

3.19 µCT analysis

Calvaria images were acquired in a SkyScan 1174 µCT scanner (Bruker, Kontich, Belgium), with a pixel size of 6.7 µm (X-ray voltage 50 kV). The Skyscan Nrecon software was used for image reconstruction by employing a modified Feldkamp algorithm. Beam hardening correction and Fourier transform–based ring artifact reduction were applied to the

reconstructed images. Area of the bone fraction was calculated for the calvarial bone–selected regions of interest using Image J software.

3.20 *In vivo* tumor EV targeting to bone

Seven-day-old CD1 mice were injected i.p. with PKH26-labeled EVs isolated from MDA-CM (12 mL collected from one 175-cm^2 flask, cell density $6.5 \times 10^4/cm^2$ injected to each mouse) or with PBS as control (number of mice/group = 9). After 5 hours, mice were euthanized, and bones were explanted and processed for lipidic extraction in chloroform-methanol (2:1 vol/vol) and 0.125% wt/vol SDS. The lipophilic PKH26 fluorescence intensity was measured by spectrofluorometry (excitation wavelength 550 nm; emission wavelength 567 nm) in the extracted lipid fraction.

Explanted femurs and tibiae were flushed out to harvest bone marrow (BM) cells, which were fixed in 4% buffered PFA and run on a FACS Melody (BD Biosciences). Cell population was verified for PKH26 content (PE laser channel). After analysis, the PE-positive population was harvested on polylysine-coated glass slides automatically by the instrument. Slides were then mounted with a slow-fade, DAPI-containing mounting medium and evaluated by epifluorescence (Axioscope; Carl Zeiss Microscopy GmbH, Jena, Germany).

Femurs were also fixed in 4% buffered PFA and decalcified in 10% EDTA for 10 days. After cryopreservation in sucrose, bones were cryoembedded in optimal cutting temperature (OCT) compound in liquid nitrogen–cooled isopentane and cut to obtain 7-µm cryosections, which were washed in PBS to remove OCT, mounted, and evaluated by confocal microscopy (Leica TCS SP5 II; Leica).

For TRAcP activity evaluation, similarly obtained slides were hydrated and imaged by conventional epifluorescence for PKH26 (tetramethylrhodamine [TRITC] filter). Then, slides were unmounted and processed for TRAcP activity by histochemistry, according to the manufacturer's instructions (Sigma Aldrich; cat#387A), mounted with DAPI, and imaged by light microscopy and epifluorescence, respectively. It should be noted that epifluorescence is not able to resolve single EVs in our experimental conditions, hence the diffused appearance of the signal in epifluorescence images.

4. RESULTS

4.1 Breast cancer–derived CM affects osteoblast differentiation

We first investigated the influence of the CM collected from the triple-negative and highly osteotropic human breast cancer cell line MDA-MB-231 (from now MDA) on osteoblasts. This treatment did not affect osteoblast metabolic activity evaluated by MTT test (Fig. 1A), although reducing their number, evaluated by crystal violet staining (Fig. 1B), as well as Alp activity (Fig. 1C), thus indicating the ability of MDA-CM to impair osteoblast differentiation. In agreement with these results, MDA-CM reduced *Cyclin D1* mRNA, as well as the transcription of genes related to osteoblast differentiation *Alp*, *Runt-related transcription factor* (*Runx*)*2*, *Osterix* (*Osx*), *Bglap*, the gene coding for the late osteoblast differentiation marker osteocalcin, and the osteoblast function marker *Collagen 1a1* (*Col1a1*), compared to untreated osteoblasts (Fig. 1D). Moreover, MDA-CM significantly increased mRNA expression of *Rankl*, whereas the Rankl decoy receptor *Osteoprotegerin* (*Opg*) and *M-csf* were not affected (Fig. 1E). Treatment with MDA-CM also increased the transcriptional expression of the inflammatory and osteoclastogenic cytokines *Interleukin* (*Il*)*1β* and *Il6*, and of *Lipocalin 2* (*Lcn2*), the latter known to have a pro-tumoral effect and to inhibit osteoblast differentiation[19,20] (Fig. 1F). Moreover, we found a significant increase of *Nitric oxide synthase 2* (*Nos2*) and a trend of increase of *Vascular endothelial growth factor* (*Vegf*) mRNAs in osteoblasts treated with MDA-CM (Fig. 1F). ELISA on osteoblast CM confirmed the increase of RANKL, IL6, and Lcn2, whereas a trend of increase in IL1β secretion was observed (Fig. 1G). Similar results were found in osteoblasts treated with CM harvested from the metastatic mouse breast cancer cell line 4T1 (Fig. 2A–D), thus indicating that the molecular players are likely conserved from mice to human.

Considering the prominent role of RANKL in bone physiopathology and starting from our previous results showing that osteoblasts release RANKL-positive EVs[13], we asked whether tumor cell CM could impact on this phenomenon. OB-EVs, isolated from untreated osteoblasts (Fig. 3A) or osteoblasts treated with MDA-CM and 4T1-CM, were subjected to FACS analysis, which revealed a significant increase of the percentage of RANKL-positive EVs compared to EVs from untreated osteoblasts (Fig. 3B,C).

Finally, we evaluated the effect of CM isolated from the less aggressive, epithelial-like, and estrogen receptor (ER)-positive human breast cancer cell line MCF7, finding no

effect on either cell viability or cell number (Fig. 4A,B), although a trend of reduction of Alp activity ($p = 0.06$) was observed compared to untreated osteoblasts (Fig. 4C). However, a significant decrease of mRNA expression of osteoblast differentiation genes (Fig. 4D) along with an increase of *Rankl* (Fig. 4E) and of inflammatory cytokines was observed in osteoblasts treated with MCF7-CM (Fig. 4F,G).

Taken together, this data shows the ability of tumor cell–released factors to influence the osteoblast transcriptional profile towards a less differentiated phenotype and to increase osteoblast production of pro-osteoclastogenic and inflammatory cytokines.

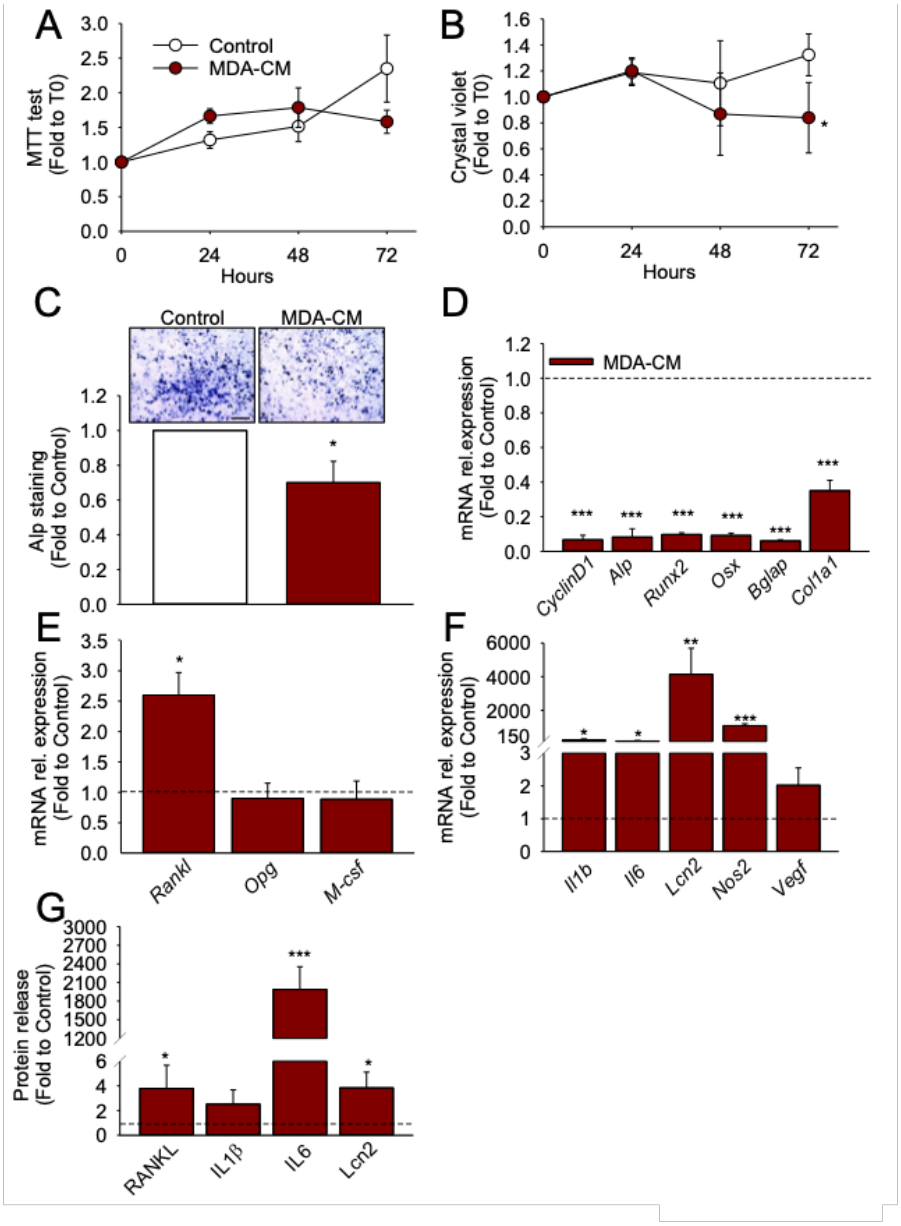

Figure 1: Effect of MDA-MB-231 conditioned medium on osteoblasts. Mouse primary osteoblasts were starved overnight in serum-free DMEM and treated with DMEM as control or with the conditioned medium collected from the human breast cancer cell line MDA-MB-231 (MDA-CM). (**A**) Cell metabolic activity evaluated by the MTT assay and (**B**) quantification of cell number by crystal violet staining at the times indicated in the abscissa. (**C**) Alkaline

phosphatase (Alp) activity evaluated by cytochemistry after 48 hours of treatment. (**D-F**) Transcriptional expression of (**D**) *Cyclin D1*, and of the osteoblast differentiating genes *Alp*, *Runt-related transcription factor 2* (*Runx2)*, *Osterix* (*Osx), Osteocalcin (Bglap)* and *Collagen 1a1* (*Col1a1).* Transcriptional expression of (**E**) the cytokines regulating osteoclastogenesis indicated in the abscissa and of (**F**) *Il1b*, *Il6*, *Lcn2*, *Nos2* and *Vegf* evaluated by real time RT-PCR. (**G**) ELISA assay to assess osteoblast release of RANKL, IL1β, IL6 and Lcn2. Data is the mean ± SD of 3 independent experiments (A,B: *P=0.04 *vs* Control, AUC; C-G: *P<0.05, **P<0.01 and ***P<0.001 *vs* Control, Student's *t*-test; dot line= control set at 1; Bar=500 µm).

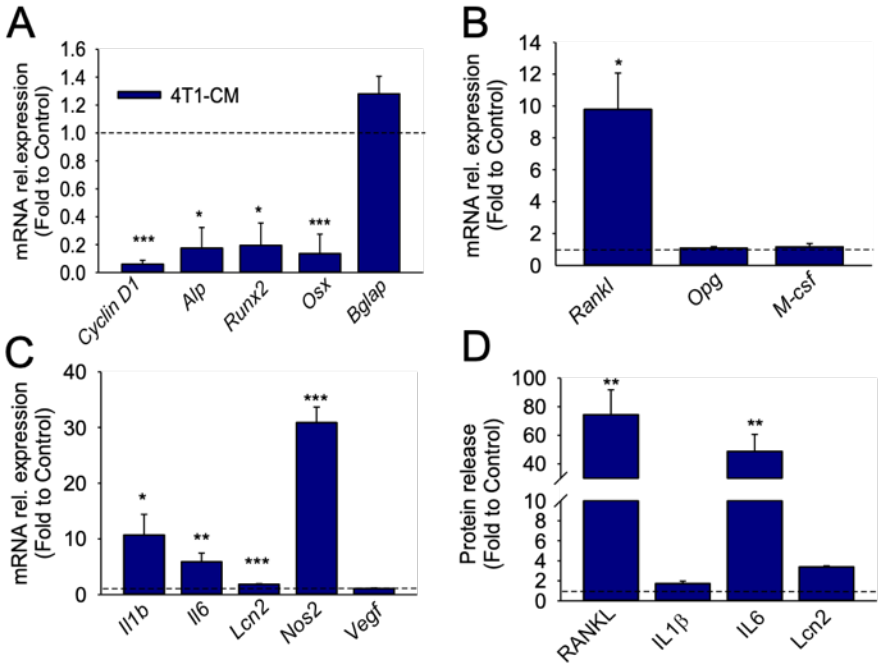

Figure 2: Effect of 4T1 conditioned medium on osteoblasts. Mouse primary osteoblasts were starved overnight in serum-free DMEM and treated with DMEM as control or with the conditioned medium collected from the mouse breast cancer cell line 4T1 (4T1-CM). After 48 hours RNA was extracted and subjected to real time RT-PCR to evaluate the expression of (**A**) Cyclin D1, and of the osteoblast differentiating genes Alp, Runx2, Osterix (Osx) and Osteocalcin (Bglap), (**B**) the cytokines regulating osteoclastogenesis indicated in the abscissa and of (**C**) Il1b, Il6, Lipocalin 2 (Lcn2), Nos2 and Vegf. (**D**) ELISA assay to assess osteoblast release of RANKL, IL1β, IL6 and Lcn2. Data is the mean ± SD of 3 independent experiments (*P<0.05, **P<0.01 and ***P<0.001 vs Control, Student's t-test; dot line= control set at 1).

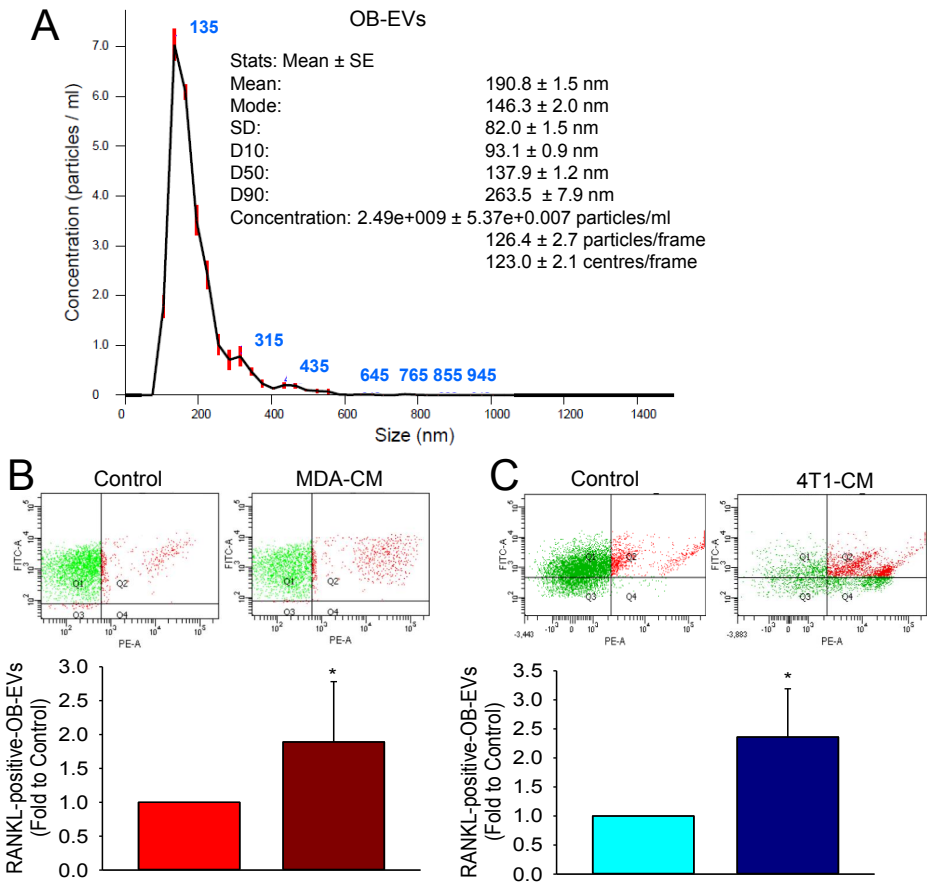

Figure 3: Effect of breast cancer conditioned medium on osteoblast release of RANKL positive EVs. (**A**) Size and concentration determination of osteoblast extracellular vesicles (OB-EVs, isolated from 12 ml of CM collected from one 175 cm^2 flask, cell density = $3.5x10^4$ cells/cm^2) by nanoparticle tracking analysis (NanoSight NS3000). Results are representative of 3 independent preparations of EVs. (**B,C**) Cytofluorimetric analysis of RANKL positive EVs released by osteoblasts untreated or pre-treated with (**B**) MDA-CM or (**C**) 4T1-CM. Data is the mean ± SD of 3 independent experiments (*P<0.05 vs Control, Student's t-test).

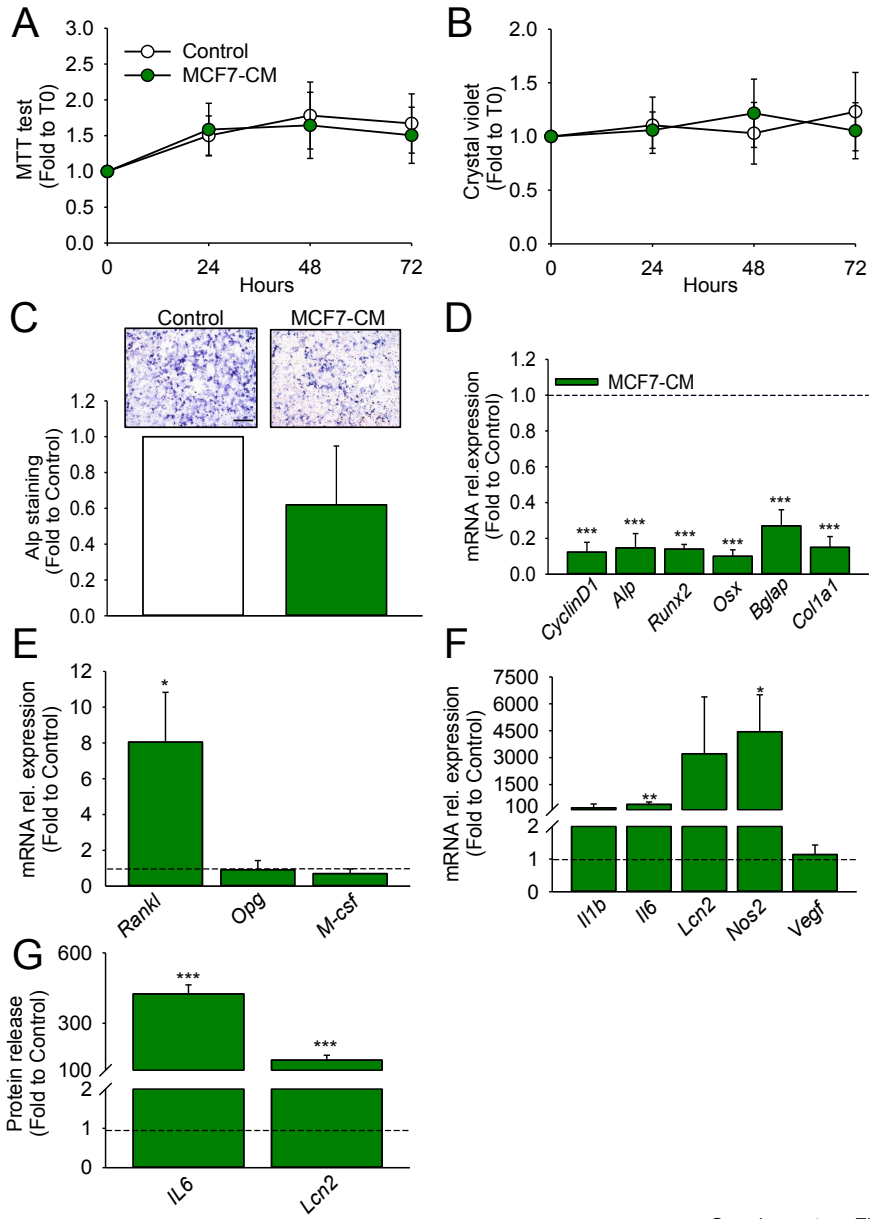

Figure 4: Effect of MCF7 conditioned medium on osteoblasts. Mouse primary osteoblasts were starved overnight in serum-free DMEM and treated with DMEM as control or with the conditioned medium collected from the human breast cancer cell line MCF7 (MCF7-CM). (**A**) Cell metabolic activity evaluated by the MTT assay and (**B**) quantification of cell number by crystal violet staining at the times indicated in the abscissa. (**C**) Alkaline phosphatase (Alp) activity evaluated after 48 hours. (**D-F**) Transcriptional expression of (**D**) *Cyclin D1*, and of the osteoblast differentiating genes *Alp*, *Runx2*, *Osterix* (*Osx), Osteocalcin (Bglap)* and *Collagen 1a1* (*Col1a1).* Transcriptional expression of (**E**) the cytokines regulating osteoclastogenesis indicated in the abscissa and of (**F**) *Il1b*, *Il6*, *Lcn2*, *Nos2* and *Vegf* evaluated by real time RT-PCR. (**G**) ELISA assay to assess osteoblast release of IL6 and Lcn2. Data is the mean ± SD of 3 independent experiments (*P<0.05, **P= 0.006 and ***P<0.001 *vs* Control, Student's *t*-test; dot line= control set at 1; Bar=500 µm).

4.2. Characterization of MDA-derived EVs

We next asked whether the alterations in osteoblast behavior were mediated by breast cancer cell–derived EVs. We isolated EVs from breast cancer cell CM after 24 hours of conditioning under starvation. Size and concentration determination were performed by

NanoSight (Salisbury, UK) (Fig. 5A); Western blot analysis on protein extracts revealed positivity for Annexin II, one of the markers of EVs[21] (Fig. 5B,C). The vesicular nature of the particles was confirmed by TEM, which showed membrane integrity and confirmed the expected EV size distribution of the MDA-EVs (Fig. 5D).

We then characterized the transcriptional profile of MDA-EVs to assess whether mRNAs involved in the regulation of bone metabolism were present. RNA from MDA-EVs was extracted, reverse transcribed, and subjected to the osteoporosis real-time array, which includes 84 genes involved in bone remodeling. Among these genes, seven met the quality controls and cutoffs determined by our analyses (Fig. 6A). We confirmed, by semiquantitative RT-PCR (Fig. 6B), that MDA-EVs shuttle mRNAs of key factors involved in osteoclast functions, such as *CLCN7*, encoding for the homodimeric chloride/proton antiporter ClC7, crucial for charge balance in the Howship lacuna, Integrin β_3 (*ITGB3*) and *CD40*, involved in osteoclast adhesion and preosteoclast fusion, respectively. Among the genes related to osteoblast functions, we found *COL1A1* and *BGLAP* (Fig. 6A,B). Transcriptional expression of *Transforming Growth Factor beta 1* (*TGFB1*) and *VEGF* were also found (Fig. 6A,B). This profile generally mirrors the transcriptional content of the cells (Fig. 5D and Fig. 6B); there are, however, some exceptions. An intriguing example is RANKL: although its expression is barely detectable in MDA cells, high levels of this mRNA were observed in MDA-EVs (Fig. 6B). However, Western blot on MDA-EVs did not show any positive signal for RANKL (Fig. 6C), whereas cytofluorometric analysis revealed a negligible percentage of RANKL-positive MDA-EVs (Fig. 6D).

Finally, to characterize the cytokine profile of MDA-EVs, they were subjected to molecular profiling by a human cytokine antibody array (Fig. 6E). CCL27 (alias CTACK), which is a positive regulator of breast cancer aggressiveness[22], was the most expressed cytokine. Among the well-expressed cytokines, there were some factors known to foster osteoclastogenesis, including IL8, Macrophage Inflammatory Protein (MIP)-1α (*alias* CCL3) and MIP-1β (*alias* CCL4), and Platelet-Derived Growth Factor (PDGF)-BB[23-26], whereas, among the angiogenic cytokines, we observed Angiopoietin 2 and VEGF. Of note, MIP-1α and PDGF-BB are also negative regulators of osteoblast differentiation[27,28].

Another cytokine expressed by MDA-EVs was oncostatin M (OSM), which potentiates preintravasation of breast cancer cells and their ability to metastasize the lung and the bone[29, 30].

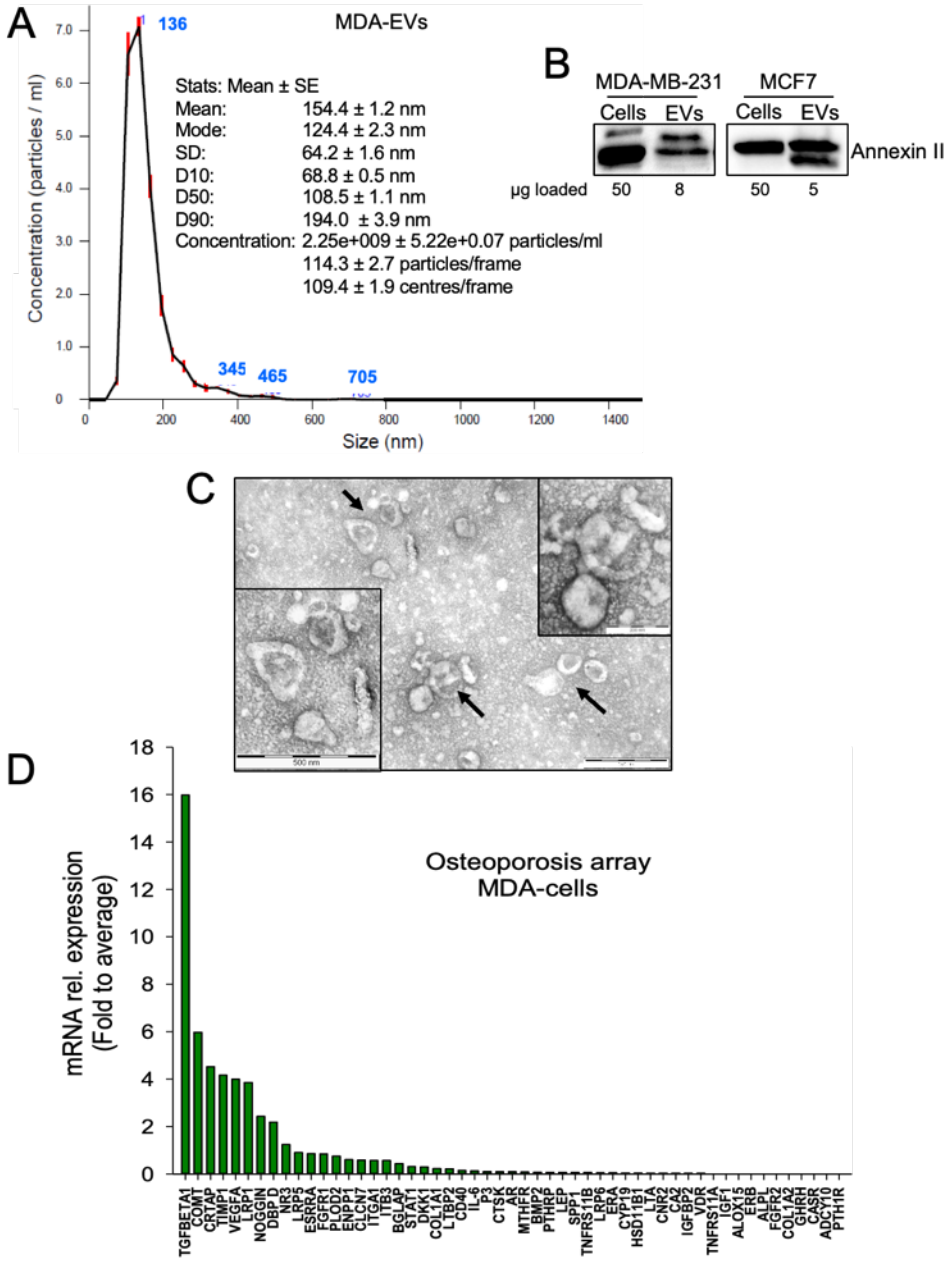

Figure 5: Characterization of breast cancer cell-derived EVs. (**A**) Size and concentration determination of MDA-MB-231 (MDA) extracellular vesicles (MDA-EVs, isolated from 12 ml of CM collected from one 175 cm^2 flask, cell density = $6.5x10^4$ cells/cm^2) by nanoparticle tracking analysis (NanoSight NS3000). (**B**) Western blot analysis for annexin II in 5 µg protein lysates extracted from MDA-MB-231 cells (50 µg) or EVs (5 µg) and MCF7 cells (50 µg) or EVs (5 µg). Results are representative of at least 3 independent preparations of EVs. (**C**) Evaluation of morphology of MDA-MB-231 isolated EVs (MDA-EVs, isolated from 12 ml of CM, collected from one 175 cm^2 flask, cell density = $6.5x10^4$ cells/cm^2) by transmission electron microscopy (arrows: MDA-EVs). (**D**) MDA-MB-231 (MDA) cells were starved for 24h, RNA was extracted and a real time RT array on osteoporosis-related genes was run, as prescribed by the manufacturer. 2^{-Ct} values were calculated, and the results were normalized by the average 2^{-Ct} value. Data are showed as fold to average 2^{-Ct} and plotted from maximum to minimum expression. Housekeeping genes were not plotted.

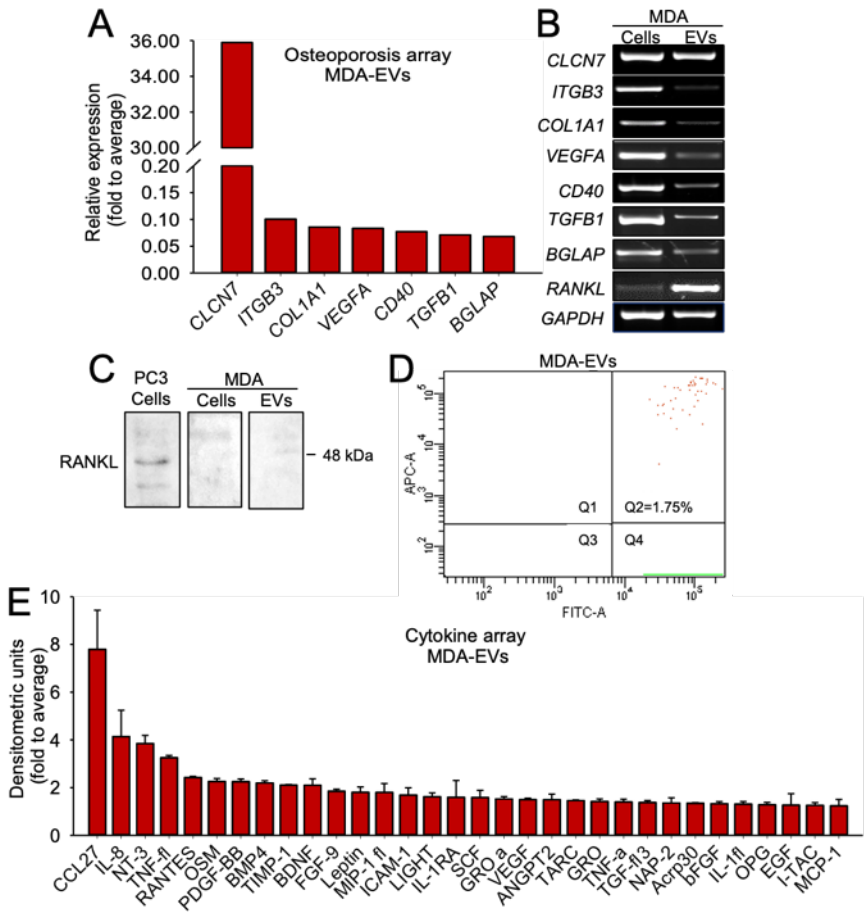

Figure 6: Transcriptional and cytokine profile of MDA-EVs. (**A**) Human osteoporosis real-time array performed on 0.1 µg of reverse-transcribed RNA extracted from MDA-EVs and subjected to a preamplification step. (**B**) Semiquantitative RT-PCR performed on 1 µg of reverse-transcribed RNA extracted from MDA-MB-231 (MDA) cells or derived EVs. (**C**) Western blot analysis to evaluate RANKL expression in PC3 cells (50 µg proteins) as positive control, MDA cells (50 µg proteins). and MDA-EVs (5 µg proteins). (**D**) Cytofluorometric analysis of RANKL-positive EVs isolated from MDA-MB-231 cells (12 mL of CM collected from one 175-cm^2 flask, cell density 6.5 × 10^4/cm^2). (**E**) Cytokine array performed on MDA-EVs protein lysates (15 µg). Result in *A* is from one MDA-EVs preparation; results in *B–E* are representative or *E* the mean ± SD of at least 3 independent preparations of MDA cells and/or MDA-derived EVs.

4.3 Effect of breast cancer–derived EVs on osteoblast behavior

We next investigated whether EVs could be responsible for the changes induced by MDA CM in osteoblasts. Interestingly, MDA-EVs reduced osteoblast metabolic activity and number (Fig. 7A,B) as well as Alp activity (Fig. 7C) compared to untreated osteoblasts. *Cyclin D1* mRNA expression was also significantly reduced, along with *Alp, Runx2, Osx, Bglap*, and *Col1a1* (Fig. 7D). Similar results were observed when osteoblasts were treated with MCF7-derived EVs (Fig. 7E–H).

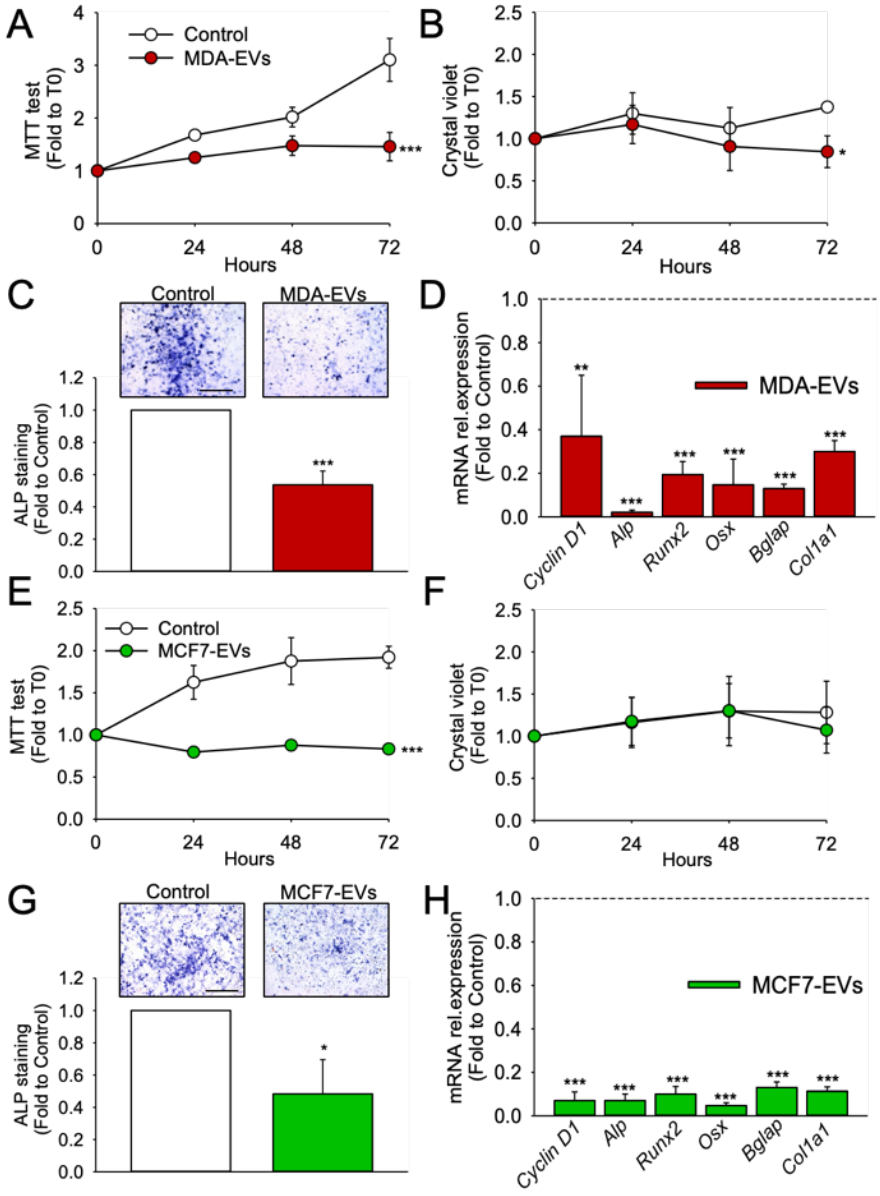

Figure 7: Effect of breast cancer–derived EVs on osteoblast differentiation. (**A–D**) Mouse primary osteoblasts were starved overnight in serum-free DMEM and treated with DMEM as control or with EVs isolated from the CM of the human breast cancer cell line MDA-MB-231 (MDA-EVs, 12 mL collected from one 175-cm^2 flask, cell density 6.5 × 10^4 cells/cm^2). (**A**) Cell metabolic activity evaluated by the MTT assay and (**B**) quantification of cell number by crystal violet staining at the times indicated in the abscissa. (**C**) Alkaline phosphatase (Alp) activity evaluated after 48 hours by cytochemical assay. (**D**) RNA was extracted and subjected to real-time RT-PCR to evaluate the expression of *Cyclin D1*, and of the osteoblast differentiating genes *Alp*, Runt-related transcription factor 2 (*Runx2*), Osterix (*Osx*), Osteocalcin (*Bglap*), and Collagen 1a1 (*Col1a1*). (**E–H**) Mouse primary osteoblasts were starved overnight in serum-free DMEM and treated with DMEM as control or with EVs isolated from the CM of the human breast cancer cell line MCF7 (MCF7-EVs, 12 mL collected from one 175-cm^2 flask, cell density 4.5 × 10^4 cells/cm^2). (**E**) Cell metabolic activity evaluated by the MTT assay and (**F**) quantification of cell number by crystal violet staining at the times indicated in the abscissa. (**G**) Alkaline phosphatase (Alp) activity evaluated after 48 hours by cytochemical assay. (**H**) RNA was extracted and subjected to real-time RT-PCR to evaluate the expression of *Cyclin D1*, and of the osteoblast differentiating genes *Alp*, *Runx2*, *Osx*, *Bglap*, and *Col1a1*. Results are the mean ± SD of 3 independent experiments (*A*,*B*,*E*: **p* = 0.01 and ****p* < 0.001 versus control, AUC; *C*,*D*,*G*,*H*: **p* < 0.05, ***p* = 0.008, and ****p* < 0.001 versus control, Student's *t* test, dot line = control set at 1; bar = 500 µm).

When we looked at the cytokines regulating osteoclastogenesis, an increase of *Rankl* and a decrease of *Opg* and *M-csf* mRNAs were observed in MDA-EV–treated osteoblasts (Fig. 8A). Moreover, MDA-EVs enhanced *Il1b, IL6, Lcn2*, and *Nos2* expression (Fig. 8B). Similar results were found in MCF7-EVs–treated osteoblasts (Fig. 8C,D).

To assess whether these differences were mirrored also at protein level, we performed ELISA assays on CM collected from EV-treated osteoblasts, finding a trend of increase of RANKL and IL1β release, whereas a significant increase of IL6 and Lcn2 were observed in osteoblasts treated with MDA-EVs (Fig. 8E). Similar results were observed with MCF7-EVs (Fig. 8F) and with 4T1-EVs (Fig. 8G-L).

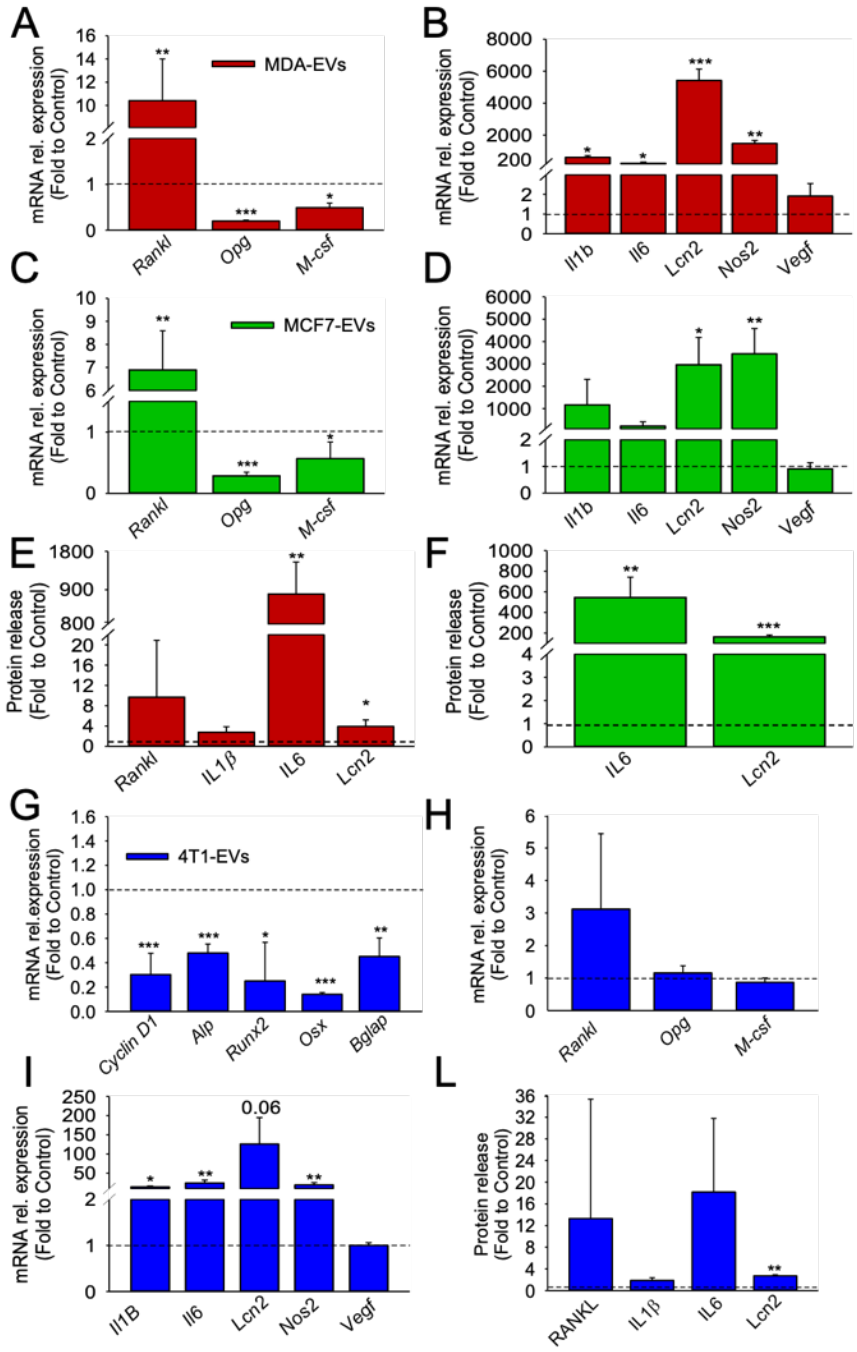

Figure 8: Effect of breast cancer–derived EVs on osteoblast. (**A–D**) Mouse primary osteoblasts were starved overnight in serum-free DMEM and treated with DMEM as control or with EVs isolated from the CM of (**A,B**) MDA-MB-231 (MDA-EVs, 12 mL collected from one 175-cm^2 flask, cell density 6.5 × 10^4 cells/cm^2) or (**C,D**) MCF7 (MCF7-EVs, 12 mL collected from one 175-cm2 flask, cell density 4.5 × 10^4 cells/cm^2). (**A,C**) Transcriptional expression of the cytokines regulating osteoclastogenesis indicated in the abscissa and of (**B,D**) *Il1b, Il6, Lcn2, Nos2,* and *Vegf* evaluated by real-time RT-PCR. (**E,F**) ELISA assay to determine the release of the cytokines indicated in the abscissa in the CM of osteoblasts left untreated or treated with (**E**) MDA-EVs or (**F**) MCF7-EVs. (**G-L**) Mouse primary osteoblasts were starved overnight in serum-free DMEM and treated with DMEM as control or with the extracellular vesicles (EVs) isolated from the conditioned medium of the mouse breast cancer cell line 4T1 (12 ml collected from one 175 cm2 flask, cell density = 6.5x104 cells/cm2). After 48 hours, (**G-I**) RNA was extracted and subjected to real time RT-PCR to evaluate the expression of (**G**) Cyclin D1, and of the osteoblast differentiating genes Alp, Runx2, Osterix (Osx) and Osteocalcin (Bglap). (**H,I**) Transcriptional expression of (**H**) the cytokines regulating osteoclastogenesis indicated in the abscissa and of (**I**) Il1b, Il6, Lcn2, Nos2 and Vegf, evaluated by real time RT-PCR. (**L**) ELISA assay to determine

osteoblast release of RANKL, IL1β, IL6 and Lcn2. Results are the mean ± SD of 3 independent experiments (*P<0.05, **P=0.005 and ***P<0.001 vs Control, Student's t-test; dot line= control set at 1).

To broadly investigate the impact of breast cancer cell–derived EVs on the release of cytokines by osteoblasts, we subjected the CM collected from untreated or MDA-EV–treated osteoblasts to a cytokine array, which allows simultaneous detection of important cytokines, chemokines, and growth factors influencing tumor growth. Along with the observed increase of IL6 and Lcn2 release (Fig. 8E), MDA-EV treatment stimulated osteoblast release of C-C motif Chemokine Ligand (CCL)-3 (alias MIP-1α), CXC motif, Chemokine Ligand (CXCL)-2 (alias MIP-2), Regenerating islet-derived protein 3 Gamma (Reg3G), and VEGF (Fig. 9A,B), and decreased OPG and WISP1 (WNT1 Inducible Signaling Pathway Protein 1) release (Fig. 9C). CCL3 has been implicated in the progression of triple-negative breast cancers[31] and in the induction of osteoclastogenesis[23]. Similarly, CXCL2 favors tumor angiogenesis and tumor-associated osteolysis[32-35]. OPG is the decoy receptor that binds RANKL and blocks its interaction with RANK; therefore, its reduced secretion favors osteoclastogenesis. Finally, WISP1 has been identified as a tumor suppressor factor in breast cancer[36], whereas Reg3G, an extracellular protein known for its antibacterial properties[37], has recently been reported to be implicated in pancreatic carcinogenesis[38].

We next asked whether the factors modulated by MDA-EVs in the osteoblast secretome were also present in the EV fraction, but this was ruled out because neither naïve OB-EVs nor OB-EVs derived from osteoblasts treated with MDA-EVs expressed these cytokines (Fig. 9D). However, naïve OB-EVs contained Angiopoietin like 3 (ANGPTL3) and IL33, whereas expression of CXCL5 was observed only in EVs isolated from osteoblasts educated by MDA-EVs (Fig. 9D).

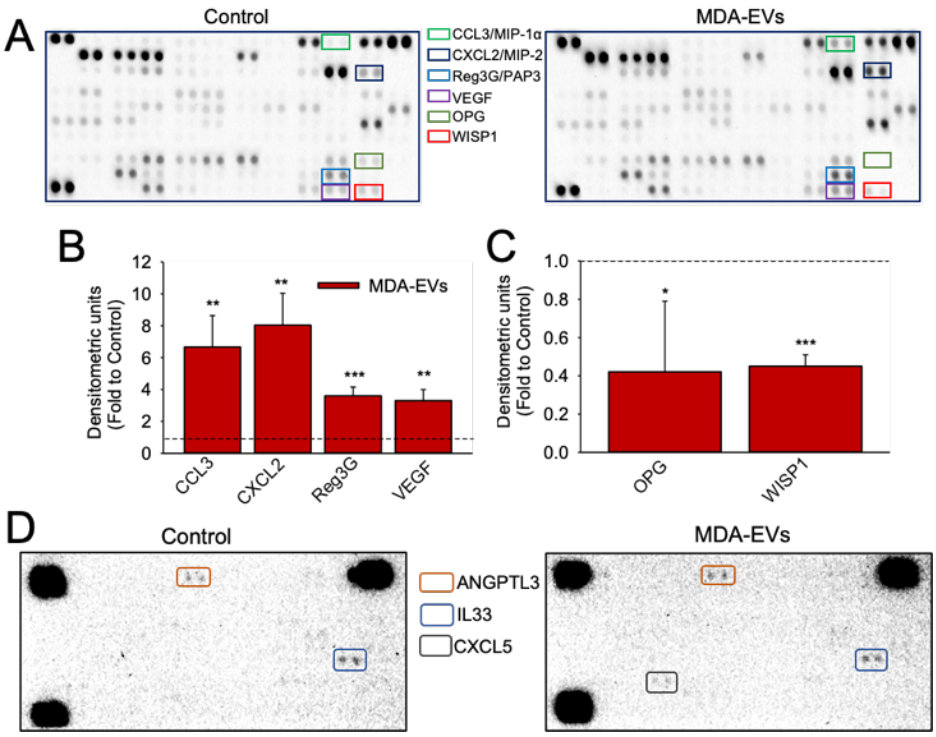

Figure 9: Effect of breast cancer derived EVs on osteoblast cytokine profile. (**A–D**) Mouse primary osteoblasts were starved overnight in serum-free DMEM and treated with DMEM as control or with the extracellular vesicles collected from the CM of the human breast cancer cell line MDA-MB-231 (MDA-EVs, isolated from 12 ml of CM collected from one 175 cm^2 flask, cell density = $6.5x10^4$ cells/cm^2). (**A-C**) After 48 hours the CM was collected from osteoblasts and subjected to cytokine array. (**A**) Representative pictures showing the membranes incubated with CM from control osteoblasts (left) or osteoblasts treated with MDA-EVs (right). (**B,C**) Densitometric analysis showing the cytokines modulated by MDA-EVs treatment, as a result of the densitometric analysis of the spots of interest normalized for the housekeeping proteins. (**D**) After 48 hours, the CM was collected from osteoblasts to isolate OB-EVs, which were lysed in RIPA buffer and subjected to cytokine array. Results are (**A**) representative or (**B,C**) the mean ± SD of 3 independent experiments (*$p < 0.05$, **$p < 0.01$, and ***$p < 0.001$ versus control, Student's t test; dot line = control set at 1).

Finally, we investigated whether the effect of MDA-EVs was persistent or it could be rescued after EV withdrawal. To this aim, osteoblasts were treated with MDA-EVs for 48 hours, then they were subjected to extensive washes to remove the EVs and cultured for additional 48 hours in DMEM. Although we observed a recovery of Alp activity after MDA-EV removal (Fig. 10A), the effects of MDA-EVs on transcriptional expression of osteoblast-differentiating and cytokines genes were persistent (Fig. 10B-D). When we looked at protein level, we found a partial recovery of the increased IL6 release (Fig. 10E) and of CXCL2 (Fig. 10F left panel and Fig.10G), thus indicating that the MDA-EV effect is mostly persistent over the timeframe of our experiment. Treatment of MDA-EVs for 96 hours instead of 48 hours also increases the release of CXCL10, CCL20, and IGFBP5 (Fig. 10F right panel; Fig. 10G); however, a partial rescue after withdrawal of EVs was only observed for the latter (Fig. 10F right panel; Fig. 10G).

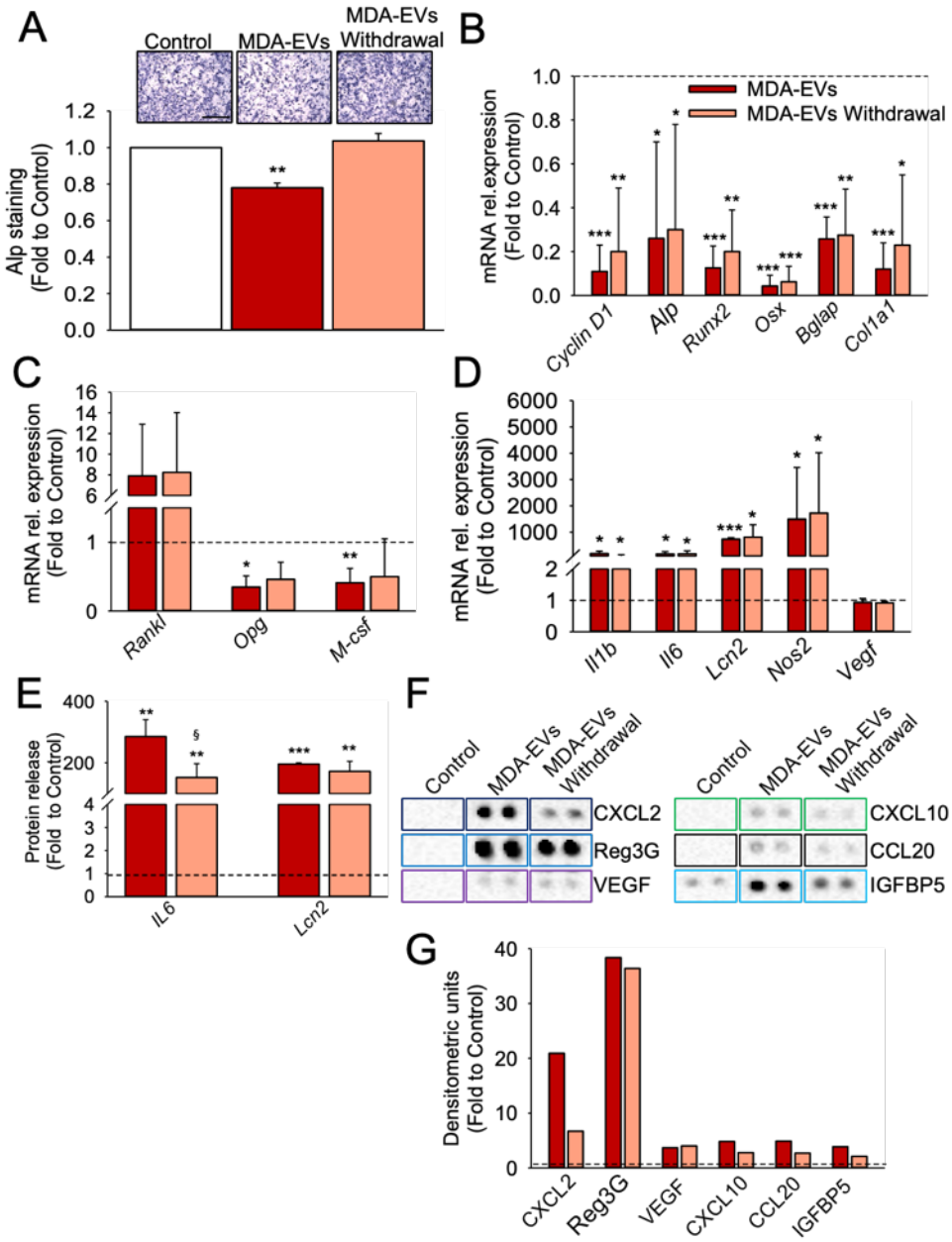

Figure 10: Persistence of MDA-EVs mediated effects on osteoblasts. Mouse primary osteoblasts were starved overnight in serum-free DMEM and treated for 96 hours with DMEM (control), MDA-EVs (12 mL of CM collected from one 175-cm^2 flask, cell density 6.5 × 10^4 cells/cm^2), or with MDA-EVs for 48 hours followed by DMEM for additional 48 hours after washing (MDA-EVs withdrawal). (**A**) Alp activity evaluated by cytochemical assay. (**B–D**) RNA was extracted and subjected to real-time RT-PCR to evaluate the expression of (**B**) Cyclin D1 and of the osteoblast-differentiating genes Alp, Runx2, Osx, Bglap, and Col1a1. (**C**) Transcriptional expression of the cytokines regulating osteoclastogenesis indicated in the abscissa and of (**D**) Il1b, Il6, Lcn2, Nos2, and Vegf evaluated by real-time RT-PCR. (**E**) ELISA assay to determine the release of the IL6 and Lcn2 by osteoblasts. Results are the mean ± SD of three independent experiments (*p < 0.05, **p < 0.01, and ***p < 0.001 versus control, §p = 0.032 versus MDA-EVs, Student's t test; bar = 500 µm). (**F,G**) Mouse cytokine array performed on the CM of osteoblasts treated as in A. (**F**) Representative dot plots for the indicated cytokines. (**G**) Densitometric analysis of the dots in F normalized for the housekeeping proteins. In F and G, results are from one cytokine array incubated with a pool of CM collected from 3 independent experiments.

Taken together, these results demonstrate the ability of MDA-EVs to influence osteoblast behavior by promoting the secretion of pro-tumoral factors and reducing the secretion of anti-osteoclastogenic factors.

4.4 Breast cancer cell–EVs and OB-EVs educated by tumor cell CM stimulate osteoclastogenesis

Osteoblasts induce osteoclastogenesis through the production of several cytokines, including RANKL, and an exacerbated osteoclast activity is the primary cause of bone metastasis–induced osteolysis. To assess whether EVs were involved in this phenomenon, we tested the effect of EVs isolated from osteoblast CM (OB-EVs) on osteoclastogenesis. Mouse primary osteoclasts were differentiated from the fraction of the bone marrow enriched in the monocyte/macrophage subpopulation in the presence of OB-EVs. Although this treatment did not induce osteoclastogenesis, a significant increase of TRAcP-positive mononuclear cells was observed upon treatment with OB-EVs isolated from osteoblasts preincubated with MDA-MB-231 CM (MDA_{CM}-OB-EVs, Fig. 11).

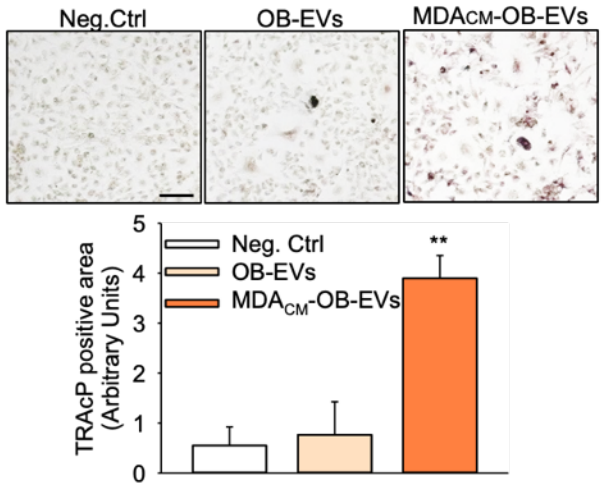

Figure 11: Effect of osteoblast EVs on osteoclastogenesis. Mouse bone marrow mononuclear cells were untreated (Neg.Ctrl), treated with osteoblast-derived EVs (OB-EVs, isolated from 6 ml of CM collected from one 75 cm^2 Petri dish, cell density = $3.5x10^4$ cells/cm^2), or with EVs isolated from osteoblasts pre-treated with MDA-CM (MDA_{CM}-OB-EVs). Inset: Representative pictures of TRAcP activity staining; graph: quantification of the TRAcP-positive area by densitometric analysis. Results are the mean ± SD of 3 independent experiments (**P<0.001, Student's *t*-test, Bar= 50 µm).

We therefore decided to repeat the experiment in the presence of suboptimal concentrations of hrRANKL (30 ng/mL). In these conditions, OB-EVs had no effect on osteoclastogenesis, whereas MDA_{CM}-OB-EVs significantly stimulated osteoclast formation (Fig. 12A).

Interestingly, we observed that MDA-EVs also induced osteoclastogenesis in the absence of RANKL (Fig. 12B), thus indicating that the exogenous RANKL cytokine is dispensable for the osteoclastogenic effect of MDA-EVs. To complete this picture, we performed an *ex vivo* experiment of calvaria culture in the presence of MDA-EVs, finding that this treatment reduced the bone volume/tissue volume (BV/TV %) (Fig. 12C). In contrast, when we employed MCF7-CM to educate OB-EVs or MCF7-EVs, we did not find any effect on osteoclastogenesis (Fig. 12D).

Finally, we assessed whether co-treatment with OB-EVs and MDA-EVs could have a synergic effect on osteoclastogenesis compared to single treatments. In this circumstance, we confirmed the effects observed with the single MDA-EVs treatment and found no further enhancement of osteoclastogenesis with the co-treatment (Fig. 12E).

Taken together, these results indicate that factors released by MDA-MB-231 cells increase the ability of OB-EVs to stimulate osteoclastogenesis.

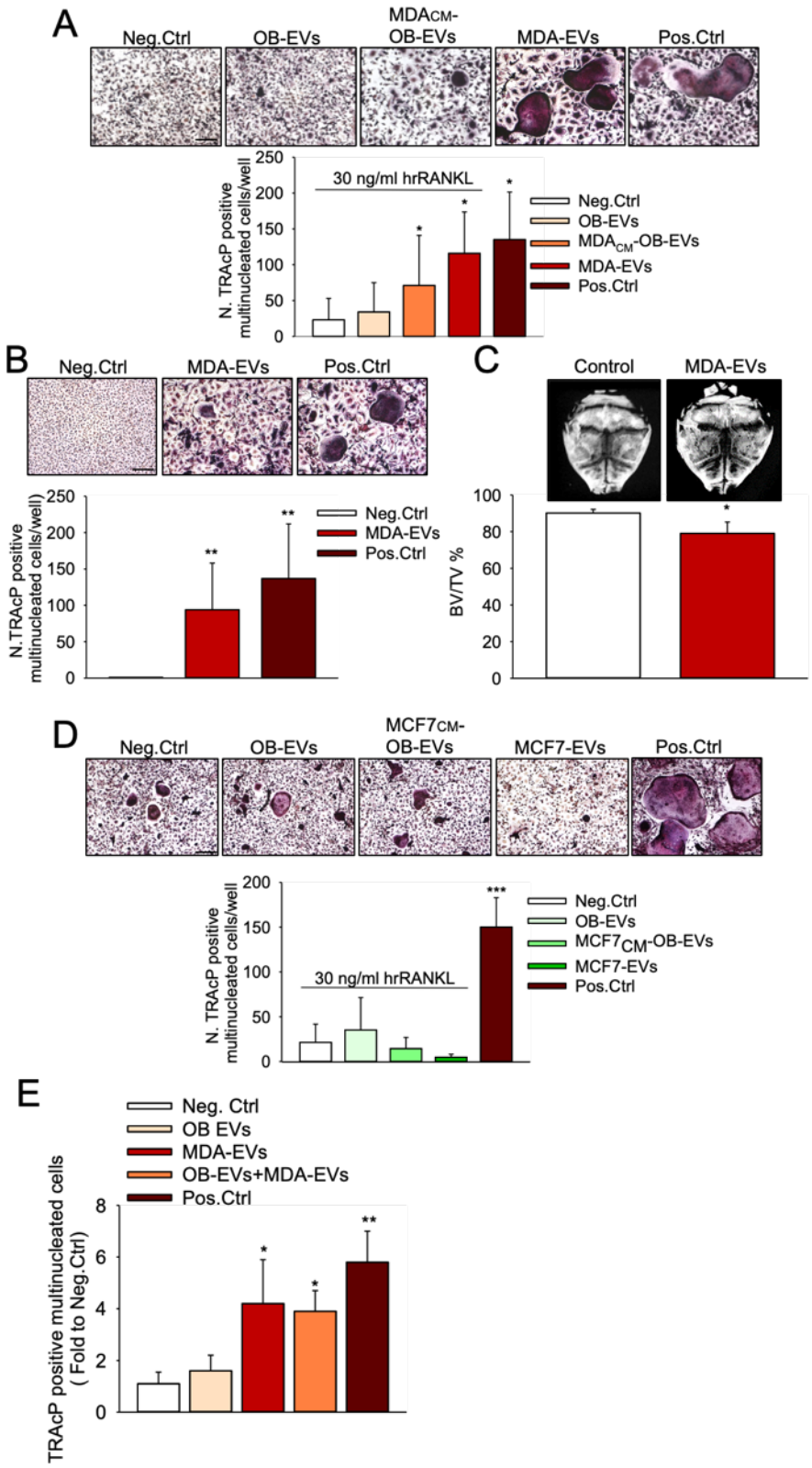

Figure 12: Effect of osteoblast-EVs and breast cancer cell–EVs on osteoclastogenesis. (**A**) Mouse bone marrow mononuclear cells were untreated (Neg.Ctrl), treated with osteoblast EVs (OB-EVs, 6 mL of CM from one 75-cm^2 Petri dish, 3.5 × 10^4 cells/cm^2) or with EVs isolated from osteoblasts pretreated with MDA-CM (MDA$_{CM}$-OB-EVs) and with MDA-EVs (6 mL of CM from one 75-cm^2 Petri dish, cell density 6.5 × 10^4 cells/cm^2) in the presence of suboptimal concentrations of hrRANKL (30 ng/mL). (**B**) Osteoclast primary cultures from mouse bone marrow were untreated (Neg.Ctrl) or treated with MDA-EVs without suboptimal concentrations of hrRANKL. (**C**) µCT analysis performed on ex vivo mouse calvariae cultures treated with MDA-

EVs (12 mL of CM from one 175-cm^2 flask, cell density 6.5×10^4 cells/cm^2). (**D**) Mouse bone marrow mononuclear cells were untreated (Neg. Ctrl), treated with OB-EVs (6 mL of CM from one 75-cm^2 Petri dish, cell density 3.5×10^4 cells/cm^2), with EVs isolated from osteoblasts pretreated with MCF7-CM ($MCF7_{CM}$-OB-EVs) or with MCF7-EVs (6 mL of CM from one 75-cm^2 Petri dish, cell density 4.5×10^4 cells/cm^2) in the presence of suboptimal concentrations of hrRANKL (30 ng/mL). Positive control (Pos.Ctrl) =120 ng/mL hrRANKL. (**E**) Mouse bone marrow mononuclear cells were left untreated (Neg. Ctrl) or treated with OB-EVs (isolated from 6 ml of CM collected from 75 cm^2 Petri dish, $3.5x10^4$ cells/cm^2) or MDA-EVs (isolated from 6 ml of CM collected from 75 cm^2 Petri dish, $6.5x10^4$ cells/cm^2), alone or in combination. Data is the mean ± SD of (A,B,D,E) 3 independent experiments or (**C**) 3 mice/group (*$p < 0.05$, **$p < 0.01$, and ***$p < 0.001$ versus Neg.Ctrl; Student's *t* test, bar = 50 µm).

4.5 Breast cancer cell–EVs and OB-EVs educated by tumor cells CM stimulate angiogenesis

Another cell population present in the bone microenvironment and participating in local tumor growth are endothelial cells. We therefore investigated the effect of OB-EVs and breast cancer cell–EVs on HUVEC behavior. OB-EV treatment did not affect cell metabolic activity, evaluated by the MTT assay (Fig. 13A), nor *in vitro* tube formation (Fig. 13B), whereas a significant increase in percent of tube branching was observed when treating with MDA_{CM}-OB-EVs or with MDA-EVs (Fig. 13B). Interestingly, when we performed *in vivo* Matrigel plug assays, OB-EVs significantly increased angiogenesis, evaluated by determination of the percent of the area covered by migrated endothelial cells over the total area of the plugs (Fig. 13C,D). This angiogenic effect of OB-EVs was much more powerful after pretreatment of osteoblasts with MDA-CM (Fig. 13D,E). Consistent with the *in vitro* results, a direct effect of MDA-EVs on in vivo angiogenesis was also observed (Fig. 13D,E). Similarly, an increase of *in vitro* tube formation was observed with EVs isolated from MCF7-CM which, however, failed to educate OB-EVs toward a proangiogenic effect (Fig. 13E). Moreover, the combination treatment with OB-EVs plus MDA-EVs did not further increase in vitro angiogenesis (Fig. 13F).

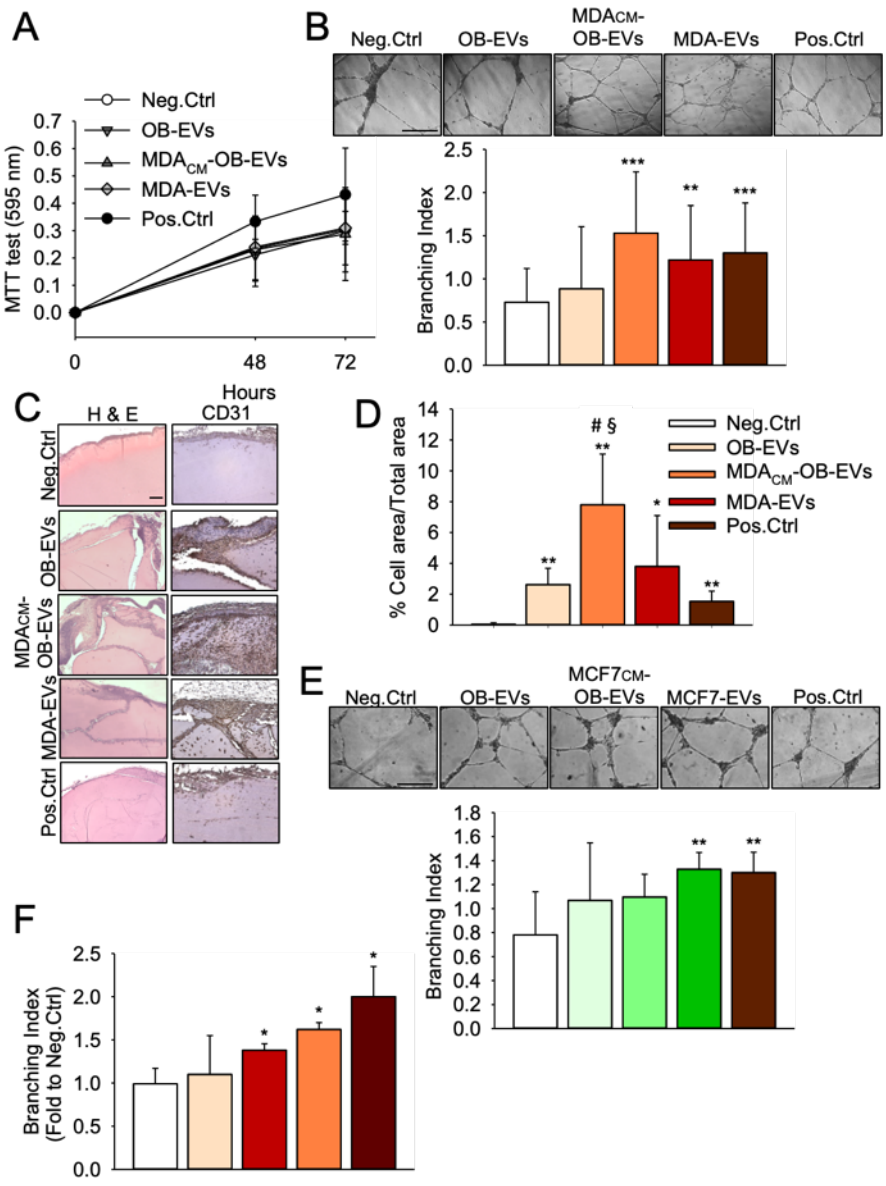

Figure 13: **Effect of osteoblast-EVs and breast cancer cell–EVs on angiogenesis.** (**A,B**) Human umbilical vein endothelial cells (HUVECs) were treated with OB-EVs (6 mL of CM from one 75-cm^2 Petri dish, cell density 3.5 × 10^4 cells/cm^2), or with EVs isolated from osteoblasts pretreated with MDA-CM (MDA$_{CM}$-OB-EVs) and with MDA-EVs (6 mL of CM from one 75-cm^2 Petri dish, cell density 6.5 × 10^4 cells/cm^2). (**A**) HUVECs Cell metabolic activity was evaluated by the MTT assay after treatment with vehicle (Neg.Ctrl), osteoblast EVs (OB-EVs), EVs isolated from osteoblasts pretreated with MDA-CM (MDA$_{CM}$-OB-EVs), MDA-EVs or endothelial growth medium (EGM)-2 (Pos.Ctrl). (**B**) in vitro tube formation assay (branching index) performed on HUVEC cells treated as described in *A*. (**C,D**) in vivo Matrigel plug assay performed by subcutaneous injection of 8-week-old male mice with 0.5 mL of Matrigel, enriched with PBS (Neg.Ctrl), OB-EVs, MDA$_{CM}$-OB-EVs, or 50 ng/mL of ECGS + 150 ng/mL VEGF (Pos.Ctrl). (**C**) Hematoxylin and eosin staining and immunohistochemistry for the endothelial marker CD31. (**D**) Quantification of the percent of cell area over the total area of the plug. (**E**) *In vitro* tube formation assay (branching index) performed on human umbilical vein endothelial cells (HUVECs) untreated or treated with osteoblast EVs (OB-EVs, 6 mL of CM from one 75-cm^2 Petri dish, cell density 2.5 × 10^4 cells/cm^2), EVs isolated from osteoblasts pretreated with MCF7-CM (MCF7$_{CM}$-OB-EVs), MCF7-EVs (6 mL of CM from one 75-cm^2 Petri dish, cell density 4.5 × 10^4 cells/cm^2), or with endothelial growth medium (EGM)-2 (Pos.Ctrl). (**F**) *In vitro* tube formation assay performed on HUVECs treated with OB-EVs (isolated from 6 ml of CM collected from 75 cm^2 Petri dish, 3.5x10^4 cells/cm^2) and with MDA-EVs (isolated from 6 ml of CM collected from 75

cm^2 Petri dish, $6.5x10^4$ cells/cm^2), alone or in combination. Pos.Ctrl = positive control, treatment with endothelial growth medium (EGM)-2. Data are the mean ± SD of (**A,B,E,F**) three independent experiments or (**C,D**) of 5 mice/group (*p<0.05, **p < 0.01 and ***p < 0.001 versus Neg.Ctrl; $^{\#}p$ = 0.004 versus OB-EVs, $^{\S}p$ = 0.001 versus Pos.Ctrl, Student's t test, in *C,D*) bar = 200 μm). ECGS = endothelial cell growth supplement.

4.6 *In vivo* breast cancer cell–EVs integration into the bone tissue

Having shown a clear effect of breast cancer–derived EVs on *in vitro* bone cells, we finally evaluated whether they were able to target and integrate into the bone tissue *in vivo*. As already shown for OB-EVs[13], we performed intraperitoneal injection of 7-day-old mice with MDA-EVs preincubated with the lipophilic fluorophore PKH26 observing, after 5 hours, a significantly higher fluorescent signal in their bones compared to bones collected from mice inoculated with PBS as vehicle (Fig. 14A). We flushed out the BM and analyzed BM cells by cytofluorometry, using the PE filter set, and found a significantly higher signal in BM cells recovered from PKH26-MDA-EV–injected mice compared to controls (Fig. 14B). However, the percentage of positive cells/total cells was low (~1%), suggesting that a small subgroup of BM cells was targeted by the MDA-EVs. Slides of sorted BM cells also confirmed the presence of PKH26-positive cells (Fig. 14C).

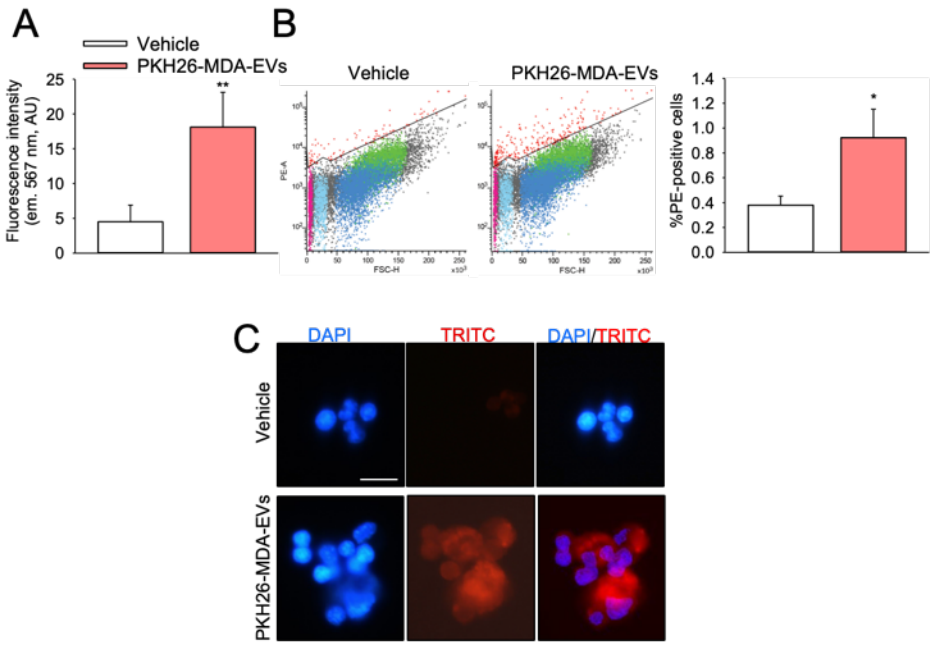

Figure 14: *In vivo* tumor cell–EVs targeting the bone. Seven-day-old mice were intraperitoneally injected with MDA-EVs (12 mL of CM collected from one 175-cm^2 flask, cell density 6.5×10^4 cells/cm^2injected to each mouse) labeled with the PKH26 fluorophore (PKH26-MDA-EVs) or with PBS (vehicle). After 5 hours, mice were euthanized and bones (forelimbs, hindlimbs, and calvariae) explanted and subjected to lipid extraction for fluorimetric analysis, cryosectioning, and confocal microscopy, while BM was flushed out for FACS analysis. (**A**)

Fluorimetric quantification of PKH26 in lipid extracts. (**B**) Representative dot plot and quantification (graph) of % of fluorescent cells, as determined with PE filter, in whole BM flushed out cells. (**C**) PE-high BM cells from PKH-MDA-EVs-injected mice were sorted onto polylysine slides by FACS, along with random BM cells from vehicle-injected mice. After mounting with DAPI, cells were observed by conventional epifluorescence. Data are the mean ± SD of (**A**) 4 mice/group and (**B,C**) 5 mice/group (*$p < 0.02$ and**$p = 0.008$ versus vehicle, Student's *t* test; bar = 25 μm). BM = bone marrow.

Finally, we analyzed cryosections of femurs explanted from PKH26-MDA-EVs or vehicle-injected mice by confocal microscopy (Fig. 15A). We observed that cells lining the trabecular bone were highly PKH26-positive in MDA-EV–injected mice (Fig. 15A). They included cells morphologically reminiscent of osteoblasts (Fig. 15B, a-a′) and multinucleated osteoclasts (Fig. 15B, b-b′). In contrast, chondrocytes were negative (Fig. 15B, c-c′). TRAcP histochemical assay on the same sections confirmed the co-localization of the PKH26 signal with TRAcP-positive multinucleated cells (Fig. 15C).

Taken together, these results showed that MDA-EVs target the bone microenvironment and are primarily taken up by osteoclasts, osteoblasts, and a few BM cells.

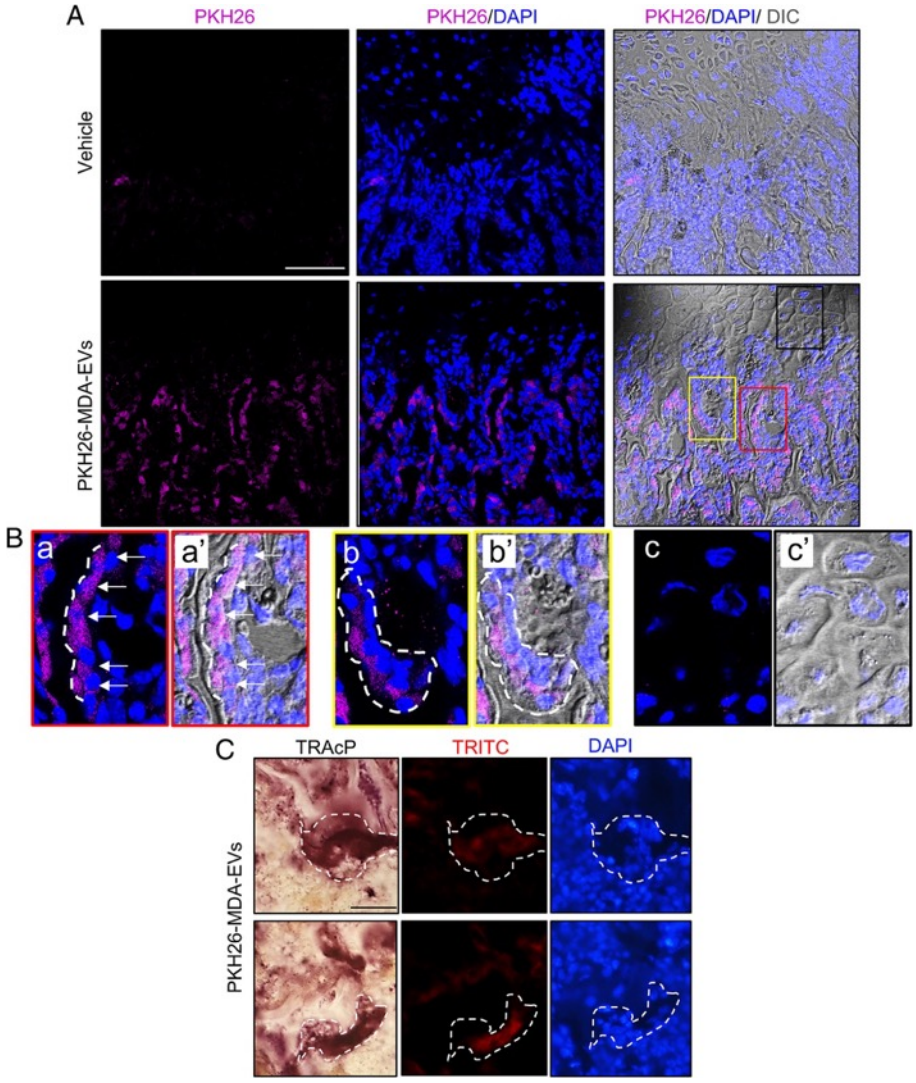

Figure 15: ***In vivo*** **tumor cell–EVs targeting the bone.** Seven-day-old mice were intraperitoneally injected with MDA-EVs (12 mL of CM collected from one 175-cm^2 flask, cell density 6.5 × 10^4 cells/cm^2 injected to each mouse) labeled with the PKH26 fluorophore (PKH26-MDA-EVs) or with PBS (vehicle). After 5 hours, mice were euthanized and femurs and calvariae were collected and fixed in 4% buffered PFA. (**A**) Femur cryosections were mounted with DAPI and observed by confocal microscopy. (**B**) Magnification of A showing representative images of (a,a′) osteoblasts, (b,b′) osteoclasts and (c,c′) chondrocytes shown as (a,b,c) PKH26/DAPI or (a′,b′,c′) PKH26/DAPI/DIC merge images. (**C**) Representative pictures of femur cryosections observed by epifluorescence microscopy to detect DAPI and PKH26 signal and stained for TRAcP activity. Images are representative of 5 mice/group (A: bar=80 µm; B: bar= 20µm; C: bar=25 µm).

5. DISCUSSION

Bone metastases represent a frequent complication in advanced breast cancer, with an occurrence of up to 70%[1]. Tumor cells generate a favorable premetastatic niche prior to their dissemination, and this process is at least in part mediated by EVs[39, 40]. Because we have previously shown that bone cells crosstalk via EVs[13], we hypothesized that EV-mediated communication between breast cancer cells and bone cells could play a role in cancer progression. In agreement with this hypothesis, we found that breast cancer cell–EVs

influence bone-resident cells both directly and indirectly. In particular, these EVs inhibited osteoblast differentiation and reduced cell number and activity, while increasing osteoclast formation in a RANKL-independent manner. Angiogenesis was also found to be increased by MDA-EVs both *in vitro* and *in vivo*. However, alteration of the crosstalk among bone-resident cells was also observed, because in osteoblasts breast cancer cell–EVs enhanced the transcription and the secretion of pro-angiogenic, pro-inflammatory, and pro-osteoclastogenic factors, which eventually increased angiogenesis and osteoclastogenesis, at least in part through tumor-educated OB-EVs.

Direct effects on osteoblasts by MDA-EVs are likely to depend on their ability to inhibit the expression of osteoblast-specific genes, including the two master transcription factors, *Runx2* and *Osx*, as well as the mature osteoblast markers *Alp*, *Bglap*, and *Col1a1*. Furthermore, the reduction in osteoblast number could be due to an induction of cell cycle arrest, as indicated by the decrease of *Cyclin D1* mRNA expression by MDA-EVs. The underlying pathways remain to be elucidated. However, we could hypothesize the involvement of the NF-κB, which would be a strong candidate given that many of its downstream targets (Il6, Il1B, Lcn2, Nos2, RANKL, CCL3, and Vegf) were strongly increased at the transcriptional and/or protein level. Although more experiments are needed to confirm the implicated molecular mechanisms, the effects appear to converge on a strong reduction of osteoblast growth, activity, and differentiation[41-44].

We also asked whether removing MDA-EVs from osteoblasts after 48 hours of treatment would result in a rescue of the observed changes in the osteoblast phenotype, finding that most of the effects exerted by MDA-EVs persist, regardless of EV removal, even at 96 hours. This might be explained by the fact that internalized EV cargo has a turnover inside the target cell, which may be longer than 48 hours. Notable exceptions include IL6, CXCL2, and IGFBP5, all showing a partial rescue, whereas a total rescue was observed for Alp activity.

Osteoclastogenesis induced by cancer cell EVs seems to be linked to RANKL in different ways. Our data shows that although MDA-EVs are RANKL-negative, they are highly enriched in mRNA coding for this factor, even compared to MDA cells. We can speculate that this mRNA can be an educating factor, potentially taken up and translated by the bone resident cells, thus contributing to the increase of osteoclastogenesis. This result is consistent with reports demonstrating functionality of proteins arising from exosomal mRNA translation[9,45]. In addition, it is interesting to note that MDA-EVs can induce osteoclastogenesis despite being RANKL-negative. Furthermore, treating osteoclast

precursors with MDA-EVs without exogenous RANKL still results in mature osteoclast formation. These results suggest that MDA-EVs foster RANKL-independent osteoclastogenesis. We can hypothesize that this process might be promoted by the shuttling of inflammatory factors that are also known to be strong inducers of osteoclastogenesis, such as IL6, IL1B, IL8, CCL3, CCL4, and PDGF-BB.

In this study, we also showed that cancer cell EVs were able to activate angiogenesis by a direct mechanism. This functional data is supported by the molecular profile of MDA-EVs, which contains pro-angiogenic mRNAs (*TGFB1*, *VEGF*) and proteins (Angiopoietin 2, VEGF). However, indirect effects are also present, showing how cancer cell EVs can deeply reprogram the bone microenvironment and alter the physiological crosstalk mechanisms to exacerbate tumor growth.

In the crosstalk between tumor cell EVs and the bone microenvironment, osteoblasts seem to play a crucial role, integrating the messages from cancer cell EVs. In fact, osteoblast preconditioning with breast cancer cell–derived factors resulted in their EVs gaining enhanced osteoclastogenic potential, indicating that the breast cancer secretome could enhance osteoblast EV–mediated osteoclastogenesis. We hypothesized that the enhanced osteoclastogenesis could be due to the enrichment of RANKL on the OB-EV surface, as demonstrated by cytofluorometry. This is consistent with several reports that suggest the implication of RANKL in cancer-mediated osteolysis[6], and with our previous work demonstrating a dampened osteoclastogenic potential in *Tnfsf11*(*Rankl*)$^{-/-}$ OB-EVs[13]. The fact that supplementation of a suboptimal concentration of RANKL is needed to induce the formation of mature osteoclasts does not subtract from the results because the number of TRAcP-positive mononuclear cells was increased even without RANKL supplementation. However, in a microenvironment such the metastatic one, many other osteoclastogenic regulators can be enhanced (i.e., soluble RANKL, Il6, CXCL2) or reduced (i.e., OPG).

On the angiogenesis side, OB-EVs enhanced *in vitro* tube formation and *in vivo* angiogenesis in plug assay experiments, following pretreatment with breast cancer cell–derived factors, even more than MDA-EVs alone. We therefore speculate that breast cancer–derived factors reprogram osteoblasts to generate a premetastatic niche, conferring both osteolytic and angiogenic potential through educated OB-EVs and soluble factors. These findings collectively demonstrate the ability of metastatic breast cancer cell–derived EVs to establish a pro-osteoclastogenic and pro-angiogenic microenvironment through the regulation of the osteoblast secretome.

Intriguingly, MCF7, a very low metastatic, ER-positive breast cancer cell line, only partially reproduced the MDA-EVs mediated effects. In fact, although osteoblast gene expression was similarly affected, MCF7 did not influence osteoblast number. Furthermore, MCF7-EVs did not cause any pro-osteoclastogenic effect and, when OB-EVs were pre-educated with MCF7 CM, they failed to induce osteoclastogenesis even with suboptimal RANKL supplementation. In contrast, MCF7-EVs showed the ability to influence in vitro angiogenesis.

Finally, our *in vivo* analyses showed that MDA-EVs were recruited by the bone microenvironment and targeted osteoclasts, osteoblasts, and a few BM cells.

In conclusion, we have profiled and evaluated the effects of osteoblast-derived and breast cancer–derived EVs on the bone microenvironment in the context of the metastatic breast cancer. As summarized in Fig. 16, we found that both secreted factors and EVs from breast cancer cells are able to condition the bone microenvironment toward an osteolytic and angiogenic phenotype, and that this occurs at least in part through the influence of the osteoblast secretome and through the alteration of the biology of their EVs. Our findings therefore collectively show a previously undescribed role for breast cancer cell–derived EVs to condition and prime the bone microenvironment for metastasis.

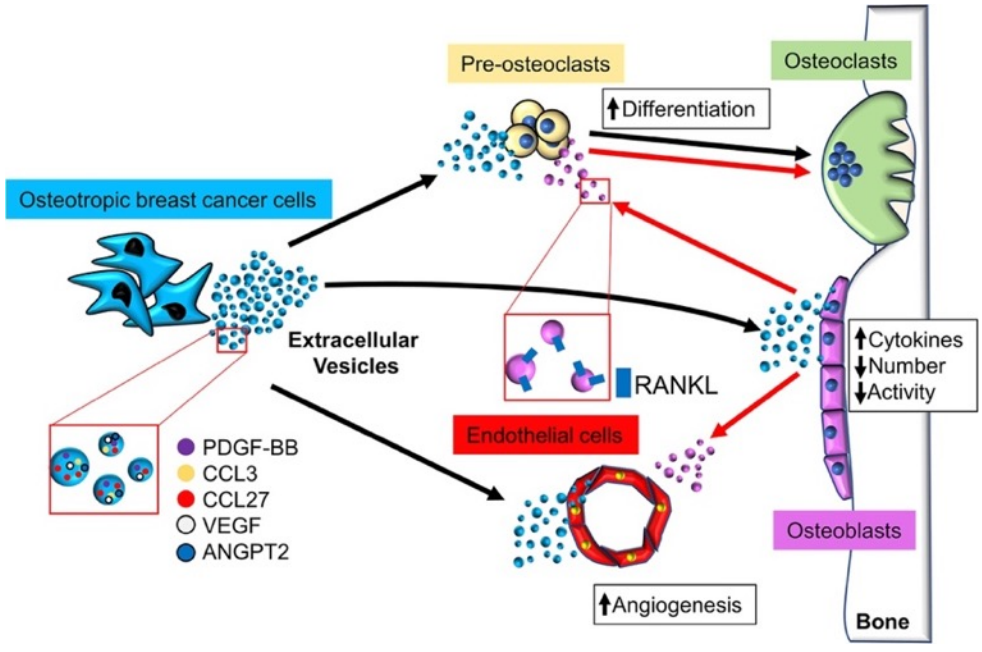

Figure 16: Proposed EV-mediated communication mechanism among cancer cells and bone cells. Osteotropic breast cancer cells release EVs that contain several molecular mediators, including PDGF-BB, CCL3, CCL27, VEGF, and ANGPT2. Cancer EVs exert several actions in the bone microenvironment: they target preosteoclasts and stimulate their differentiation to multinucleated OCs, osteoblasts increasing their cytokine production, while reducing their number and activity, and endothelial cells, which increases angiogenesis. Furthermore, cancer-released factors can increase osteoblast production of RANKL-positive EVs, which further stimulate

osteoclastogenesis and angiogenesis. This series of changes mediated by breast cancer cells EVs result in a deep reprogramming of the bone microenvironment, which makes it more favorable for cancer growth and engraftment.

6. REFERENCES

1. Coleman, R. E. & Rubens, R. D.The clinical course of bone metastases from breast cancer. *Br J Cancer* **55**, 61–6 (1987).
2. Coleman, R. E., Smith, P. & Rubens R. D. Clinical course and prognostic factors following bone recurrence from breast cancer. *Br J Cancer* **77**, 336–40 (1998).
3. Lacey, D.L.,Timms, E., Tan, H. L. *et al*. Osteoprotegerin ligand is a cytokine that regulates osteoclast differentiation and activation. *Cell* **93**, 165–76 (1998).
4. Yasuda, H. Y., Shima, N., Nakagawa, N. *et al*. Osteoclast differentiation factor is a ligand for osteoprotegerin/osteoclastogenesis-inhibitory factor and is identical to TRANCE/RANKL. *Proc Natl Acad Sci USA* **95**, 3597–602, (1998).
5. Cappariello, A., Maurizi, A., Veeriah, V. & Teti, A. The Great Beauty of the osteoclast. *Arch Biochem Biophys* **558**, 70–8 (2014).
6. Maurizi, A & Rucci, N. The osteoclast in bone metastasis: player and target. *Cancers (Basel)* **10**, 218 (2018).
7. Cox, T. R., Rumney, R. M. H., Schoof, E. M., *et al*. The hypoxic cancer secretome induces pre-metastatic bone lesions through lysyl oxidase. *Nature* **522**, 106–10 (2015).
8. Becker, A., Thakur, B. K., Weiss, J. M., Kim, H. S., Peinado, H. & Lyden, D. Extracellular vesicles in cancer: cell-to-cell mediators of metastasis. *Cancer Cell* **30**, 836–48 (2016).
9. Valadi, H., Ekström, K., Bossios, A., Sjöstrand, M., Lee, J. J. & Lötvall, J. O. Exosome-mediated transfer of mRNAs and microRNAs is a novel mechanism of genetic exchange between cells. *Nat Cell Biol* **9**, 654–9 (2007).
10. Gangoda, L., Liem, M., Ang, C. S. *et al*. Proteomic profiling of exosomes secreted by breast cancer cells with varying metastatic potential. *Proteomics* **17**, 1–5 (2017).
11. Hashimoto, K., Ochi, H., Sunamura, S. *et al*.Cancer-secreted hsa-miR-940 induces an osteoblastic phenotype in the bone metastatic microenvironment via targeting ARHGAP1 and FAM134A. *Proc Natl Acad Sci USA* **115**, 2204–9 (2018).
12. Tiedemann, K., Sadvakassova, G., Mikolajewicz, N. *et al*. Exosomal release of L-plastin by breast cancer cells facilitates metastatic bone osteolysis. *Transl Oncol* **12**, 462–74 (2019).

13. Cappariello, A., Loftus, A., Muraca, M., Maurizi, A., Rucci, N. & Teti, A. Osteoblast-derived extracellular vesicles are biological tools for the delivery of active molecules to bone. *J Bone Miner Res* **33**, 517–33 (2018).
14. Marzia, M., Sims, N. A., Voit, S. *et al*. Decreased c-Src expression enhances osteoblast differentiation and bone formation. *J Cell Biol* **151**, 311–20 (2000).
15. Rucci, N., Rufo, A., Alamanou, M. *et al*. The glycosaminoglycan-binding domain of PRELP acts as a cell type-specific NF-kappaB inhibitor that impairs osteoclastogenesis. *J Cell Biol* **187**, 669–83 (2009).
16. Kruger, S., Abd-Elmageed, Z. Y., Hawke, D. H. *et al*. Molecular characterization of exosome-like vesicles from breast cancer cells. *BMC Cancer* **14**, 44 (2014).
17. Kubota, Y., Kleinman, H. K., Martin, G. R. & Lawley, T. J. Role of laminin and basement membrane in the morphological differentiation of human endothelial cells into capillary-like structures. *J Cell Biol* **107**, 1589–98 (1995).
18. Peramuhendige, P., Marino, S., Bishop, R. T. *et al*. TRAF2 in osteotropic breast cancer cells enhances skeletal tumor growth and promotes osteolysis. *Sci Rep* **8**, 39 (2018).
19. Rucci, N., Capulli, M., Piperni, S. G. *et al*. Lipocalin 2: a new mechanoresponding gene regulating bone homeostasis. *J Bone Miner Res* **30**, 357–68 (2015).
20. Ören, B., Urosevic, J., Mertens, C. *et al*. Tumor stroma-derived lipocalin-2 promotes breast cancer metastasis. *J Pathol* **239**, 274–85 (2016).
21. Théry, C., Amigorena, S., Raposo, G & Clayton, A. Isolation and characterization of exosomes from cell culture supernatants and biological fluids. *Curr Protoc Cell Biol*. Chapter 3, **22**, 1–29 (2006).
22. Lin, H. Y., Sun, S. M., Lu, X. F. *et al*. CCR10 activation stimulates the invasion and migration of breast cancer cells through the ERK1/2/MMP-7 pathway. *Int Immunopharmacol* **51**, 124–30 (2017).
23. Oba, Y., Lee, J. W., Ehrlich, L.A. *et al*. MIP-1 alpha utilizes both CCR1 and CCR5 to induce osteoclast formation and increase adhesion of myeloma cells to marrow stromal cells. *Exp Hematol* **33**, 272–8 (2005).
24. Sabokbar, A., Mahoney, D. J., Hemingway, F. & Athanasou, N. A. Non-canonical (RANKL-independent) pathways of osteoclast differentiation and their role in musculoskeletal diseases. *Clin Rev Allergy Immunol* **51**, 16–26 (2016).
25. Xuan, W.,Feng, X., Qian, C. *et al*. Osteoclast differentiation geneexpression profiling reveals chemokine CCL4 mediates RANKL-induced osteoclast migration and

invasion via PI3K pathway. *Cell Biochem Funct.* **35**, 171–7 (2017).

26. Li, D. Q., Wan, Q. L., Pathak, J. L. & Li, Z. B. Platelet-derived growth factor BB enhances osteoclast formation and osteoclast precursor cell chemotaxis. *J Bone Miner Metab* **35**, 355–65 (2017).
27. Vallet, S., Pozzi, S., Patel, K. *et al*. A novel role for CCL3 (MIP-1α) in myeloma-induced bone disease via osteocalcin downregulation and inhibition of osteoblast function. *Leukemia* **25**, 1174–81 (2011).
28. Kubota, K., Sakikawa, C., Katsumata, M., Nakamura, T. & Wakabayashi, K. Platelet-derived growth factor BB secreted from osteoclasts acts as an osteoblastogenesis inhibitor factor. *J Bone Miner Res* **17**, 257–65 (2002).
29. Tawara, K., Bolin, C., Kancisky, J. *et al*. OSM potentiates preintravasation events, increases CTC counts, and promotes breast cancer metastasis to the lung. *Breast Cancer Res* **20**, 53 (2018).
30. Bolin, C., Tawara, K., Sutherland, C. *et al*. Oncostatin M promotes mammary tumor metastasis to bone and osteolyitic bone degradation. *Genes Cancer* **3**, 117–30 (2012).
31. Roberti, M. P., Arriaga, J. M., Bianchini, M. *et al*. Protein expression changes during human triple negative breast cancer cell line progression to lymph node metastasis in a xenografted model in nude mice. *Cancer Biol Ther* **13**,1123–40 (2012).
32. Palacios-Arreola, M. I., Nava-Castro, K.E., Castro, J.I., García-Zepeda E., Carrero, J. C. & Morales-Montor J. The role of chemokines in breast cancer pathology and its possible use as therapeutic targets. *J Immunol Res* **2014**, 849720 (2014).
33. Strieter, R. M., Burdick, M. D., Mestas, J., Gomperts, B., Keane, M. P. & Belperio, J. A. Cancer CXC chemokine networks and tumor angiogenesis. *Eur J Cancer* **42**, 768–78 (2006).
34. Ben-Baruch, A. The multifaceted roles of chemokines in malignancy. *Cancer Metastasis Rev* **25**, 357–71 (2006).
35. Hardaway, A. L., Herroon, M. K., Rajagurubandara, E. & Podgorski, I. Marrow adipocyte-derived CXCL1 and CXCL2 contribute to osteolysis in metastatic prostate cancer. *Clin Exp Metastasis* **32**, 353–68 (2015).
36. Davies, S. R., Watkins, G., Mansel, R. E., Jiang & W. G. Differential expression and prognostic implications of the CCN family members WISP-1, WISP-2 and WISP-3 in human breast cancer. *Ann Surg Oncol* **14**, 1909–18 (2007).
37. Johansson, M. E., Hansson, G.C. Microbiology. Keeping bacteria at a distance. *Science*. **334**, 182–3 (2011).

38. Li, Q., Wang, H., Zogopoulos, G. *et al*. Reg proteins promote acinar-to-ductal metaplasia and act as novel diagnostic and prognostic markers in pancreatic ductal adenocarcinoma. *Oncotarget* **7**, 77838–53 (2016).
39. Kaplan, R. N., Rafii, S. & Lyden, D. Preparing the "soil": the premetastatic niche. *Cancer Res* **66**, 11089–93 (2006).
40. Peinado, H., Zhang, H., Matei, I. R. *et al*. Pre-metastatic niches: organ-specific homes for metastases. *Nat Rev Cancer* **17**, 302–17 (2017).
41. De Benedetti, F., Rucci, N., Del Fattore, A. *et al*. Impaired skeletal development in interleukin-6-transgenic mice: a model for the impact of chronic inflammation on the growing skeletal system. *Arthritis Rheum* **54**, 3551-63 (2006).
42. Peruzzi, B., Cappariello, A., Del Fattore, A., Rucci, N., De Benedetti, F., Teti, A. C-Src and IL-6 inhibit osteoblast differentiation and integrate IGFBP5 signalling. *Nat Commun* **3**, 630 (2012).
43. Del Fattore, A., Cappariello, A., Capulli, M. *et al*. An experimental therapy to improve skeletal growth and prevent bone loss in a mouse model overexpressing IL-6. *Osteoporos Int* **25**, 681-92 (2014).
44. Capulli, M., Ponzetti, , M., Maurizi, A. *et al*. A complex role for Lipocalin 2 in bone metabolism: global ablation in mice induces osteopenia caused by an altered energy metabolism. *J Bone Miner Res* **33**, 1141–53 (2018).
45. Mao, L., Li, X., Gong, S. *et al*. Serum exosomes contain ECRG4 mRNA that suppresses tumor growth via inhibition of genes involved in inflammation, cell proliferation, and angiogenesis. *Cancer Gene Ther* **25**, 248–59 (2018).

Chapter 3

"Anti-osteoblastogenic, pro-inflammatory and pro-angiogenic effect of extracellular vesicles isolated from the human osteosarcoma cell line MNNG/HOS"

Published in BONE, 2021. Vol. 153: Pag. 116130 (doi: 10.1016/j.bone.2021.116130).

Ucci, A.*, Cappariello, A.*, Ponzetti, M., Tennant, F., Loftus, A. E. P., Shefferd, K., Maurizi, A., Delle Monache, S., Teti, A., Rucci, N.

*Equal contributors

1. ABSTRACT

Extracellular Vesicles (EVs) are becoming increasingly recognized as integral signaling vehicles in several types of cancers, including bone malignancies. However, the specific mechanisms by which EVs influence osteosarcoma progression have not been fully determined. We evaluated the effects of EVs derived from the human osteosarcoma cell line MNNG/HOS (MNNG/HOS-EVs) on bone resident cells. We found that MNNG/HOS-EVs are internalized by osteoblasts and osteoclasts *in vitro*, with potent inhibitory effects on osteoblast metabolic activity, cell density and alkaline phosphatase activity. Consistently, MNNG/HOS-EVs reduced the expression of cell cycle and pro-osteoblastogenic genes, whilst increasing transcriptional expression and protein release of pro-osteoclastogenic/inflammatory cytokines (RANKL, Il1b, Il6 and Lcn2), pro-tumoral cytokines (CCL2,5,6,12 and CXCL1,2,5) and the metalloproteinase MMP3. MNNG/HOS-EVs did not induce osteoclast differentiation, while promoting *in vitro* and *in vivo* angiogenesis. Intriguingly, EVs derived from another osteosarcoma cell line (U2OS) reduced ALP activity but had no other effect on osteoblast phenotype. MNNG/HOS-EVs were also found to dramatically increase Serpin b2 expression in osteoblasts. To evaluate the significance of this finding, osteoblasts were forced to overexpress Serpin b2, which however did not affect osteoblast differentiation, while *Il6* and *Lcn2* mRNAs were up regulated. Overall, we shed light on the interactions of osteosarcoma EVs with the cells of the bone microenvironment, identifying key anti-osteoblastogenic, pro-inflammatory and pro-angiogenic factors that could contribute to osteosarcoma expansion.

2. INTRODUCTION

Osteosarcoma is a rare bone tumor having a worldwide incidence of around 3 cases/million per year[1]. Nevertheless, osteosarcoma is the most common primary bone malignancy, predominantly affecting adolescents and accounting for the 5% of all pediatric tumors[2]. Histologically, osteosarcoma is a transformed mesenchymal cell population characterized by a compact core of heterogeneous spindle-shaped cells producing an immature, osteoid-like matrix[3]. While patients with localized disease have a 10-years survival rate of 70%, this is reduced to 10-20% for patients with metastases, which most often affect lungs[4,5]. Therefore, the identification of targetable pathways underlying osteosarcoma onset, progression and metastasis is crucial to improve the prognosis of patients.

Bone tissue is continuously renewed by a critical turnover mechanism named bone remodeling, which involves a series of highly coordinated interactions between the bone-forming osteoblasts and bone-resorbing osteoclasts[6]. Osteoblast-osteoclast crosstalk is mediated by a combination of autocrine, paracrine and juxtacrine signaling. Key examples are the Receptor Activator of NF-κB Ligand (RANKL)/RANK axis and the Macrophage-Colony Stimulating Factor (M-CSF)/c-fms axis, which together stimulate osteoblast-mediated osteoclast formation[7,8]. Activated osteoclasts release H^+ ions and proteases in the underlying resorption lacuna. The former promotes the dissolution of the mineralized matrix, exposing the organic matrix, which is then degraded by the latter[9]. This leads to the subsequent release of pro-osteoblastogenic factors stored in the bone matrix, which stimulate osteoblasts to orchestrate new bone formation and thereby complete the remodeling process[10].

In osteosarcoma, the balance of the remodeling process is disrupted to favor tumor progression. Interestingly, primary osteosarcoma develops in sites where a very active bone remodeling is supposed to occur. They include the metaphysis of long bone, such as distal femur, proximal tibia and proximal humerus, which are the most common sites for osteosarcoma[11,12]. It is quite clear that osteosarcoma cells reduce osteoblast differentiation, tipping the balance of the remodeling process towards net bone loss[13,14], while the role played by osteoclasts in osteosarcoma development seems to be more complex. Indeed, in recent reports a dual role for osteoclasts emerged: they support osteosarcoma development in the early stages of tumorigenesis, while their numbers decrease in later stages[15,16,17]. Some reports show that the lower is the osteoclast number in the primary site, the shorter is the time to presentation of clinical signs of pulmonary metastasis[17,18].

Angiogenesis is another key process in osteosarcoma development and progression. In fact, intratumoral micro vessel density, an index of tumor angiogenesis, is reported as a negative prognostic factor, and several anti-angiogenic compounds have been tested in clinical trials in the attempt to improve the poor prognosis of high-grade osteosarcoma patients[19]. Therefore, mechanisms that underpin the interaction between osteosarcoma cells and bone resident cells hold high potential as a therapeutic target for osteosarcoma.

Extracellular vesicles (EVs) are membrane-enclosed structures that can transfer molecular cargoes between cells, with potent effects on the recipient cells' phenotype under both physiological and pathological conditions[20]. Notably, there is growing evidence that osteosarcoma progression is facilitated by an EV-mediated crosstalk between osteosarcoma cells and cells resident in the tumor microenvironment. Biochemical analysis of osteosarcoma-derived EVs revealed an enrichment of pro-osteoclastogenic cytokines such as CD9, RANKL and TGF-β, the latter of which is known to drive pro-osteoclastic IL-6 production in mesenchymal stem cells and tumorigenesis in later stages of cancer[21,22]. Consistently, in our recent report we showed the ability of osteotropic breast cancer-derived EVs to stimulate osteoclastogenesis and angiogenesis and at the same time inhibit osteoblast differentiation, thus creating a favorable *milieu* for osteolytic bone metastases development[23].

Based on this finding, in our study we sought to broadly investigate an EV-mediated crosstalk between osteosarcoma cells and bone cells. We found that treatment of bone cells with osteosarcoma-EVs promotes a series of anti-osteoblastogenic, pro-inflammatory and pro-angiogenic events that are likely to contribute to the tumor expansion.

3. MATERIALS AND METHODS

3.1 Materials

Dulbecco's modified Minimum Essential Medium (DMEM), Fetal Bovine Serum (FBS), penicillin, streptomycin and trypsin were from GIBCO (Uxbridge, UK). Sterile plasticware was from Falcon Becton- Dickinson (Cowley, Oxford, UK) or Costar (Cambridge, MA, USA). The 3-(4,5-dimethylthiazol-2-yl)-2,5-diphenyltetrazolium (MTT) bromide reduction assay (cat# M2128) was purchased by Sigma Aldrich Co. (St. Louis, MO, USA). The RNeasy MiniTM kit (cat#74104), the RT^2 First Strand Kit (cat# 330401) and the Human Osteoporosis RT^2 Profiler PCR Array (cat# PAHS-170Z) were from Qiagen

(Düsseldorf, Germany). The SYBR Green reagent (cat# QT605) was from Bioline (Memphis, TM, USA), the DreamTaq Green master mix (cat# K1081) was from Thermo Scientific (Waltham, MA, USA), the Eurosafe (cat #EMR440001) was from Euroclone (Milan, Italy). The 5-chloromethylfluoresceindiacetate (CMFDA, cat#C7025) was from Thermo Fisher Scientific (Waltham, MA, USA). The anti-Vegf (cat#sc-7269) -Annexin II (cat# sc-9061) and β-Actin (cat#sc-81,178) antibodies were from Santa Cruz Biotechnology Inc. (Santa Cruz, CA); anti-CD63 antibody (cat#143902) was from BioLegend (San Diego, CA, USA), anti-Serpin b2 antibody (cat#ab137588) was from Abcam (Cambridge, UK). The mouse XL Cytokine Array Kit (cat#ARY028) was purchased from R&D Systems (Minneapolis, MN, USA), while the EIA kits for Tartrate Resistant Acid Phosphatase (TRAcP) 5b (cat# SB-TR103) were from Immunodiagnostic Systems (Park Boldon, UK). The Matrigel Matrix (cat#354262) was purchased by Corning (Corning, NY, USA), the *in vitro* Angiogenesis Assay (cat#ECM625) was from Millipore (Burlington, MA, USA). The endothelial cell growth supplement (ECGS, cat#354006) was from BD Biosciences (Franklin Lakes, NJ, USA).

3.2 Animals

All procedures involving animals and their care were conducted in conformity with national and international laws and policies (European Economic Community Council Directive 86/609, OJ L 358, 1, December 12, 1987; Italian Legislative Decree 4.03.2014 n.26, *Gazzetta Ufficiale della Repubblica Italiana* no. 61, March 4, 2014; National Institutes of Health guide for the Care and Use of Laboratory Animals, National Institutes of Health Publication no. 85–23, 1985) and the Animal Research: Reporting of *in Vivo* Experiments (ARRIVE) guidelines. Animal procedures received approval by the Italian Ministry of Health authority (Approval N. 173/2016-PR).

3.3 Cell lines

The human osteosarcoma cell line MNNG/HOS and U2OS were obtained from the European Collection of Authenticated Cell Cultures (ECACC, Salisbury, UK) and grown in DMEM supplemented with 10% FBS, 100 IU/ml penicillin, 100 µg/ml streptomycin, and 2 mM L-glutamine. Human umbilical vein endothelial cells (HUVECs) were purchased from Lonza (Basel, Switzerland) and cultured in endothelial cell growth medium (EGM)-2. All cells were grown in a humidified 95% air/5% CO_2 incubator at 37 °C.

3.4 Extracellular vesicles (EVs) isolation

EVs were isolated according to Cappariello *et al*[24] and Loftus *et al*[23]. Upon reaching 80% confluence, MNNG/HOS and U2OS cells were washed in PBS and starved in serum-free DMEM to prevent contamination from FBS-EVs. After 24 h, conditioned medium (CM) was collected and sequentially centrifuged at 300 *g*, 4 °C for 5 min to remove dead cells and at 5000 *g*, 4 °C for 25 min to remove membrane debris. The supernatant was collected and transferred to a Beckman L7–65 ultracentrifuge in a Beckman SW41-Ti rotor and centrifuged at 100,000 *g*, at 9 °C for 70 min. Supernatant was discarded, while the pellet, containing EVs, was resuspended in PBS, TRIzol or RIPA buffer according to the experimental needs.

3.5 Transmission electron microscopy (TEM)

Five µl of EVs isolated from MNNG/HOS conditioned medium (12 ml collected from one 175 cm^2 flask, cell density = 6.5 × 10^4 cells/cm^2) were put onto Formvar-coated grids and allowed to air-dry. Grids were washed in PBS and fixed in 1% glutaraldehyde for 5 min. Samples were washed in distilled water and contrasted with 4% uranyl-oxalate solution for 5 min. Grids were air-dried for 10 min and observed under a Philips CM 30 TEM, 80 kV.

3.6 EV internalization assay

Extracellular vesicles derived from 12 ml of CM collected from one 175 cm^2 flask, cell density = 6.5 × 10^4 cells/cm^2, were incubated at 37 °C with the membrane-permeant green fluorescent dye 5-chloromethylfluoresceindiacetate (CMFDA) for 30 min followed by 5 min at 37 °C with the red fluorescent membrane-labeling dye PKH26 (Sigma-Aldrich; #MINI26-1KT). Then, the EVs were washed in PBS and ultracentrifuged at 100,000 *g*, at 4 °C for 70 min. Finally, EVs were resuspended in PBS for the treatment. Target cells were incubated with stained or unstained EVs for 24 h before microscopic assessment of internalization.

3.7 Osteoblast primary cultures

Calvariae from 7-day-old CD1 mice were explanted, cleaned free of soft tissues, and digested three times with 1 mg/ml Clostridium histolyticum type IV collagenase and 0.25%

trypsin, for 15, 30 and 45 min at 37 °C, with gentle agitation. Supernatant from the first digestion was discarded, while those of the second and third digestion were centrifuged at 300 *g* for 7 min and cells were resuspended and cultured in DMEM plus 10% FBS. At confluence, cells were trypsinized and plated according to the experimental protocol.

3.8 Alkaline phosphatase (ALP) activity assay

Primary mouse osteoblasts were fixed in 4% buffered paraformaldehyde (PFA) for 15 min and washed twice with PBS. Alp activity was evaluated cytochemically by the Sigma-Aldrich kit#85, according to the manufacturer's instruction.

3.9 Mineralization assay

For mineralization assay, standard medium (DMEM+10% FBS) was supplemented with 10 mM β-glycerophosphate and 50 µg/ml ascorbic acid. Osteoblasts were cultured for 7 days with or without MNNG/HOS-EVs prior to assay for mineralization by von Kossa staining.

3.10 Osteoclast primary cultures

Femurs and tibiae of 7-day-old CD1 mice were cleaned of soft tissues and cut with sterile blade. Bone marrow was collected, diluted 1:1 in Hank's Balanced Salt Solution (HBSS), layered over Histopaque 1077 solution and centrifuged at 400*g* for 30 min. Cells of the buffy coat were recovered, washed twice with HBSS, resuspended in DMEM plus 10% FBS and plated in culture dishes at a density of 1×10^6 cells/cm^2 [25]. After 3 h, cultures were washed with PBS to remove non-adherent cells and maintained for 7 days in the same medium supplemented with 50 ng/ml human recombinant (hr)Macrophage- Colony Stimulating Factor (M-CSF, negative control) and with hrM-CSF plus 120 ng/ml hrRANKL as positive control. According to the experimental protocol, cultures were also treated with 50 ng/ml M-CSF plus MNNG/HOS-EVs or osteoblast CM (dilution 1:4) or osteoblast CM pre-treated with MNNG/HOS-EVs (dilution 1:4). Multinucleated mature osteoclasts were detected by cytochemical staining of Tartrate Resistant Acid Phosphatase (TRAcP) activity according to the manufacturer's instructions, and the number of nuclei was counted by counterstaining with DAPI. TRAcP-positive area was evaluated using NIH ImageJ.

3.11 Bone resorption assay

Mature osteoclasts obtained after 7 days of culture with hrM-CSF and hrRANKL, as above described, were detached by trypsin/EDTA procedure, replated onto bone slices in equal numbers and cultured for further 3 days with or without MNNG/HOS-EVs. Afterwards, bone slices were collected, cells were gently removed, and slices were stained with 0.1% toluidine blue to detect the resorption pits. Quantification of the pits was performed using the NIH Image J software.

3.12 Evaluation of bone turnover markers on conditioned media

Conditioned media from osteoclasts cultured on bone slices were harvested at endpoint, centrifuged at 400 *g* for 10 min to remove cells and subjected to EIA assay for TRAcP determination following the manufacturer's instruction.

3.13 Cell metabolic activity

Metabolic activity was assessed by the 3-(4,5-dimethylthiazol-2-yl)-2,5-diphenyltetrazolium (MTT) bromide reduction assay, following the manufacturer's protocol.

3.14 Crystal violet assay

Osteoblasts and HUVECs cell density were assessed by crystal violet nuclear staining. Cells were fixed in 4% buffered PFA for 15 min, washed twice in PBS, then stained with 0.5% crystal violet in 20% methanol for 5 min before rinsing with distilled water and air drying for 15 min. Crystal violet was then dissolved in 100 µl of methanol and the absorbance was evaluated at 595 nm in an ELISA plate reader.

3.15 *In vitro* tube formation assay

In vitro tube formation assay was performed according to Kubota *et al*[26] and Loftus *et al*[23]. Fifteen-well µ-slides were coated with Matrigel and allowed to solidify at 37 °C for 30 min, then 1.5 × 10^4/well HUVECs were plated and treated with MNNG/HOS-EVs, U2OS-EVs or Endothelial Growth Medium (EGM)-2 (dilution 1:3) as positive control. After 16 h, tube formation was evaluated under an inverted light microscope. Pictures were taken

and the % of branching points/area was evaluated (Branching Index) using an ImageJ extension plugin for angiogenesis analysis.

3.16 Matrigel plug assay

Eight-week-old male mice were subcutaneously injected (ventral area) with 0.4 ml Matrigel plus 0.1 ml PBS (negative control), 0.1 ml of EVs isolated from MNNG/HOS CM (MNNG/HOS-EVs) or 0.1 ml containing endothelial cell growth supplement (ECGS) plus 150 ng/ml hrVEGF as positive control. After 10 days mice were sacrificed, the plugs were removed, fixed in 4% buffered PFA, and processed for histological analysis.

3.17 RT^2 profiler real time PCR array

RNA was isolated from MNNG/HOS cells and from MNNG/HOS-EVs using the RNeasy Mini kit (Qiagen), then the RNA was retrotranscribed employing the RT^2 First Strand Kit (Qiagen), according to the manufacturer's instructions. cDNAs were mixed with the RT SYBR Green qPCR master mix and dispensed in the wells of the human osteoporosis PCR array. Wells were subjected to real-time PCR (Stratagene MX 3000P), following the manufacturer's instructions. Array data were automatically analyzed by a dedicated online software (Qiagen).

3.18 Comparative real time RT-PCR

RNA was extracted using TRIzol reagent, then 1 μg of RNA was reverse-transcribed into cDNA using the Moloney Murine Leukemia Virus (M-MLV) reverse transcriptase and subjected to real time RT-PCR using primer pairs and amplification conditions described in Table 1. All reactions were carried out using a SYBR green based master mix containing ROX as reference dye. Data were analyzed *via* dedicated software (MxPro, Stratagene, La Jolla, CA) using the ΔΔCt method and Gapdh was chosen as the housekeeping gene.

Table 1: Mouse primer sequences (5' to 3'). Primers were designed to anneal at 60°C.

Gene ID	Forward primer	Reverse primer
Gapdh	TGGCAAAGTGGAGATTGTTGC	AAGATGGTGATGGGCTTCCCG
Alp	CCAGCAGGTTTCTCTCTTGG	CTGGGAGTCTCATCCTGAGC

Runx2	AACCCACGGCCCTCCCTGAACTCT	ACTGGCGGGGTGTAGGTAAAGGTG
Rankl	CCAAGATCTCTAACATGACG	CACCATCAGCTGAAGATAGT
Opg	AAAGCACCCTGTAGAAAACA	CCGTTTTATCCTCTCTACACTC
Osx	TGCTTCCCAATCCTATTTGC	AGAATCCCTTTCCCTCTCCA
Bglap	TTCTGCTCACTCTGCTGACC	GGGACTGAGGCTCCAAGGTA
Col1a1	GTCCCTCTGGAAATGCTGGAC	GACCGGGAAGACCGACCA
M-csf	GCTCCTGCCTACCAAGACTG	GCTGTCCCACCCTTTGAATA
Il1b	GCCCATCCTCTGTGACTCAT	AGGCCACAGGTATTTTGTCG
Il6	GAGGATACCACTCCCAACAGACC	AAGTGCATCATCGTTGTTCATACA
Lcn2	CCAGTTCGCCATGGTATTTT	CACACTCACCACCCATTCAG
Nos2	CACCTTGGAGTTGACCCAGT	ACCACTCGTAGTTGGGATGC
Vegf	CCCTTCCTCATCTTCCCTTC	CACCGATCTGGGAGAGAGAG
Serpin b2	AATCCCAAACCTGCTACCCG	TCTCATGCGAGTTCACACGG
p16INK	CGAACTCGAGGAGAGCCATC	CATCATCACCTGAATCGGGGT
Glb1	GCCTATTGGAATGGTGCCAAC	GGATACCCAGAGCTTCAGCC
p21	ATCCAGACATTCAGAGCCACAG	CATGAGCGCATCGCAATCAC
P19ARF	TCGCAGGTTCTTGGTCACTG	CCCATCATCATCACCTGGTCC
Lamin B1	GCTGCTGCTCAATTATGCCAA	TAACTGCTTTTTGGCGGCAG
Cyclin D1	TCAAGTGTGACCCGGACTG	ATGTCCACATCTCGCACGTC
Aurka	AATATGCGCCCCTTGGAACA	CCACCCGAAGTCTGCAATCT
Ki67	AGAGCTAACTTGCGCTGACT	TCAATACTCCTTCCAAACAGGCA
Ercc5	GACCTTGGCAAAGAGAAGGCA	TCCCCAAGTCCAACGCTATC
Ccl2	ATGCAGTTAATGCCCCACTC	TTCCTTATTGGGGTCAGCAC

3.19 Endpoint RT-PCR

RNA was extracted using TRIzol reagent, reverse transcribed using the M-MLV reverse transcriptase and subjected to PCR amplification with the DreamTaq Green master

mix using primer pairs and amplification conditions described in Table 2. The PCR products were run in a 2% agarose gel stained with an ethidium bromide substitute (Eurosafe Gold) to detect the amplified DNA bands under UV.

Table 2: Human primer sequences (5' to 3'). Primers were designed to anneal at 60°C.

Gene ID	Forward primer	Reverse primer
BGLAP	GACTGTGACGAGTTGGCTCA	GCCCACAGATTCCTCTTCTG
CATHK	CTTCCAATACGTGCAGCAGA	CCGAGCCAAGAGAGCATATC
CD40	GAGATCAATTTTCCCGACGA	GCTCCAGGGTGAAGTGAGAG
CLCN7	GATTTCAAGATCTTCGAGTACTTCC	TGATTCGAAACATGGTCAGC
GAPDH	CCATCTTCCAGGAGCGAGAT	CAGTGATGGCATGGACTGTG
ITGB3	GACAAGGGCTCTGGAGACAG	ACTGGTGAGCTTTCGCATCT
OPG	GGCAACACAGCTCACAAGAA	GTGTCTTGGTCGCCATTTTT
SOST	GAGCAGCCATCACAAACTCA	CAAGTCCCACGTGGAAGAAT
VEGF	CTACCTCCACCATGCCAAGT	GCAGTAGCTGCGCTGATAGA

3.20 Cytokine array

One ml of conditioned media recovered from mouse primary osteoblasts treated with MNNG/HOS-EVs or with PBS as control were incubated overnight at 4 °C with the nitrocellulose membranes of the Mouse XL Cytokine Array Kit, which includes 111 capture antibodies printed in duplicate. The membranes were then washed three times and incubated with the detection antibody cocktail for 1 h at room temperature. After 3 washes, a 30 min incubation with the Streptavidin-HRP solution was performed, then membranes were washed and incubated with the Chemi Reagent mix for the detection of the positive spots by chemiluminescence. For data analysis, the intensity of each spot was determined by densitometry, and the average background subtracted. Protein expression was normalized by calculating the ratio between the signal intensity of the protein of interest and that of the housekeeping proteins.

3.21 Western blot analysis

Mouse primary osteoblasts, MNNG/HOS or U2OS cells and MNNG/HOS- or U2OS-EVs were lysed in RIPA buffer containing phosphatase and protease inhibitors. Fifty µg of cell protein and 8 µg of EV protein lysates were resolved by 12% SDS-PAGE under reducing conditions and transferred to nitrocellulose membranes. Blots were incubated with the primary antibody for 1 h at room temperature or overnight at 4 °C, washed and incubated with the appropriate HRP-conjugated secondary antibody for 1 h at room temperature. Protein bands were visualized with a chemiluminescence reaction kit, according to the manufacturer's instructions and imaged on a BioRad ChemiDoc XR Gel Imaging System.

3.22 Statistics

Results are expressed as the mean ± SD of at least three independent experiments, as specified in the figure legends. Statistical analyses were performed using the unpaired Student's *t*-test, conducted either on raw data or on the curves, according to the type of data. The statistical method is indicated in the figure legends. A p value ≤ 0.05 was considered statistically significant.

4. RESULTS

4.1 MNNG/HOS-EV characterization and bone transcriptional profiling

We first characterized the EVs isolated from MNNG/HOS conditioned media. EV size was confirmed by NanoSight, which also allowed to determine the EV concentration per preparation (Fig. 1A). The typical EV biomarkers, Annexin II and CD63, were enriched in the EV protein lysates *versus* the source cells (Fig. 1B). CD63 showed a broad band, consistent with the extensive glycosylation of this member of the tetraspanin family (Fig. 1B). The vesicular nature of the isolated particles was confirmed by TEM, which also showed the EV membrane integrity (Fig. 1C). Altogether, these results fulfil the requirements described in the MISEV2018 guidelines[27] to define a vesicular fraction as EVs.

We next investigated the transcriptional profile of the MNNG/HOS-EVs to assess if they expressed mRNAs typical of bone cells. To this end, the RNA from MNNG/HOS-EVs was subjected to the RT^2 Profiler Real Time PCR Array, which includes 84 genes involved in the bone remodeling process. Twelve of these genes met the quality controls and cut-offs

determined by our analysis (Table 3) and most of them were confirmed by semiquantitative RT-PCR (Fig. 1D). Interestingly, MNNG/HOS-EVs contained mRNAs of key factors involved in osteoclast functions [*Cathepsin K (CATHK), Chloride Voltage-Gated Channel 7 (CLCN7), Integrin β3 (ITGB3)* and *CD40*], as well as genes associated with the osteoblast phenotype [*COL1A1, Bone Gamma-carboxyglutamic Acid-containing Protein (BGLAP), Osteoprotegerin (OPG)* and *Sclerostin (SOST)*]. This profile mirrors the transcriptional content of the MNNG/HOS cells (Fig. 1D).

Table 3 – Osteoporosis RT² array results on HOS-EVs mRNA. The raw gene expression value (2^{-Ct}) of genes with an amplification threshold cycle (Ct) < 20 are reported. Results are from one MNNG/HOS-EVs preparation.

Gene name	Gene symbol	mRNA expression (2^{-Ct})
Chloride voltage-gated channel 7	*CLCN7*	1.56E-04
Cathepsin K	*CTSK*	3.12E-06
Interleukin-6 receptor α	*IL6RA*	2.36E-06
Vascular endothelium growth factor A	*VEGFA*	1.56E-06
Integrin β3	*ITGB3*	1.50E-06
Osteoprotegerin	*OPG*	1.39E-06
Sclerostin	*SOST*	1.38E-06
Collagen 1 α1 chain	*COL1A1*	1.34E-06
Cluster of differentiation 40	*CD40*	1.33E-06
Bone gamma-carboxyglutamic acid-containing protein	*BGLAP*	1.07E-06
Transforming growth factor β1	*TGFB1*	1.06E-06
Interleukin-6	*IL6*	9.94E-07

4.2 MNNG/HOS-EVs integration into recipient bone cells *in vitro*

We next investigated whether MNNG/HOS-EVs were actively internalized by bone cells. MNNG/HOS-EVs were double-labeled with the intra-vesicular green-fluorescent dye, CMFDA, and with the red-fluorescent membrane dye, PKH26. Mouse primary osteoclasts and osteoblasts were then incubated with these EVs for 24 h. Confocal microscopy demonstrated that PKH26 and CMFDA fluorescence was detectable in both cell types,

suggesting internalization of MNNG/HOS-EVs by these recipient bone cells (Fig. 1E,F). Negative controls treated with unstained EVs confirmed specificity of the signal (Fig. 1G,H).

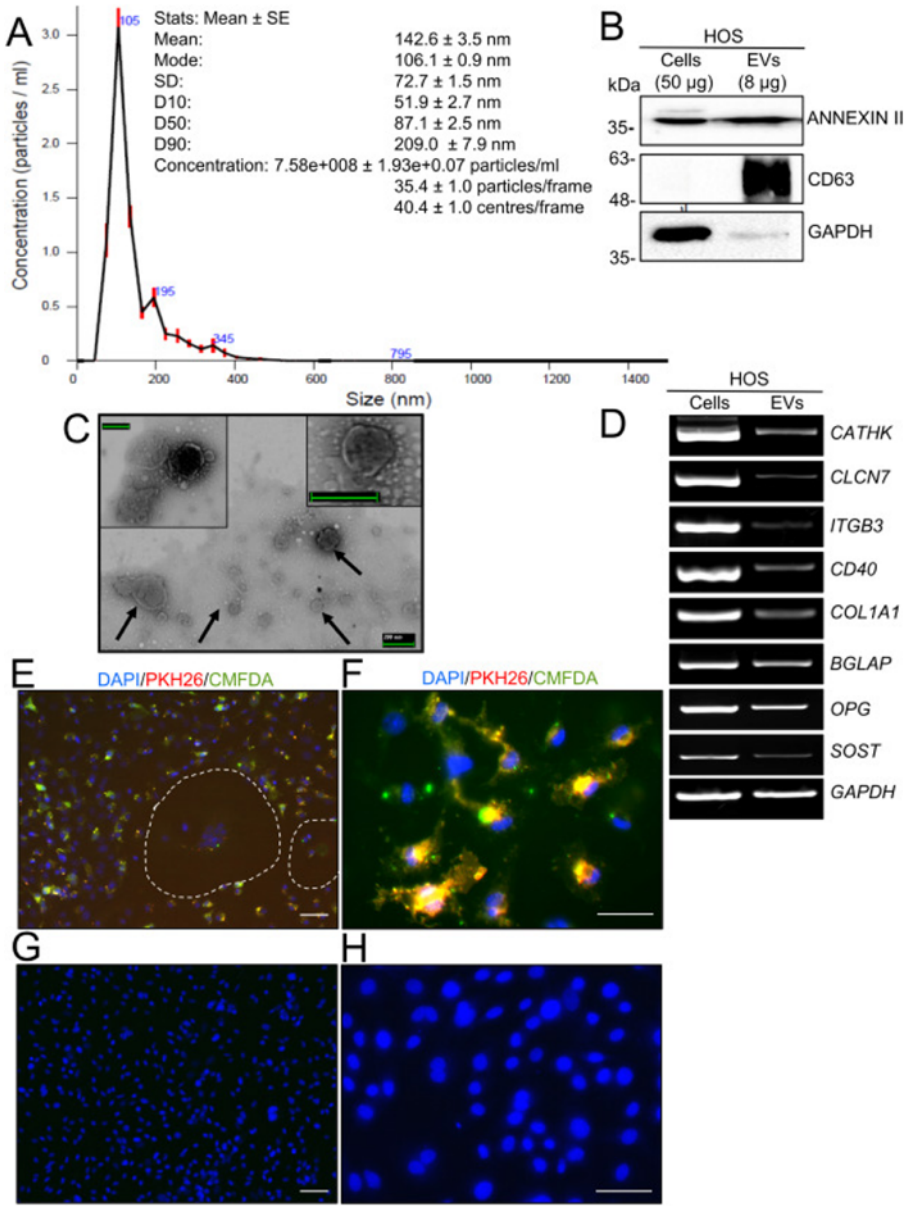

Figure 1: Characterization of MNNG/HOS-EVs. MNNG/HOS cells were starved in serum-free DMEM for 24 h and EVs were isolated from their conditioned medium (CM) by ultracentrifugation. (**A**) Size and concentration determination of MNNG/HOS-EVs (isolated from 12 ml of CM collected from one 175 cm^2 flask, cell density = 6.5×10^4 cells/cm^2) by nanoparticle tracking analysis (NanoSight NS3000). (**B**) Western blot for the EV markers ANNEXIN II and CD63, and for GAPDH as loading control in protein lysates extracted from MNNG/HOS cells and MNNG/HOS-EVs (50 and 8 µg, respectively). (**C**) Evaluation of MNNG/HOS-EVs morphology by transmission electron microscopy. Arrows: MNNG/HOS-EVs. (**D**) Semi-quantitative RT-PCR of MNNG/HOS cells and MNNG/HOS-EVs RNA to assess transcriptional expression of *Cathepsin K (CATHK), Chloride voltage-gated channel 7 (CLCN7), Integrin Beta 3 (ITGB3), CD40, Collagen Type 1 alpha 1 (COL1A1), BGLAP* encoding for *Osteocalcin, Osteoprotegerin (OPG), Sclerostin (SOST),* and *Glyceraldehyde-3-Phosphate Dehydrogenase (GAPDH)*. (**E,F**) Representative fluorescence micrographs of (**E**) primary murine bone marrow mononuclear cells and (**F**) primary murine osteoblasts incubated with MNNG/HOS-EVs previously labeled with CMFDA (green cytoplasmic dye) and PKH26 (red lipophilic dye) for 24 h. Cells were also stained

with the nuclear dye DAPI. (**G,H**) Representative images of the negative control performed on (**G**) primary murine bone marrow mononuclear cells and (**H**) primary murine osteoblasts incubated with unlabeled MNNG/HOS-EVs. Data are (A) the mean or (B–H) representative of 3 independent preparations (scale bar: C = 200 nm; E,G = 20 μm; F,H = 10 μm).

4.3 Effect of MNNG/HOS-EVs on osteoblast differentiation and activity

We next evaluated the effect of MNNG/HOS-EVs on primary osteoblast cultures. We measured osteoblast cell density by crystal violet staining and observed that it was reduced *versus* control at all timepoints investigated (Fig. 2A). Metabolic activity, evaluated by the MTT assay, was also decreased (Fig. 2B), along with Alp activity, investigated by cytochemistry (Fig. 2C,D). Since MNNG/HOS-EVs affect osteoblast number, we quantified the number of Alp positive cells over total number of cells, the latter evaluated by neutral red counterstaining. Under these conditions, we still found a significant decrease of Alp activity (Fig. 2E) thus suggesting that MNNG/HOS-EVs affect both osteoblast number and differentiation. To investigate whether MNNG/HOS-EVs could also affect osteoblast activity, cells were maintained in culture in presence of osteogenic medium (10 mM β-glycerophosphate +50 μg/ml ascorbic acid). We observed a trend of increase ($p = 0.09$) of % Alp positive cells in control cultures at 7 days *versus* 2 days of culture. However, we could not observe any differences in the % Alp positive cells in cultures treated with MNNG/HOS-EVs compared to control, neither at 2 nor at 7 days of culture (Fig. 2F). At day 7 of culture, we also noted a trend of reduction ($p = 0.08$) of the total cell number in MNNG/HOS-EVs treated osteoblasts compared to control (Fig. 2G). Next, we performed von Kossa staining to detect the formation of nuclei of mineralization, finding no significant differences (Fig. 2H). Of note, we should specify that the latter analysis was performed at 7 days of culture, since when cultures were prolonged over this time, we observed a complete detachment of the cell monolayer subjected to treatment with EVs. Finally, the transcriptional profile showed that MNNG/HOS-EVs induced significant downregulation of the cell cycle associated genes *Cyclin D1, Aurora kinase A (Aurka), Ki67* and *Excision repair cross-complementing 5 (Ercc5)* (Fig. 2I), the latter involved in DNA repair. Moreover, the mRNA expression of osteoblast differentiating genes, including *Alp, Runt related transcription factor 2 (Runx2), Osterix (Osx), Collagen 1a1 (Col1a1)* and *Bglap*, was also reduced by treatment with MNNG/HOS-EVs (Fig. 2I).

To broaden the scope of our investigation, osteoblasts were treated with EVs isolated from the human osteosarcoma epithelial cell line U2OS (Fig. 3A), which however did not influence their number (Fig. 3B) or metabolic activity (Fig. 3C). Intriguingly, Alp activity,

evaluated by densitometry, showed a slight reduction in osteoblasts treated with U2OS-EVs (Fig. 3D,E).

Taken together, these results suggest a negative role for MNNG/HOS-EVs on osteoblast differentiation, while U2OS-EVs were able to reduce Alp activity, but not osteoblast metabolic activity or number.

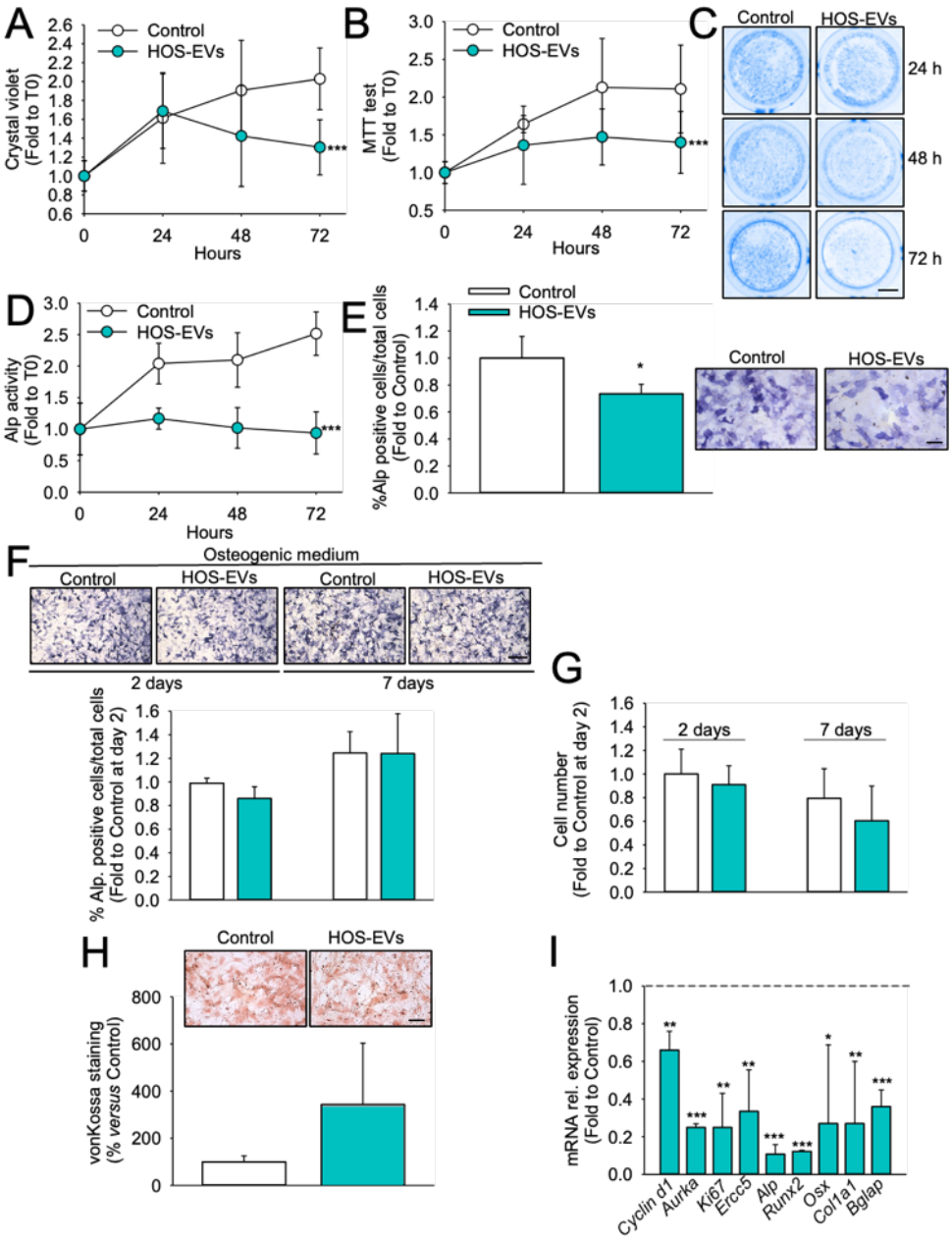

Figure 2: Effect of MNNG/HOS-EVs on osteoblasts. (**A-E**) Primary murine osteoblasts were starved in serum-free DMEM overnight and cultured in DMEM as control or with MNNG/HOS-EVs (isolated from 12 ml of CM collected from one 175 cm^2 flask, cell density = 6.5 × 10^4 cells/cm^2) for the times indicated in the abscissa. (**A**) Cell density estimated by crystal violet staining. (**B**) Cell metabolic activity assessed by the MTT assay. (**C**) Cytochemical staining of Alp activity (scale bar = 2 mm); (**D**) densitometric quantification of Alp positive cells and (**E**) quantification of the percent of Alp positive cells over total cells after 48 h, expressed as fold to control (inset: Alp activity staining, scale bar =100 µm). (**F– H**) Primary murine osteoblasts were

cultured for 2 and 7 days in osteogenic medium (10 mM β-glycerophosphate and 50 µg/ml ascorbic acid) supplemented or not with MNNG/HOS-EVs (isolated from 12 ml of CM collected from one 175 cm^2 flask, cell density = 6.5 × 10^4 cells/cm^2). (**F**) Quantification of the percentage of Alp positive cells over total cells (scale bar =500 µm) and of (**G**) total cell number. (**H**) Evaluation of the mineralization after 7 days of culture by von Kossa staining (scale bar =100 µm). (**I**) Primary murine osteoblasts were treated as described in (A), then the RNA was extracted, reverse transcribed and subjected to real time RT-PCR to evaluate the transcriptional expression of the cell cycle genes *Cyclin d1, Aurka, Ki67 and Ercc5* and osteoblastogenic genes *Alp, Runx2, Osx, Col1a1 and Bglap*. Results are the mean ± SD of 3 independent experiments (*p < 0.05, **p < 0.01, and ***p < 0.001 versus control, Student's t-test; dot line = control set at 1).

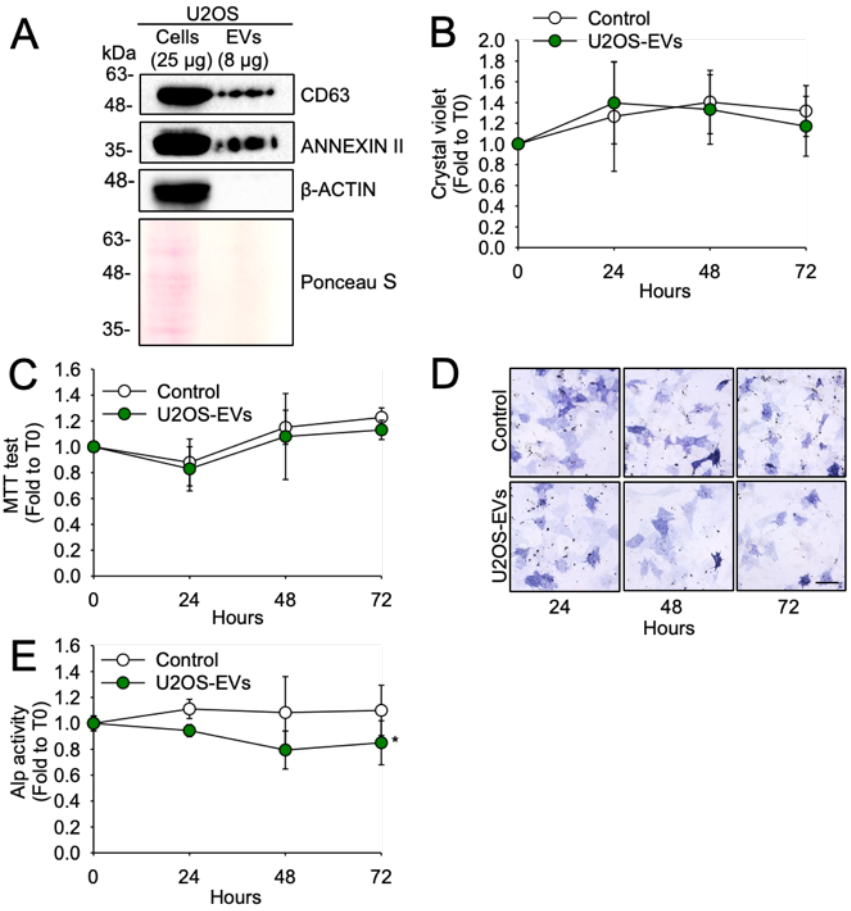

Figure 3. Effect of U2OS-EVs on osteoblast differentiation. (**A**) Western blot for the EV markers Annexin II and CD63 in protein lysates extracted from U2OS cells and U2OS-EVs (25 and 8µg, respectively). (**B-E**) Primary murine osteoblasts were starved in serum-free DMEM overnight and cultured in DMEM as control or were treated with U2OS-EVs (isolated from 12 ml of CM collected from one 175 cm^2 flask, cell density = 6.5x10^4 cells/cm^2) for the times indicated in the abscissa. (**B**) Cell density estimated by crystal violet staining. (**C**) Cell metabolic activity assessed by the MTT assay. (**D**) Cytochemical staining of Alp activity (scale bar = 100 µm); (**E**) densitometric quantification of Alp activity at the times indicated in the abscissa. Results are the mean ± SD of 3 independent experiments.

4.4 Effect of MNNG/HOS-EVs on osteoclast differentiation and activity

We then evaluated the effect of MNNG/HOS-EVs on primary osteoclast cultures. TRAcP cytochemical activity (Fig. 4A) revealed a positive signal in mouse bone marrow mononuclear cells treated with MNNG/HOS-EVs compared to the negative control where, as expected, cells were TRAcP negative (Fig. 4A,B). Indeed, when looking at the size of these cells, we observed significantly more TRAcP-positive mono/ binucleated cells compared to untreated cultures, while medium or large osteoclasts (number of nuclei >3) were not present (Fig. 4C). The positive control, obtained by treatment of bone marrow mononuclear cells with 120 ng/ml hrRANKL, confirmed the ability of the culture to form multinucleated osteoclasts in standard osteoclastogenic conditions (Fig. 4A-C). Interestingly, DAPI staining showed a significantly lower number of cells in MNNG/HOS-EV-treated cultures compared to both negative and positive controls (Fig. 4D), suggesting impairment of osteoclast precursor expansion. To better characterize the phenotype of the TRAcP positive cells arising from the treatment of bone marrow mononuclear cells with MNNG/HOS-EVs, we performed immunofluorescence for the mouse macrophage marker F4/80[28,29], which is usually lost during osteoclastogenic differentiation, but is well expressed in precursor cells. The results show that, as expected, the % of F4/80-positive cells is strongly reduced in the positive control *versus* negative control, while MNNG/HOS-EVs treated cells are in between, and do not lose expression of F4/80 completely, which could indicate a switch to- wards a macrophage phenotype (Fig. 4E). We then further characterized these cells by gene expression analysis to confirm whether there was a switch towards a macrophage phenotype, and whether fusion genes were affected. The results showed that, compared to mature osteoclasts (PosCtrl) the macrophage marker integrin Subunit Alpha M (*Itgam*, a.k.a. CD11b)[30] was unremarkable in MNNG/HOS-EVs treated cells, whereas *Rank*, a pre-osteoclast/osteoclast marker[31], and the important fusion genes macrophage fusion receptor (*Mfr*) and *Cd44* were strongly downregulated in MNNG/HOS-EVs treated cells compared to PosCtrl (Fig. 4F).

We next allowed osteoclasts to differentiate in presence of 120 ng/ml rhRANKL and after 7 days of culture mature osteoclasts were detached and replated onto bone slices in equal numbers to assess their activity in the presence MNNG/HOS-EVs. However, this treatment did not alter the resorption pit formation, compared to untreated osteoclasts (Fig. 4G). Evaluation of TRAcP activity on CM collected from these cultures confirmed that the number of osteoclasts plated for the two experimental conditions was similar (Fig. 4H). To investigate whether MNNG/HOS-EVs could exert a pro-osteoclastogenic effect through

osteoblasts, we treated osteoclast precursors with CM harvested from osteoblasts pretreated with MNNG/HOS-EVs, finding no effect (Fig. 5).

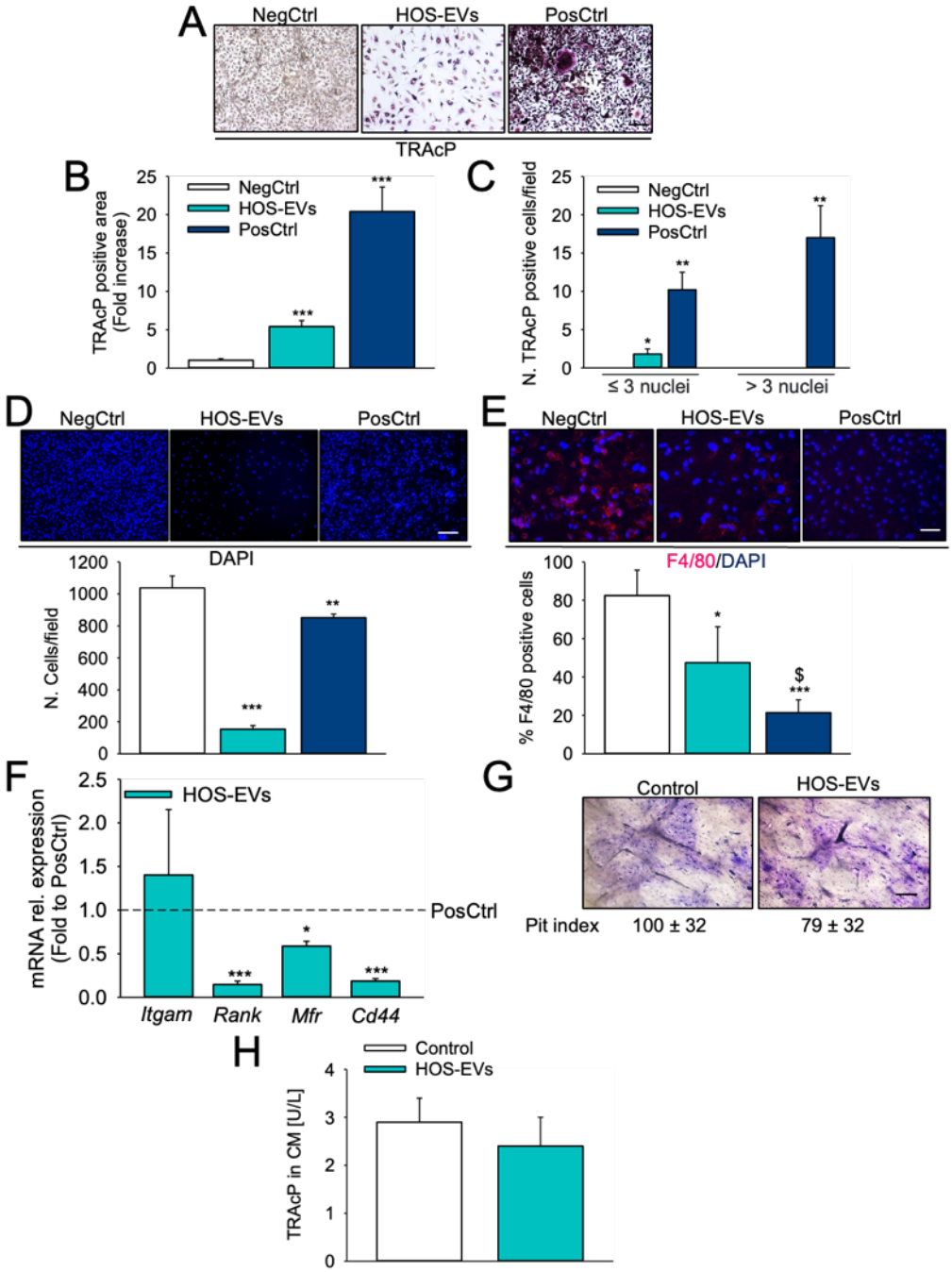

Figure 4. Effect of MNNG/HOS-EVs on osteoclast differentiation and function. (**A-F**) Mouse bone marrow mononuclear cells were untreated (NegCtrl), treated with MNNG/HOS-EVs or with hrRANKL (120 ng/ml) (PosCtrl). (**A**) Cytochemical evaluation of TRAcP activity to assess the number of TRAcP positive multinucleated cells (scale bar = 50 μm). (**B**) Quantification of TRAcP positive area by software-assisted analysis. (**C**) Evaluation of TRAcP positive cell numbers stratified according to the number of nuclei (TRAcP-positive cells with a number of nuclei ≤3 or > 3). (**D**) Cells were counterstained with DAPI to assess cell density (scale bar = 100 μm). (**E**) Mouse bone marrow mononuclear cells were treated as described above, fixed and subjected to immunofluorescence staining for the F4/80 macrophage marker. F4/ 80+ cells were counted and reported as % of the total cells, assessed by DAPI staining (scale bar =50 μm). (**F**) Mouse bone

marrow mononuclear cells were treated with MNNG/HOS-EVs or with hrRANKL (PosCtrl) as described in (A), then RNA was extracted, reverse transcribed and subjected to real time PCR to evaluate the expression of Integrin Subunit Alpha M (*Itgam*), *Rank*, Macrophage fusion receptor (*Mfr*) and *Cd44*. (**G,H**) Mouse bone marrow mononuclear cells were treated with hrRANKL (120 ng/ml). After 7 days of culture mature osteoclasts were detached, replated onto bone slices, and cultured for additional 3 days in presence of MNNG/ HOS-Evs. (**G**) Pit index and representative images of pits (scale bar = 100 µm); (**H**) ELISA assay to determine TRAcP activity in the conditioned media (CM) collected from the osteoclast cultures performed onto bone slices. Results are the mean ± SD of at least 3 independent experiments (*p = 0.03, **p < 0.01 and ***p < 0.001 versus NegCtrl, $p < 0.05 *versus* HOS-Evs, (F)*p < 0.05 and ***p < 0.001 *versus* PosCtrl, Student's t-test).

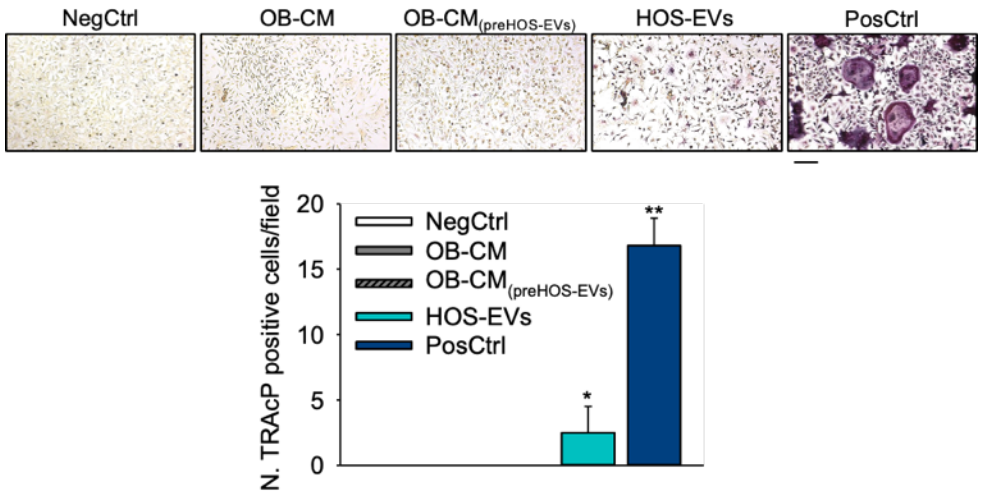

Figure 5. Effect of osteoblast conditioned medium on osteoclast differentiation. Mouse bone marrow mononuclear cells were untreated (NegCtrl), treated with osteoblast conditioned medium (OB-CM, dilution 1:4), conditioned medium from osteoblasts pretreated with MNNG/HOS-EVs ($OB\text{-}CM_{preHOS\text{-}EVs}$), MNNG/HOS-EVs (HOS-EVs) or with hrRANKL (120 ng/ml) (PosCtrl). TRAcP activity to assess the number of TRAcP positive cells (scale bar = 50µm). Results are the mean ± SD of 4 independent experiments (*p = 0.04 and **p = 0.007 *versus* NegCtrl, Student's t test).

4.5 Effect of MNNG/HOS-EVs on osteoblast inflammatory and osteoclastogenic cytokines

Cancer cells colonizing the bone stimulate osteoblasts to express factors promoting tumor growth[32]. To assess whether this effect could be mediated by EVs, the transcriptional expression of inflammatory and osteoclast-regulating cytokines was analyzed in primary osteoblasts treated with MNNG/HOS-EVs. Of note, MNNG/HOS-EVs increased the transcriptional expression of *C-c motif chemokine ligand 2 (Ccl2), Interleukin 1b (Il1b)* and *Il6*, known to inhibit osteoblasts and stimulate osteoclast function[9,10], and *Lipocalin 2 (Lcn2)* (Fig. 6B), which in our hand proved to inhibit osteoblast differentiation[33]. We also found a trend of upregulation of the pro-osteoclastogenic cytokine *Rankl* in MNNG/HOS-EV-treated osteoblasts compared to control, while *Opg* and *Csf1* were unchanged (Fig. 6A).

Upregulation of RANKL, IL1β, IL6 and Lcn2 was also confirmed at protein level, as demonstrated by ELISA assay carried out on conditioned media (CM) of osteoblasts treated with MNNG/HOS-EVs (Fig. 6C).

To widen our investigation on the impact of MNNG/HOS-EVs in the release of cytokines by osteoblasts, CM collected from untreated or MNNG/HOS-EV-treated osteoblasts were subjected to a cytokine array, which allows simultaneous detection of the most important cytokines, chemokine and growth factors influencing tumor growth (Fig. 6D). MNNG/HOS-EVs stimulated osteoblast release of C–C motif Chemokine Ligand (CCL)2 (Fig. 6D,E), whose upregulation was also observed at transcriptional level (Fig. 6B), as well as CCL5, 6 and 12, CXC motif Chemokine Ligand (CXCL) 1, 2 (*alias* macrophage inflammatory protein-2) and 5 (also known as LPS-induced chemokine, LIX) and Matrix Metalloprotease (MMP) 3 (Fig. 6D,E).

Dissecting the influence of MNNG/HOS-EVs on osteoblasts allowed us to identify another molecule highly modulated both at transcriptional and protein level: Serpin b2, *alias* Plasminogen Activator Inhibitor (PAI)-2 (Fig. 7A). Western blot analysis confirmed the increase of Serpin b2 at protein level, (Fig. 7B) showing a positive signal at the expected molecular weight, that is 47 kD, and a lower band, which could represent a cleaved form, as described by Ye *et al*[34]. Intriguingly, Serpin b2 was not derived from MNNG/HOS cells since they showed no expression both at the transcriptional (Fig. 7C) and protein level (Fig. 7D). Serpin b2 is overexpressed in some tumors compared to normal tissues and has been associated with a poor prognosis in cancer patients[35]. It is also involved in the regulation of cellular senescence[36]. We therefore transiently transfected osteoblasts with Serpin b2 (Fig. 7E,F). This overexpression did not affect Alp activity (Fig. 7G), while investigating the transcriptional expression of osteoblastogenic genes a trend of reduction ($p = 0.06$) was observed for *Alp* (Fig. 7H). Of note, Serpin b2 overexpression failed to affect the mRNA of genes regulating osteoclastogenesis, while it significantly upregulated *Il6* and *Lcn2* mRNA, and a trend of increase was observed for *Il1b* (Fig. 7I). Finally, since Serpin b2 is known to play a role in cell senescence, we evaluated whether its overexpression could affect this process in osteoblast by analyzing the expression of *Glb1*, encoding for the senescence gene β galactosidase 1, *p19ARF* and *Lamin B1*, finding them reduced in Serpin b2 overexpressing osteoblasts, while *p16INK*, and *p21* mRNAs were unchanged compared to controls (Fig. 7L).

Taken together, these results highlight an inhibitory effect of MNNG/HOS-EVs on osteoblast differentiation as well as a stimulatory effect on osteoblast's expression and release of pro-inflammatory and pro-tumoral cytokines.

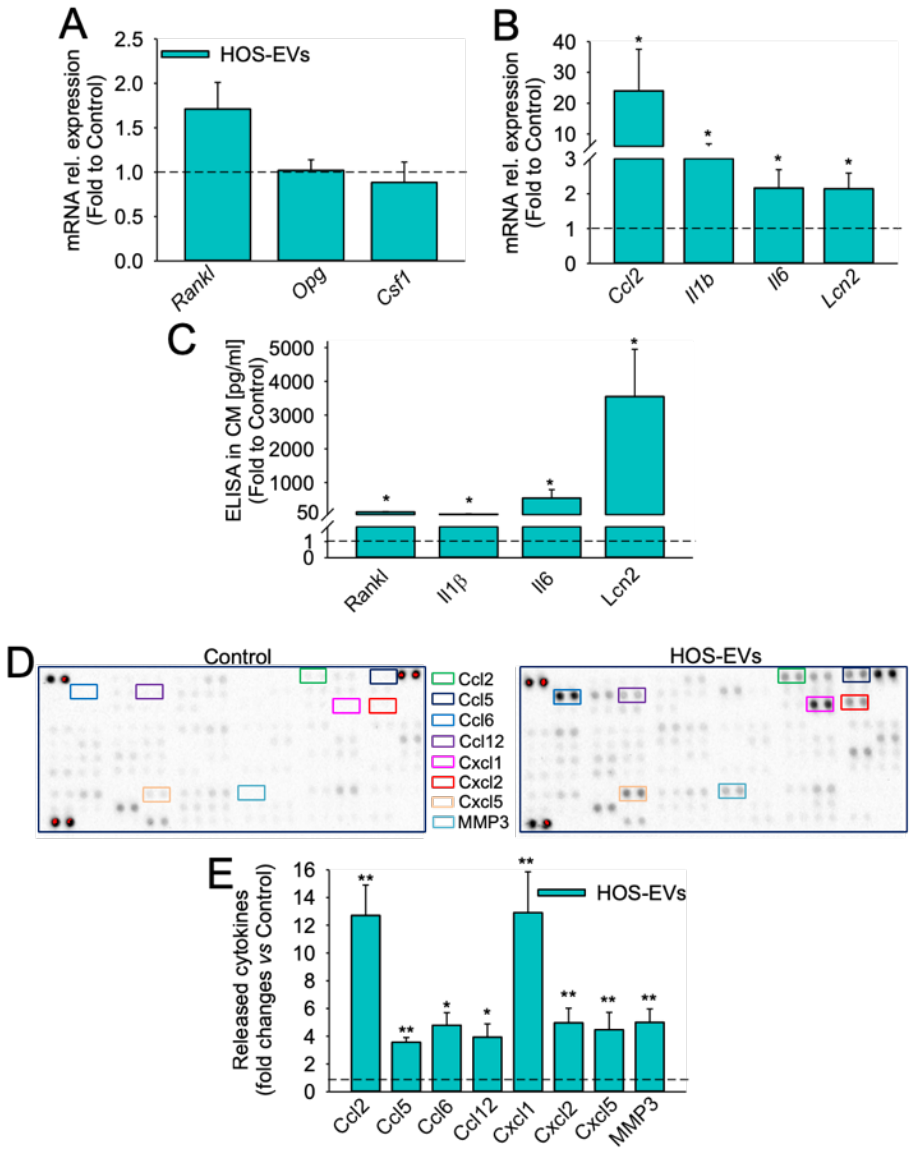

Figure 6. Effect of MNNG/HOS-EVs on osteoblast cytokine profile. Primary murine osteoblasts were starved overnight in serum-free DMEM, then cells were untreated (DMEM) or treated with MNNG/HOS-EVs (isolated from 12 ml of CM collected from one 175 cm^2 flask; cell density = 6.5 × $10^4/cm^2$). After 24 h, conditioned media (CM) were collected, while osteoblasts RNA was subjected to real time RT-PCR analysis. (**A,B**) Transcriptional expression of (**A**) osteoclast regulating factors *Rankl, Opg* and *Csf1* and (**B**) pro-inflammatory cytokines *Ccl2, Il1b, Il6 and Lcn2*. (**C**) ELISA assay to evaluate the release of RANKL, IL1β, IL6 and Lcn2 in the CM of control or MNNG/HOS-EV treated osteoblasts. (**D,E**) Cytokine array performed on the CM of control and MNNG/HOS-EV treated osteoblasts. (**D**) Representative images of membranes incubated with CM from untreated osteoblasts (Control) or MNNG/HOS-EV treated osteoblasts. (**E**) Evaluation of secreted cytokines modulated by treatment with MNNG/HOS-EVs, as determined by densitometric analysis of spots of interest that were normalized for the housekeeping genes. Results are (D) representative or (A-C,E) the mean ± SD of at 3 independent experiments (*$p < 0.05$ and **$p < 0.01$ *versus* control, Student's t-test; dot line = control set at 1).

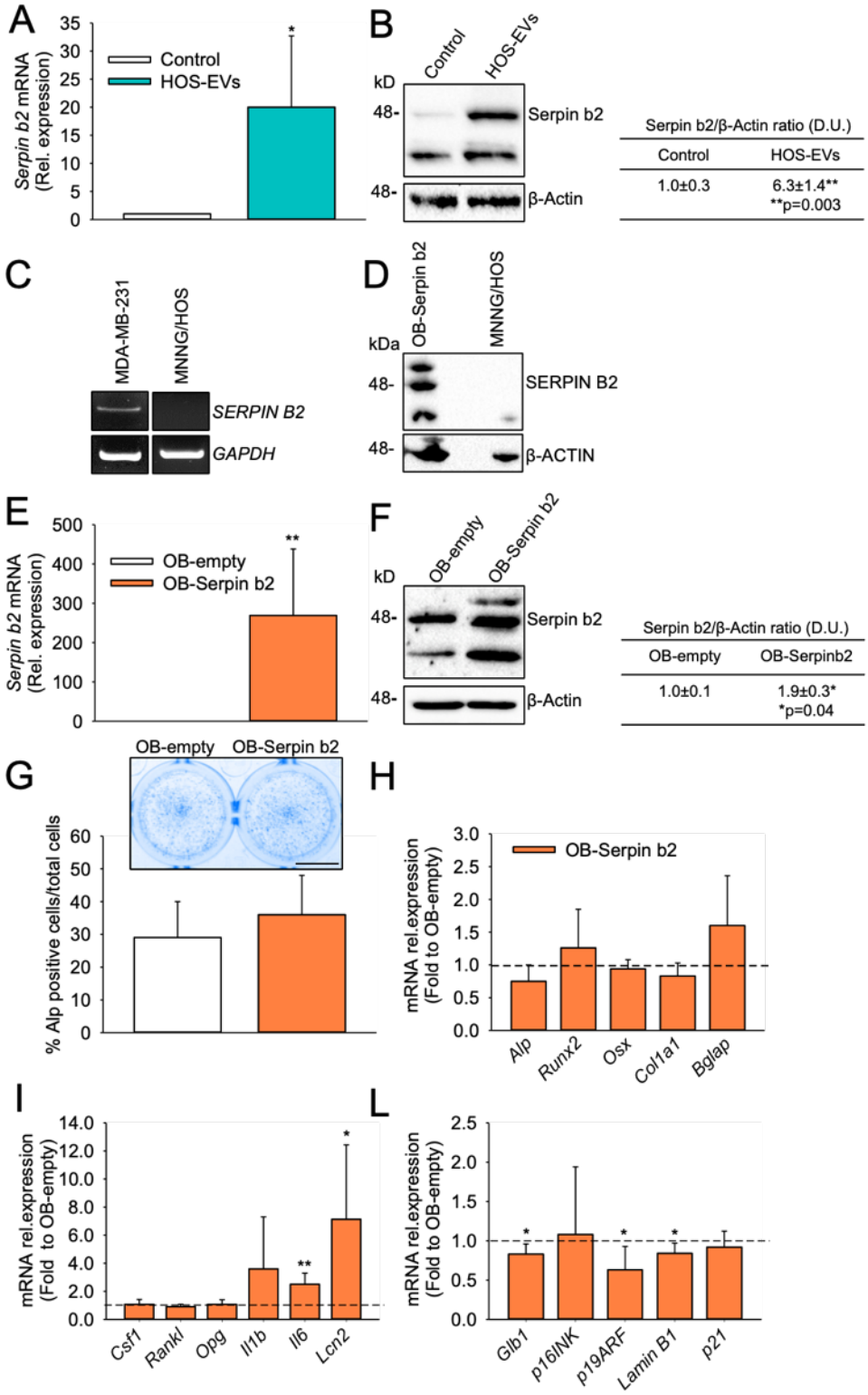

Figure 7. Effect of Serpin b2 overexpression on osteoblasts. (**A,B**) Mouse primary osteoblasts were starved in serum-free DMEM overnight and cultured in DMEM as control or treated with MNNG/HOS-EVs. (**A**) Real time RT-PCR to evaluate the expression of *Serpin b2*. (**B**) Western blot to evaluate protein expression of Serpin b2. The table on the right shows Serpin b2/β-actin ratio evaluated by densitometric analysis of the band of the specific molecular weight for Serpin b2 (47 kD). (**C**) Transcriptional expression of *SERPIN B2* in MDA-MB-231 and MNNG/HOS

cells by semiquantitative RT-PCR. *GAPDH* = housekeeping gene. MDA-MB-231 mRNA was employed as positive control. (**D**) Western blot to analyse SERPIN B2 protein in MNNG/HOS-EVs and in osteoblasts overexpressing Serpin b2 (OB-Serpin b2), the latter employed as positive control. Filter was stripped and reprobed with an anti-β-ACTIN antibody. (**E– L**) Mouse primary osteoblasts were transiently transfected with an empty (OB-empty) or Serpin b2-expressing plasmid (OB-Serpin b2) using the AMAXA nucleofection procedure. (**E**) Real time RT-PCR to evaluate the expression of *Serpin b2* in transfected osteoblasts. (**F**) Western blot to evaluate the protein expression of *Serpin b2* in transfected osteoblasts; the table on the right shows Serpin b2/β-actin ratio evaluated by densitometric analysis of the band of the specific molecular weight for Serpin b2 (47 kD). (**G**) Cytochemical Alp activity performed on osteoblasts transfected with an empty (OB-empty) or Serpin b2-overexpression plasmid (OB-Serpin b2) (Inset, scale bar =5 mm). Osteoblasts were also counterstained with neutral red to assess the % of Alp positive cells/total cells (graph). (**H– L**) Real time RT-PCR to evaluate the expression of the (**H**) osteoblastogenic genes *Alp, Runx2, Osx, Col1a1* and *Bglap*, (**I**) osteoclast modulating (*Csf1, Rankl* and *Opg*) and inflammatory (*Il1b, Il6 and Lcn2*) cytokines, and (**L**) senescence-associated genes *Glb1, p16INK, p19ARF, Lamin B1* and *p21*. In (A,B,D,E) data are representative or the mean ± SD of three independent experiments (*p = 0.045 versus Control, Student's t-test); in (E,H-L) data are the mean ± SD of 6 independent experiments (*p < 0.017 and **p < 0.004 versus empty plasmid, Student's t-test; dot line = control set at 1).

4.6 Effect of MNNG/HOS-EV on angiogenesis

Given the relevance of blood supply in tumor growth, we evaluated whether MNNG/HOS-EVs could have any effects on angiogenesis. HUVEC cells were cultured in Endothelial Growth Medium (EGM)-2, to allow differentiation of endothelial cells and used as positive control, or in endothelial basal medium (EBM), which is the same medium without pro-angiogenic factors (negative control). MNNG/HOS-EVs treatment prevented the reduction of cell density observed in HUVECs maintained in EBM medium alone, as demonstrated by the crystal violet staining (Fig. 8A). Consistently, *in vitro* angiogenesis, evaluated by tube formation assay, was also fostered by MNNG/HOS-EVs, with an effect similar to that obtained in the presence of the EGM-2 pro-angiogenic medium (Fig. 8B). This result was reproduced *in vivo* by the Matrigel plug assay (Fig. 8C). Interestingly, among the genes involved in angiogenesis, *Angiopoietin 2 (ANGPT2), Fibroblast Growth Factor 2 (FGF2)* and *Vascular Endothelial Growth Factor (VEGF)* mRNAs were present in both MNNG/HOS cells and derived EVs (Fig. 8D,E), while and enrichment of the VEGF Receptor (VEGFR) was observed in MNNG/HOS-EVs (Fig. 8E). Immunofluorescence and ELISA assays on MNNG/HOS cells and on protein lysates from MNNG/HOS-EVs, respectively, also revealed the presence of VEGF (Fig. 8F,G). Taken together, these results indicate the ability of osteosarcoma derived-EVs to fuel *in vitro* tube formation, likely through a VEGF/ANGPT2/FGF2-mediated mechanism. At variance with MNNG/HOS-EVs, U2OS-EVs had no effect on *in vitro* angiogenesis of HUVEC cells (Fig. 9).

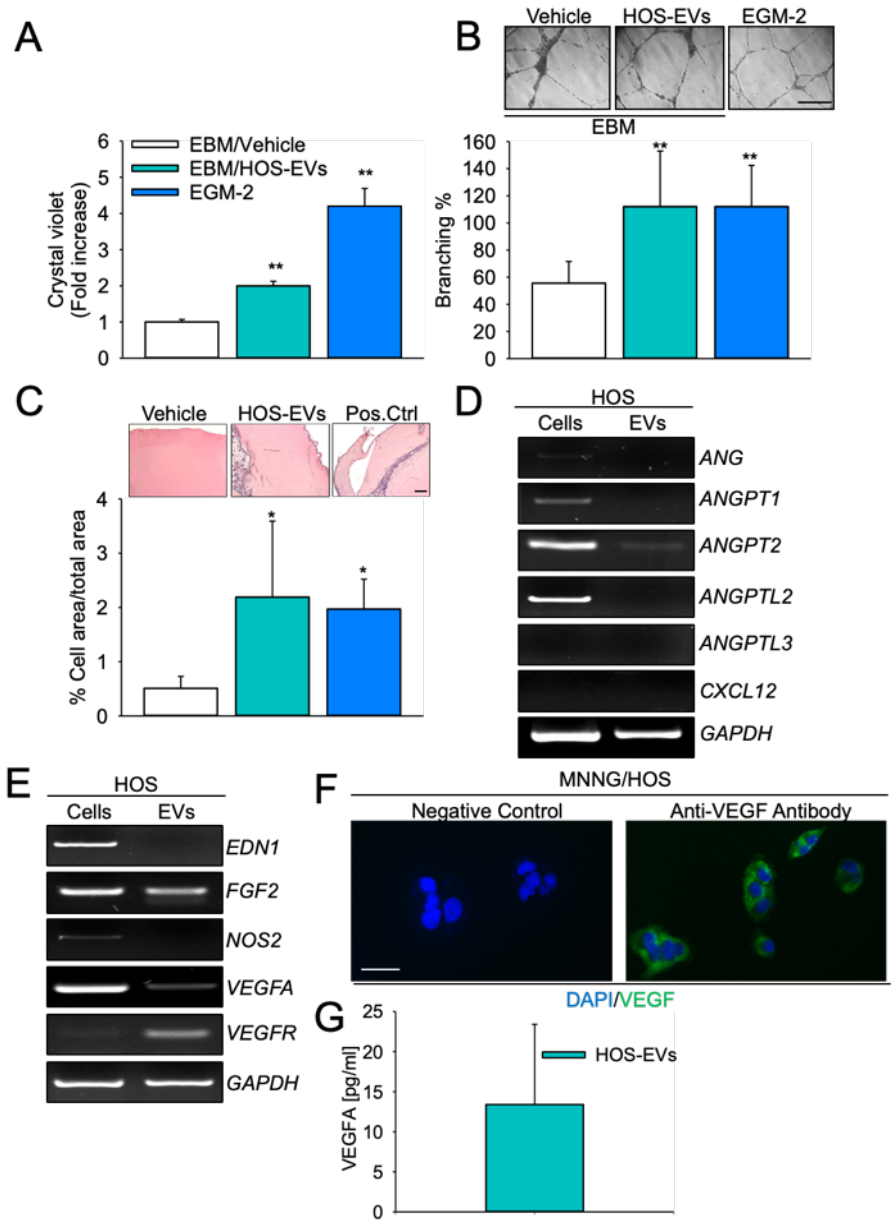

Figure 8. Effect of MNNG/HOS-EVs on angiogenesis. Human umbilical vein endothelial cells (HUVECs) were cultured in endothelial basic medium (EBM) as negative control, EBM plus MNNG/HOS-EVs (isolated from 12 ml of CM collected from one 175 cm^2 flask, cell density = 6.5×10^4 cells/cm^2) or endothelial growth medium (EGM)-2 as Positive control. (**A**) HUVEC cell density estimated by crystal violet staining. (**B**) *In vitro* tube formation assay on HUVECs to assess percent of branching following treatment with EBM, MNNG/HOS-EVs and EGM-2. (C) *In vivo* Matrigel plug assay by subcutaneous injection of 8-week-old male mice with 0.5 mL of Matrigel, plus PBS (Neg.Ctrl), MNNG/HOS-EVs or 50 ng/ml of ECGS +150 ng/ml VEGF (Pos.Ctrl). Data are the mean ± SD of (**A,B**) three independent experiments or (**C**) 5 mice/group (** $p < 0.01$ versus EBM, Student's t-test; scale bar = 200 µm). (**D,E**) Semiquantitative RT-PCR to evaluate the transcriptional expression of (**D**) *Angiogenin (ANG), Angiopoietin 1 (ANGPT1), ANGPT2, Angiopoietin Like 2 (ANGPTL2), ANGPTL3, Chemokine (C-X-C motif) ligand 12 (CXCL12),* (**E**) *Endothelin 1 (EDN1), Fibroblast Growth Factor 2 (FGF2), Nitric oxide 2 (NOS2), Vascular Endothelial Growth Factor A (VEGFA)* and *VEGF Receptor (VEGFR)* in MNNG/HOS cells and in MNNG/HOS-EVs. GAPDH = housekeeping gene. Pictures are representative of 3 different cells/EVs preparations. (**F**) Immunofluorescence analysis to assess VEGF expression in MNNG/HOS cells. Cells were also stained with the nuclear dye DAPI; left panel = negative control (scale bar = 40 µm). (**G**) ELISA on MNNG/HOS-EV protein lysates. Pictures are representative and the graph is the mean ± SD of 3 independent EV preparations.

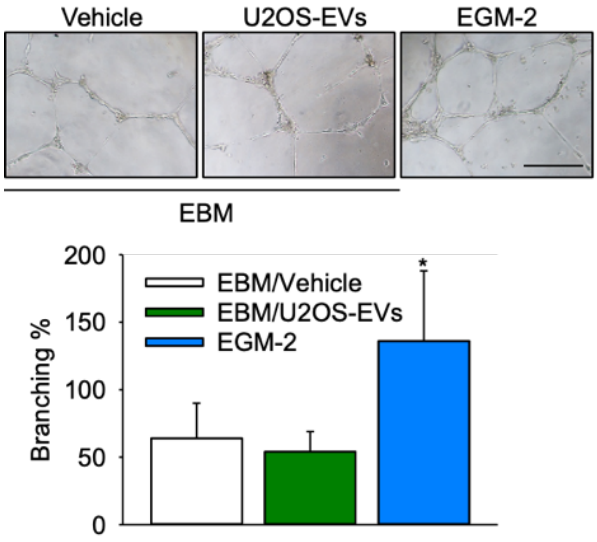

Figure 9. Effect of U2OS-EVs on angiogenesis. Human umbilical vein endothelial cells (HUVECs) were cultured in endothelial basic medium (EBM) as negative control, EBM plus U2OS-EVs (isolated from 12 ml of CM collected from one 175 cm^2 flask, cell density= $6.5x10^4$ cells/cm^2) or endothelial growth medium (EGM)-2 as Positive control. After 18 hours *in vitro* tube formation was evaluated by assessing the percent of branching formed. Pictures are representative and the graph is the mean ± SD of 3 independent experiments (*$p<0.05$ vs EBM/Vehicle, Student's t-test. Scale bar = 200µm).

5. DISCUSSION

Osteosarcoma is a rare primary tumor which mainly affects long bones, with a high morbidity in early childhood[1,3]. Indeed, tumor cells induce substantial changes in the bone microenvironment to prepare a fertile soil for their own growth and, despite important advances in this field, many aspects of osteosarcoma biology still need to be elucidated. Recently, EVs have been identified as key players in tumorigenesis and spreading of cancer cells to bone, both for primary tumors and metastases[37].

In line with this evidence, we observed that EVs from the MNNG/HOS human osteosarcoma cell line can affect bone resident cells, namely osteoblasts, osteoclasts and endothelial cells. As for the former, MNNG/HOS-EVs are internalized by cultured osteoblasts, eventually inducing decrease in their density, metabolic activity, and differentiation. Interestingly, the latter effect seems to be only partially dependent on the cell number-reducing effect, since the % of Alp-positive cells was also reduced. This effect was less evident when cells were put into osteogenic medium, a condition that strongly induces osteoblast differentiation, where also mineralization ability was unchanged, although the brevity of the experiment is a limitation for the latter evaluation. Furthermore, although the regulation was not significant ($p = 0.08$), MNNG/HOS-EVs seemed to reduce cell number at 7 days of mineralization, similarly to what we observed in non-osteogenic conditions.

Deregulation of osteoblast homeostasis is an effect known to be typically induced by tumor cells colonizing the bone. As a key example, the osteoblast molecular reprogramming carried out by tumor cells creates a permissive environment for breast cancer cells growth in the bone and is at least partially accomplished *via* EVs[23,38]. In this work we show that this concept may also apply to a primary bone tumor like osteosarcoma. In particular, we found that several cytokines involved in chemotaxis and inflammation are released by osteoblasts under MNNG/HOS-EVs treatment, such as CCL2, 5, 6 and 12. Interestingly, the release of CXCL1, 2 and 5 is also increased after osteoblast treatment with MNNG/HOS-EVs. These results agree with recent findings demonstrating the involvement of CXCL1 in supporting osteosarcoma cell metastatization to lungs[39], and the role of CXCL2 in inhibiting osteoblast proliferation and differentiation[40]. Moreover, it has been shown that CXCL5 supports invasion and migration of osteosarcoma cells in both autocrine and paracrine ways[41]. Similarly, we found that MMP3 secretion by osteoblasts is increased after MNNG/HOS-EVs treatment. Interestingly, a recent work aimed at screening for critical genes involved in osteosarcoma, identified *MMP3* as one of the genes predictive of osteosarcoma metastasis[42]. Therefore, our work seems to strengthen the involvement of this metalloprotease in the osteosarcoma context and points out a role for osteosarcoma EVs in determining the osteoblast ectoenzyme profile.

In line with the observed changes in the pro-inflammatory molecular profile of osteoblasts, MNNG/HOS-EVs increased the expression of Serpin b2, also known as PAI-2. Elsafadi and colleagues recently characterized the molecular profile of two human bone marrow stromal cell lines with opposite ability to promote bone formation, finding that non-bone forming stromal cells present with upregulation of Serpin b2 compared to bone forming stromal cells[115]. In our hands, the exogenous overexpression of Serpin b2 in osteoblasts does not recapitulate the negative effect of MNNG/HOS-EVs on osteoblast differentiation, except for a slight but significant reduction of *Alp* mRNA. However, Serpin b2-overexpressing osteoblasts showed a pro-inflammatory gene expression profile, which suggests that this molecule may switch the bone microenvironment into an inflammatory condition through the MNNG/HOS-EVs.

In the tumor context, the role of Serpin b2 seems to be quite controversial, with pro and antitumoral effects according to the type of cancer[35,44,45]. Jin *et al* demonstrated that Serpin b2 upregulation promotes breast cancer metastasis to lungs, which is also the preferential secondary site for osteosarcoma, and reduces patient survival[46]. Another recognized role for Serpin b2 is in cell senescence[36]. However, we found a decrease in *Glb1,*

p19ARF and *Lamin B1* mRNAs, which indeed should be increased by senescence, while the transcription of other genes associated with cell senescence was not influenced by the overexpression of Serpin b2 in osteoblasts, thus ruling out the hypothesis that Serpin b2 could induce osteoblast senescence.

Although the effect of MNNG/HOS-EVs on osteoblast is quite clear, the response of osteoclast precursors to the treatment was less obvious. We showed that MNNG/HOS-EVs can be internalized by these cells, eventually leading to an increase of TRAcP positive mononuclear cells, which would suggest a pro-osteoclastogenic effect. However, this does not lead to the formation of mature multinucleated osteoclasts. In fact, while the TRAcP-positive area was increased by the treatment with MNNG/HOS-EVs, the number of TRAcP-positive cells with ≥3 nuclei was unremarkable *versus* the negative control. At the same time, a clear effect in reducing the number of these mononuclear precursors is observed, in line with an at least partial differentiation effect. We also noticed an increase of F4/80 positive cells compared to positive control-treated osteoclast precursors when treating with MNNG/HOS-EVs, accompanied by a reduction of *Rank* expression, but no change in *Itgam* expression. These results indicate that there could be a switch towards a macrophage phenotype, although not complete, and a deficit in fusion genes induced by MNNG/HOS-EVs, which is consistent with the phenotype observed, where precursors did not fuse into mature osteoclasts, but remained as single/binucleated cells. Additionally, we assessed whether MNNG/HOS-EVs could influence mature osteoclasts activity through the classical pit assay and evaluation of TRAcP release in the conditioned medium. However, this was not the case. It is also interesting to note that treating mature osteoclasts with MNNG/HOS-EVs results in scarce internalization (Fig. 1E), despite these cells have substantially more developed endocytic activity compared to osteoblasts, which is consistent with the absence of direct effects found by treating osteoclasts with MNNG/HOS-EVs.

Osteoblasts are key regulators of osteoclast differentiation, and since their secretome is affected by treatment with MNNG/HOS-EVs, we assessed whether an indirect effect on osteoclastogenesis was being carried out by MNNG/HOS-EVs through osteoblasts. However, conditioned medium from MNNG/HOS-EV-treated osteoblasts did not induce osteoclast differentiation. Nevertheless, the osteoblast secretome induced by the treatment with MNNG/HOS-EVs could be advantageous for tumor growth, rather than osteoclast differentiation, also considering that inflammation is a hallmark of cancer and promotes its progression.

Angiogenesis is a crucial mechanism for supporting invasiveness and metastatization of osteosarcoma, and EVs from different tumors have been described to directly fuel this process[47]. Consistently with such reports, we found that MNNG/HOS-EVs increase HUVEC cell number as well as angiogenesis both *in vitro* and *in vivo*, while there was no effect on endothelial cell motility. Moreover, this direct effect could be VEGF-mediated, as suggested by the evidence that MNNG/HOS-EVs contain both VEGF transcript and protein. These results agree with what observed by Perut *et al.*[48] who found that endothelial cells internalize osteosarcoma derived-EVs and their miRNA and protein content stimulate angiogenesis. Additionally, VEGF could be only one of the players in the angiogenesis-inducing effect of MNNG/HOS-EVs, since they also contain mRNAs for other important pro-angiogenic factors, including FGF2 and ANGPT2.

To expand the scope of the work, we used another human osteosarcoma cell line, U2OS, to evaluate the effect of their EVs on osteoblast phenotype. This cell line is peculiar, since it shows fast growth rate, invasion, and migration *in vitro* (comparable or higher than MNNG/HOS), but at variance with MNNG/HOS, does not grow efficiently *in vivo*[49]. U2OS-EVs did not affect osteoblast cell density or metabolic activity, while reducing Alp activity, and were unable to increase angiogenesis. This difference in phenotype might mean that MNNG/HOS-EVs have a better ability to reprogram the microenvironment to their advantage *in vitro*, but whether this is a determinant of their different behavior *in vivo* is to be demonstrated.

In conclusion, we have profiled and evaluated the effects of osteosarcoma derived-EVs in the bone microenvironment, finding that they are able to dramatically impair osteoblast differentiation, alter osteoblasts secretome by inducing the release of proinflammatory and pro-tumoral factors, and stimulate angiogenesis. Taken together, our findings show a previously undescribed role for osteosarcoma derived EVs in the changes that eventually favor osteosarcoma growth and aggressiveness.

6. REFERENCES

1. Mirabello, L., Troisi, R. J. & Savage, S. A. International osteosarcoma incidence patterns in children and adolescents, middle ages, and elderly persons. *Int J Cancer* **125**, 229–234 (2009).
2. Ottaviani, G. & Jaffe, N. The epidemiology of osteosarcoma. *Cancer Treat Res* **152**, 3–13 (2009).

3. Brown, H. K., Schiavone, K., Gouin, F., Heymann, M.-F. & Heymann, D. Biology of bone sarcomas and new therapeutic developments. *Calcif Tissue Int* **102**, 174–195 (2018).
4. Jackson, T. M., Bittman, M. & Granowetter, L. Pediatric malignant bone tumors: a review and update on current challenges, and emerging drug targets. *Curr Probl Pediatr Adolesc Health Care* **46**, 213–228 (2016).
5. Jafari, F., Javdansirat, S., Sanaie, S., *et al.* Osteosarcoma : a comprehensive review of management and treatment strategies. *Ann Diagn Pathol* **49**, 151654 (2020).
6. Del Fattore, A., Teti, A. & Rucci, N. Bone cells and the mechanisms of bone remodelling. *Front Biosci* **4**, 2302–21 (2012).
7. Lacey, D. L., Timms, E., Tan, H. L., *et al.* Osteoprotegerin ligand is a cytokine that regulates osteoclast differentiation and activation. *Cell* **93**, 165-176 (1998).
8. Fuller, K., Owens, J., Jagger, C., Wilson, A., Moss, R. & Chambers, T. Macrophage colony-stimulating factor stimulates survival and chemotactic behavior in isolated osteoclasts. *J Exp Med* **178**, 1733-1744 (1993).
9. Cappariello, A., Maurizi, A., Veeriah, V. & Teti, A. The great beauty of the osteoclast. *Arch Biochem Biophys* **558**, 70–78 (2014).
10. Capulli, M., Paone, R. & Rucci, N. Osteoblast and osteocyte: games without frontiers. *Arch Biochem Biophys* **561**, 3–12 (2014).
11. Muscolo, D. L., Campaner, G., Aponte-Tinao, L. A., Ayerza, M. A. & Santini-Araujo, E. Epiphyseal primary location for osteosarcoma and ewing sarcoma in patients with open physis. *J Pediatr Orthop* **23**, 542–545 (2003).
12. Buch, A., Sawlani, V., Chandanwale, S. & Kumar, H. Diaphyseal osteosarcoma with varying histomorphologic patterns. *Adv Biomed Res* **3**, 33 (2014).
13. Thomas, D. M., Johnson, S. A., Sims, N. A., *et al.* Terminal osteoblast differentiation, mediated by runx2 and p27 KIP1, is disrupted in osteosarcoma. *J Cell Biol* **167**, 925–934 (2004).
14. Haydon, R. C., Luu, H. H. & He, T. C. Osteosarcoma and osteoblastic differentiation: a new perspective on oncogenesis. *Clin Orthop Relat Res* **454**, 237–246 (2007).
15. Avnet S., Longhi A., Salerno M., *et al.* Increased osteoclast activity is associated with aggressiveness of osteosarcoma. *Int J Oncol* **33**, 1231–1238 (2008).
16. Endo-Munoz, L., Cumming, A., Rickwood, D., *et al.* Loss of Osteoclasts Contributes to Development of Osteosarcoma Pulmonary Metastases. *Cancer Res* **70**, 7063-7072 (2010).

17. Endo-Munoz, L., Evdokiou, A. & Saunders, N. A. The role of osteoclasts and tumour-associated macrophages in osteosarcoma metastasis. *Biochim Biophys Acta* **1826**, 434–442 (2012).
18. Endo-Munoz, L., Cumming, A., Sommerville, S., Dickinson, I. & Saunders, N. A. Osteosarcoma is characterised by reduced expression of markers of osteoclastogenesis and antigen presentation compared with normal bone. *Br J Cancer* **103**, 73–81 (2010).
19. Xie, L., Ji, T. & Guo, W. Anti-angiogenesis target therapy for advanced osteosarcoma. *Oncol Rep* **38**, 625–636 (2017).
20. Valadi, H., Ekström, K., Bossios, A., Sjöstrand, M., Lee, J. & Lötvall, J. Exosome-mediated transfer of mRNAs and microRNAs is a novel mechanism of genetic exchange between cells. *Nat Cell Biol* **9**, 654–659 (2007).
21. Garimella, R., Washington, L., Issacson, J., *et al.* Extracellular membrane vesicles derived from 143B osteosarcoma cells contain pro-osteoclastogenic cargo: a novel communication mechanism in osteosarcoma bone microenvironment. *Transl Oncol* **7**, 331–340 (2014).
22. Baglio, S., Lagerweij, T., Pérez-Lanzòn, M., *et al.* Blocking tumor-educated MSC paracrine activity halts osteosarcoma progression. *Clin Cancer Res* **23**, 3721–33 (2017).
23. Loftus, A., Cappariello, A., George, C., *et al.* Extracellular Vesicles From Osteotropic Breast Cancer Cells Affect Bone Resident Cells. *J Bone Miner Res* **35**, 396-412 (2020).
24. Cappariello, A., Loftus, A., Muraca, M., Maurizi, A., Rucci, N. & Teti, A. Osteoblast-derived extracellular vesicles are biological tools for the delivery of active molecules to bone. *J Bone Miner Res* **33**, 517–533 (2017).
25. Rucci, N., Rufo, A., Alamanou, M., *et al.* The glycosaminoglycan-binding domain of PRELP acts as a cell type-specific NF-κB inhibitor that impairs osteoclastogenesis. *J Cell Biol* **187**, 669–683 (2009).
26. Kubota, Y., Kleinman, H. K., Martin, G. R. & Lawley, T. J. Role of laminin and basement membrane in the morphological differentiation of human endothelial cells into capillary-like structures. *J Cell Biol* **107**, 1589–1598 (1995).
27. Théry, C., Witwer, K. W., Aikawa, E., *et al.* Minimal information for studies of extracellular vesicles 2018 (MISEV2018): a position statement of the International Society for Extracellular Vesicles and update of the MISEV2014 guidelines. *J*

Extracellular vesicles 7:1535750 (2018).

28. Austyn, J. M. & Gordon, S. F4/80, a monoclonal antibody directed specifically against the mouse macrophage. *Eur J Immunol* **11**, 805–815 (1981).
29. Morris, L., Graham, C. F. & Gordon, S. Macrophages in haemopoietic and other tissues of the developing mouse detected by the monoclonal antibody F4/80. *Development* **112**, 517–526 (1991).
30. Tanaka, T. Encycopedia of Immunobiology. *Academic Press* **3**, 505–511 (2016).
31. Wright, H. L., McCarthy, H. S., Middleton, J. & Marshall, M. J. RANK, RANKL and osteoprotegerin in bone biology and disease. *Curr Rev Musculoskelet Med* **2**, 56–64 (2009).
32. Ponzetti, M. & Rucci, N. Switching homes: how cancer moves to bone. *Int J Mol Sci* **21**, 1–25 (2020).
33. Rucci, N., Capulli, M., Piperni, S. G., *et al.* Lipocalin 2: a new mechanoresponding gene regulating bone homeostasis. *J Bone Miner Res* **30**, 357–368 (2015).
34. Ye, R. D., Wun, T. C. & Sadler, J. E. Mammalian protein secretion without signal peptide removal. Biosynthesis of plasminogen activator inhibitor-2 in U-937 cells. *J Biol Chem* **263**, 4869–4875 (1988).
35. Su, S. C., Lin, C. W., Yang, W. E., Fan, W. L. & Yang, S. F. The urokinase-type plasminogen activator (uPA) system as a biomarker and therapeutic target in human malignancies. *Expert Opin Ther Targets* **20**, 551–566 (2016).
36. Hsieh, H. H., Chen, Y. C., Jhan, J. R. & Lin, J. J. The serine protease inhibitor serpinB2 binds and stabilizes p21 in senescent cells. *J Cell Sci* **130**, 3272–3281 (2017).
37. Cappariello, A. & Rucci, N. Tumour-derived extracellular vesicles (EVs): a dangerous 'message in a bottle' for bone. *Int J Mol Sci* **20**, 4805 (2019).
38. Bussard, K. M., Venzon, D. J. & Mastro, A. M. Osteoblasts are a major source of inflammatory cytokines in the tumor microenvironment of bone metastatic breast cancer. *J Cell Biochem* **111**, 1138–1148 (2010).
39. Chao, C. C., Lee, C. W., Chang, T. M., Chen, P. C. & Liu, J. F. CXCL1/CXCR2 paracrine axis contributes to lung metastasis in osteosarcoma. *Cancers* **12**, 459 (2020).
40. Yang, Y., Zhou, X., Li, Y., *et al.* CXCL2 attenuates osteoblast differentiation by inhibiting the ERK1/2 signaling pathway. *J Cell Sci* **132**, (2019).
41. Dang, H., Wu, W., Wang, B., *et al.* CXCL5 plays a promoting role in osteosarcoma

cell migration and invasion in autocrine- and paracrine-dependent manners. *Oncol Res* **25**, 177-186 (2017).

42. Fan, H., Lu, S., Wang, S. & Zhang, S. Identification of critical genes associated with human osteosarcoma metastasis based on integrated gene expression profiling. *Mol Med Rep* **20**, 915–930 (2019).
43. Elsafadi, M., Shinwari, T., Al-Malki, S., *et al.* Convergence of TGFβ and BMP signaling in regulating human bone marrow stromal cell differentiation. *Sci Rep* **9**, 17827 (2019).
44. Zhang, X. M., Wang, T., Hu, P., Li, B., Liu, H. & Cheng Y. F. SERPINB2 overexpression inhibited cell proliferation, invasion and migration, led to G2/M arrest, and increased radiosensitivity in nasopharyngeal carcinoma cells. *J Radiat Res* **60**, 318–327 (2019).
45. Harris, N. L. E., Vennin, C., Conway, J. R. W., *et al.* SerpinB2 regulates stromal remodelling and local invasion in pancreatic cancer. *Oncogene* **36**, 4288–4298 (2017).
46. Jin, T., Suk Kim, H., Ki Choi, S., *et al.* microRNA-200c/141 upregulates SerpinB2 to promote breast cancer cell metastasis and reduce patient survival. *Oncotarget* **8**, 32769–32782 (2017).
47. Feng, Q., Zhang, C., Lum, D., *et al.* A class of extracellular vesicles from breast cancer cells activates VEGF receptors and tumour angiogenesis. *Nat Commun* **8**, 14450 (2017).
48. Perut, F., Roncuzzi, L., Zini, N., Massa, A. & Baldini, N. Extracellular nanovesicles secreted by human osteosarcoma cells promote angiogenesis. *Cancers* **11**, *779* (2019).
49. Lauvrak, S. U., Munthe, E., Kresse, S. H., *et al.* Functional characterisation of osteosarcoma cell lines and identification of mRNAs and miRNAs associated with aggressive cancer phenotypes. *Br J Ca* **15**, 2228-2236 (2013).

Chapter 4

"Conclusions"

CONCLUSIONS

During my PhD I focused my research to study the effects of extracellular vesicles (EVs) derived from osteosarcoma cells and osteotropic breast cancer cells on bone resident cells.

There are consistent data in the literature showing that bone is a preferential site for cancer dissemination[1,2,3]. EVs are released from multiple cell types and regulate intercellular communication[4]. In recent years, several studies have been emerging on the involvement of EVs not only in normal bone physiology, as mediator of the osteoblast-osteoclast crosstalk[5,6], but also in tumors onset and dissemination[7,8,9]. However, their role in the bone metastatic process is quite complex and has not been completely understood to date, thus becoming a hot topic in the field of cancer research (see **Chapter 1**).

Based on these premises, since bone tissue is one of the most common sites for breast cancer metastases, in **Chapter 2** of this thesis we evaluated the EV-mediated interaction between the osteotropic human breast cancer MDA-MB-231 cell line, and bone resident cells. We demonstrated the ability of tumor cells-derived EVs to increase osteoclastogenesis as well as *in vitro* and *in vivo* angiogenesis, and, at the same time, to inhibit osteoblast differentiation and activity, exerting a direct role on bone physiopathology. Our findings are consistent with the fact that there is a growing body of evidence supporting that metastatic cancer cells use the EVs for educating bone cells toward a microenvironment favoring their homing[10,11,12]. Moreover, in our hands secreted factors deriving from MDA-MB-231 conditioned medium have an educational, previously undescribed, effect on osteoblasts, increasing the osteoclastogenic and angiogenic potential of EVs isolated from the latter and potentially promoting osteolysis, taking part to the vicious cycle, thus altering the balance between bone resident cells and creating a pro-metastatic environment[13]. However, the implicated molecular pathways remain to be elucidated through further studies.

In line with these findings, focusing on the mechanisms underlying the progression of bone primary tumors, in **Chapter 3** we investigated the interactions of EVs derived from the human osteosarcoma cell line MNNG/HOS with bone resident cells. We demonstrated *in vitro* that MNNG/HOS-EVs treatment reduced osteoblast differentiation, while enhancing their release of pro-inflammatory cytokines and pro-tumoral factors, disrupting the balance underlying the bone remodelling process and contributing to a pro-tumoral effect. It is interesting to note that we observed that MNNG/HOS-EVs promote angiogenesis, both *in vitro* and *in vivo*. We also found that they dramatically increase Serpin b2 expression in

murine osteoblasts, probably linked to the observed EVs-mediated pro-inflammatory effect on bone[14]. Although further experiments are needed, this could lead us to identify EVs-derived key factors potentially involved in the observed deregulation of osteoblast homeostasis during the progression of a primary bone tumor like the osteosarcoma.

Intriguingly, the studies discussed in this dissertation underline the importance of EVs in bone cancers, both primary and secondary, which has been an understudied issue to date. In particular, osteoblasts, master-regulatory cells in the bone microenvironment, are hijacked by cancer-EVs, which not only reduce their differentiation, but also induce them to release factors involved in the progression of the tumors themselves. It is interesting to think that EVs do not necessarily act locally, but can also be transported in the bloodstream and act in an endocrine-like fashion, thus influencing bone cells from the primary site, potentially creating pre-metastatic niches in the case of breast cancer. Therefore, blocking the action of EVs would not only result in a potential rescue of the vicious cycle, but it could also prevent bone metastatization. In this regard, there are several drugs that are able to stop EVs production and secretion, such as manumycin A, GW4869, imipramine, pantethine, tipifarnib, neticonazole, climbazole, and ketoconazole[15], and it would be interesting to evaluate whether these compounds exert any effect on bone tumor growth and metastasis.

Furthermore, it will also be important to investigate the other side of the coin: the effects of microenvironment-derived EVs on tumor cells. This could indicate whether cancer-influenced bone cells also secrete EVs that favor tumor growth, thus increasing the rationale for blocking EVs production in a cancer setting. On the other side, one could use biotechnologically engineered EVs based on the naturally-occurring ones, that are already programmed to target cancer or bone cells, as drug-delivery-systems able to counteract bone metastasis as well as osteosarcoma growth.

In conclusion, the work done during my PhD allowed us to better understand and characterize EVs as important means of communication between bone cells and both primary and metastatic tumor cells, adding another piece to the complex puzzle underlying the current study on the composition and the role of tumor derived-EVs in bone physiopathology. The obtained results may represent a starting point for further studies, aimed at the identification of new biomarkers or targetable pathways involved in the tumor-bone microenvironment EV-mediated interactions, necessary for the development of novel therapeutic approaches to counteract tumor onset or metastatic progression in bone and to improve patients' life quality and/or expectancy.

REFERENCES

1. Yin, J. J., Pollock, C. B. & Kelly, K. Mechanisms of cancer metastasis to the bone. *Cell Res* **15**, 57–62 (2005).
2. Virk, M. S. & Lieberman, J. R. Tumor metastasis to bone. *Arthritis Res Ther* **9**, 1–10 (2007).
3. Coleman, R. E. Metastatic bone disease: clinical features, pathophysiology and treatment strategies. *Cancer Treat Rev* **27**, 165–176 (2001).
4. György, B., Szabò, T. G., Pàsztòi, M., *et al.* Membrane vesicles, current state-of-the-art: emerging role of extracellular vesicles. *Cell Mol Life Sci* **68**, 2667–2688 (2011).
5. Deng, L., Wang, Y., Peng, Y., *et al.* Osteoblast-derived microvesicles: a novel mechanism for communication between osteoblasts and osteoclasts. *Bone* **79**, 37–42 (2015).
6. Cappariello, A., Loftus, A., Muraca, M., Maurizi, A., Rucci, N. & Teti, A. Osteoblast-derived extracellular vesicles are biological tools for the delivery of active molecules to bone. *J Bone Miner Res* **33**, 517–533 (2018).
7. Zhao, H. Achreja, A., Iessi, E., *et al.* The key role of extracellular vesicles in the metastatic process. *Biochim Biophys Acta Rev Cancer* **1869**, 64–77 (2018).
8. Becker, A. Thakur, B. K., Weiss, J. M., Kim, H. S., Peinado, H. & Lyden, D. Extracellular vesicles in cancer: cell-to-cell mediators of metastasis. *Cancer Cell* **30**, 836–848 (2016).
9. Kahlert, C. & Kalluri, R. Exosomes in tumor microenvironment influence cancer progression and metastasis. *J Mol Med* **91**, 431–437 (2013).
10. Li, S. & Wang, W. Extracellular vesicles in tumors: a potential mediator of bone metastasis. *Front Cell Dev Biol* **9**, 639514 (2021).
11. Cappariello, A. & Rucci, N. Extracellular vesicles in bone tumors: how to seed in the surroundings molecular information for malignant transformation and progression. *Front Oncol* **11**, 3654 (2021).
12. Xavier, C. P. R., Caires, H. R., Barbosa, M. A. G, *et al.* The role of extracellular vesicles in the hallmarks of cancer and drug resistance. *Cells* **9**, 1–34 (2020).
13. Loftus, A., Cappariello, A., George, C., *et al.* Extracellular vesicles from osteotropic breast cancer cells affect bone resident cells. *J Bone Miner Res* **35**, (2020).
14. Ucci, A., Cappariello, A., Ponzetti, M., *et al.* Anti-osteoblastogenic, pro-inflammatory and pro-angiogenic effect of extracellular vesicles isolated from the human osteosarcoma cell line MNNG/HOS. *Bone* **153**, 116130 (2021).

15. Catalano, M. & O' Driscoll, L. Inhibiting extracellular vesicles formation and release: a review of EV inhibitors. *J Extracell Vesicles* **9**, 1703244 (2019).

Chapter 5

"Achievements"

CURRICULUM VITAE

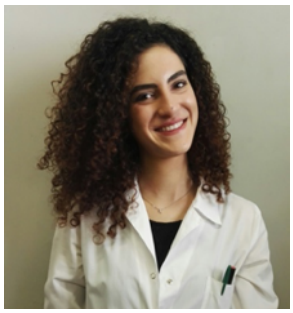

Argia Ucci

Born in Lanciano (Italy), 9th November 1992,
Italian Citizenship

OrcidID QR code

ADDRESS

Via G. Mameli, 6
66034, Lanciano (CH), Italy

Mobile: +39 3405064578
E-mail : argiaucci@gmail.com
argia.ucci@graduate.univaq.it

ACADEMIC DEGREES

22/04/2017	Master's degree in Medical Biotechnologies *summa cum laude*, University of L'Aquila, Italy.
31/03/2015	Bachelor's degree in Biotechnologies *summa cum laude*, University of L'Aquila, Italy.

PROFESSIONAL EXPERIENCES AND POSITIONS

02/2022-to date	Research Assistant (assegnista di ricerca) in the University of L'Aquila, Italy, in the "Skeletal Disease laboratory" headed by Prof. Nadia Rucci.
07/2019-09/2019	Secondment of 3 months, under the RUBICON (Training network for Research on molecUlar and Biomechanical Interactions in CONnective tissue disorders) project, in Prof. Danny Chan laboratory, School of Biomedical Sciences, University of Hong Kong.
11/2018-11/2021	PhD candidate in Experimental Medicine in the University of L'Aquila, Italy, in the "Skeletal Disease laboratory" headed by Prof. Nadia Rucci.
07/2017-09/2017	Secondment of 3 months, under the RUBICON project, in Prof. Shireen Lamande and Prof. John Bateman laboratory, Murdoch Children's Research Institute (MCRI) in Melbourne, Australia.

01/2017-
10/2018 Research fellowship in the "Skeletal Disease Laboratory", supervised by Prof. Nadia Rucci, University of L'Aquila, Italy.

2015-2016 Student training in the "Skeletal Disease Laboratory", supervised by Prof. Nadia Rucci, University of L'Aquila, Italy.

2013-2014 Student training in the "Bone Biopathology Laboratory" headed by Prof. Anna Maria Teti, Department of Biotechnological and Applied Clinical Sciences, University of L'Aquila, Italy.

OTHER EXPERIENCES AND INITIATIVES

2018-2021 Volunteering: member and chair of the "Student Group" in the Thursday Morning Science (TMS) group, University of L'Aquila, Italy.
2015-2020 Telethon fundraiser, L'Aquila, Italy.

NATIONAL AND INTERNATIONAL MEETINGS

- ECTS (European Calcified Tissue Society) international congress, 7-10 May 2022
- 33rd AICC (Associazione Italiana Colture Cellulari) conference in Turin, Italy, 22-24 November 2021
- III International AICC Exosome meeting, 7-8 June 2021
- ECTS international congress, 6-8 May 2021
- ECTS international congress, 22-24 October 2020
- ECTS Digital Masterclass for PhD Students, Trainees and Young Investigators, 23-25 June 2020
- ECTS international congress and RUBICON meeting in Budapest, Hungary, 11-14 May 2019
- MBE (Matrix Biology Europe) meeting in Manchester, United Kingdom, 21-24 July 2018
- RUBICON meeting in Manchester, United Kingdom, 20-21 July 2018
- RUBICON meeting in Salzburg, Austria, 16-17 May 2017
- ECTS international congress in Rome, Italy, 14-17 May 2016

PUBLIC SPEAKING AND CONFERENCE PRESENTATIONS

- Oral communication and poster – ECTS international congress, 7-10 May 2022
- Oral communication – III International AICC Exosome meeting, 7-8 June 2021
- Presentation of my PhD work – ECTS Digital Masterclass for PhD Students, Trainees and Young Investigators, 23-25 June 2020
- Presentation of the secondment completed in Melbourne, Australia – RUBICON meeting, Manchester, United Kingdom, 20-21 July 2018

- Seminar entitled "Working in Melbourne for the RUBICON project: my experience and data" – TMS event, University of L'Aquila, Italy, 5 October 2017

AWARDS

- **Best oral presentation award –** III International AICC Exosome meeting, 7-8 June 2021

PEER REVIEWED PUBLICATIONS

- **Ucci A**, Rucci N, Ponzetti M. *"Liquid biopsies in primary and secondary bone cancers"*. Cancer Drug Resistance, 2022. doi: 10.20517/cdr.2022.17.

- Ponzetti M, **Ucci A**, Maurizi A, Giacchi L, Teti A, Rucci N. *"Lipocalin 2 influences bone and muscle phenotype in the MDX mouse model of duchenne muscular dystrophy"*. International Journal of Molecular Sciences (IJMS), 2022. doi: 10.3390/ijms23020958.

- **Ucci A***, Cappariello A*, Ponzetti M, Tennant F, Loftus AEP, Shefferd K, Maurizi A, Delle Monache S, Teti A, Rucci N. *"Anti-osteoblastogenic, pro-inflammatory and pro-angiogenic effect of extracellular vesicles isolated from the human osteosarcoma cell line MNNG/HOS"*. Bone, 2021. 153:116130. doi: 10.1016/j.bone.2021.116130. **Equal contributors*

- Ponzetti M, Aielli F, **Ucci A**, Cappariello A, Lombardi G, Teti A, Rucci N. *"Lipocalin 2 increases after high-intensity exercise in humans and influences muscle gene expression and differentiation in mice".* Journal of Cellular Physiology, 2021. doi: 10.1002/jcp.30501.

- Loftus A, Cappariello A, George C, **Ucci A**, Shefferd K, Green A, Paone R, Ponzetti M, Delle Monache S, Muraca M, Teti A, Rucci N. *"Extracellular vesicles from osteotropic breast cancer cells affect bone resident cells"*. Journal of Bone and Mineral Research (JBMR), 2020. doi: 10.1002/jbmr.3891.

- Maurizi A, Capulli M, Curle A, Patel R, **Ucci A**, Côrtes JA, Oxford H, Lamandè SR, Bateman JF, Rucci N, Teti A. "*Extra-skeletal manifestations in mice affected by Clcn7-dependent autosomal dominant osteopetrosis type 2 clinical and therapeutic implications*". Bone Research, 2019. doi: 10.1038/s41413-019-0055-x.

Date of preparation: June 2022 Argia Ucci